

MIT Open Access Articles

A Statistical Study of the Subauroral Polarization Stream Over North American Sector Using the Millstone Hill Incoherent Scatter Radar 1979–2019 Measurements

The MIT Faculty has made this article openly available. **Please share** how this access benefits you. Your story matters.

Citation: Aa, Ercha, Erickson, Philip J., Zhang, Shun#Rong, Zou, Shasha, Coster, Anthea J. et al. 2020. "A Statistical Study of the Subauroral Polarization Stream Over North American Sector Using the Millstone Hill Incoherent Scatter Radar 1979–2019 Measurements." *Journal of Geophysical Research: Space Physics*, 125 (10).

As Published: <http://dx.doi.org/10.1029/2020ja028584>

Publisher: American Geophysical Union (AGU)

Persistent URL: <https://hdl.handle.net/1721.1/140925>

Version: Author's final manuscript: final author's manuscript post peer review, without publisher's formatting or copy editing

Terms of Use: Article is made available in accordance with the publisher's policy and may be subject to US copyright law. Please refer to the publisher's site for terms of use.



1 **A statistical study of the subauroral polarization**
2 **stream over North American sector using the Millstone**
3 **Hill incoherent scatter radar 1979–2019 measurements**

4 **Ercha Aa^{1,2}, Philip J. Erickson¹, Shun-Rong Zhang¹, Shasha Zou³, Anthea J.**
5 **Coster¹, Larisa P. Goncharenko¹, and John C. Foster¹**

6 ¹Haystack Observatory, Massachusetts Institute of Technology, Westford, MA, USA.

7 ²National Space Science Center, Chinese Academy of Sciences, Beijing, China.

8 ³Department of Climate and Space Sciences and Engineering, University of Michigan, Ann Arbor, MI,
9 USA.

10 **Key Points:**

- 11 • Key features of North American SAPS and associated N_e , T_i , and T_e were an-
12 alyzed using four-decade Millstone Hill IS radar measurements
- 13 • North American SAPS climatology in terms of MLT, season, geomagnetic activ-
14 ity, solar activity, and IMF condition was comprehensively studied
- 15 • Both ion and electron temperatures exhibit moderate enhancement around SAPS,
16 with similar geomagnetic but different solar activity dependence

This is the author manuscript accepted for publication and has undergone full peer review but has not been through the copyediting, typesetting, pagination and proofreading process, which may lead to differences between this version and the [Version of Record](#). Please cite this article as doi: [10.1029/2020JA028584](https://doi.org/10.1029/2020JA028584)

Corresponding author: P. J. Erickson, pje@mit.edu

Abstract

This work conducts a statistical study of the subauroral polarization stream (SAPS) feature in the North American sector using Millstone Hill incoherent scatter radar measurements from 1979 to 2019, which provides a comprehensive SAPS climatology using a significantly larger database of radar observations than was used in seminal earlier works. Key features of SAPS and associated electron density (Ne), ion temperature (Ti), and electron temperature (Te) are investigated using a superposed epoch analysis method. The characteristics of these parameters are investigated with respect to magnetic local time, season, geomagnetic activity, solar activity, and interplanetary magnetic field orientation, respectively. The main results are as follows: (1) Conditions for SAPS are more favorable for dusk than near midnight, for winter compared to summer, for active geomagnetic periods compared to quiet time, for solar minimum compared to solar maximum, and for IMF conditions with negative By and negative Bz . (2) SAPS is usually associated with a midlatitude trough of 15–20% depletion in the background density. The SAPS-related trough is more pronounced in the postmidnight sector and near the equinoxes. (3) Subauroral ion and electron temperatures exhibit a 3–8% (50–120 K) enhancement in SAPS regions, which tend to have higher percentage enhancement during geomagnetically active periods and at midnight. Ion temperature enhancements are more favored during low solar activity periods, while the electron temperature enhancement remains almost constant as a function of the solar cycle. (4) The electron thermal content, $Te \times Ne$, in the SAPS associated region is strongly dependent on $1/Ne$, with Te exhibiting a negative correlation with respect to Ne .

1 Introduction

The subauroral polarization stream (SAPS), which was first introduced by Foster and Burke (2002) as a synthesis of previous observational and theoretical work, refers to persistent westward plasma flows driven by enhanced poleward electric fields in the subauroral ionosphere equatorward of the electron auroral precipitation zone. SAPS is predominantly observed in the dusk-midnight magnetic local time (MLT) sector during periods of geomagnetic storms and substorms with a typical width of 3–5°, velocity magnitudes of several hundred m/s or larger, and collocated poleward electric field strengths exceeding 20 mV/m (Foster & Vo, 2002; Erickson et al., 2011). SAPS encompasses a number of occasionally embedded phenomena, including a broader region of smaller drifts (Yeh et al., 1991), as well as latitudinally narrow channels (1–2°) of intense localized westward flow (>1,000 m/s) with stronger electric fields (>50 mV/m), known as polarization jets (Galperin et al., 1974), subauroral ion drifts (SAID) (Anderson et al., 1993, 2001; Spiro et al., 1979), or subauroral electric fields (Karlsson et al., 1998). The presence of SAPS in the coupled ionosphere-magnetosphere plays an important role in controlling the formation and evolution of some large-scale features with significant space weather effects, such as enhanced ion vertical flows (H. Wang & Lühr, 2013), main ionospheric trough (Muldrew, 1965; Spiro et al., 1978; Rodger, 2008), storm-enhanced density plumes (Foster et al., 2007; Zou et al., 2013, 2014), and sunward-convecting plasmaspheric drainage plumes (Goldstein et al., 2004). For these reasons, SAPS/SAID have been extensively studied for several decades using both space-based and ground-based observations. For example, SAID/SAPS signatures can be derived from *in-situ* satellite measurements of ion drifts and electric fields in the ionosphere and/or inner magnetosphere, such as those measured by the Defense Meteorological Satellite Program (DMSP) (e.g., Yeh et al., 1991; Anderson, 2004; Goldstein et al., 2005; Huang & Foster, 2007; H. Wang et al., 2008, 2011; He et al., 2014, 2018; Landry & Anderson, 2018), Van Allen Probes (Foster et al., 2014; Califf et al., 2016; Lejosne & Mozer, 2017), and Magnetospheric Multiscale (MMS) spacecraft (Erickson et al., 2016). Also, the Super Dual Auroral Radar Network (SuperDARN) radars can observe large-scale plasma convection measurements of SAPS continuously over extended periods (e.g., Parkinson et al., 2005; Oksavik et al., 2006; Ebihara et al., 2009; Makarevich et al., 2009; Zou, Lyons, Wang, et al., 2009; Clausen et al., 2012; Nagano

et al., 2015; Kunduri et al., 2017, 2018; Z. Wang et al., 2019). Moreover, the altitudinal and time-dependent characteristics (plasma velocities, densities, temperature) on SAPS can also be remotely studied by using powerful incoherent scatter radar techniques (Foster & Burke, 2002; Foster & Vo, 2002; Erickson et al., 2011; Zou, Lyons, Nicolls, et al., 2009).

Various mechanisms have been proposed to interpret SAPS generation, including (1) Voltage source mechanism: During enhanced geomagnetic activity intervals, the inner boundary of the ion plasma sheet penetrates closer to Earth compared to that of electron plasma sheet in the premidnight sector due to their energy spectra difference. This misalignment of the ion and electron boundaries results in a radially outward polarization electric field in the inner magnetosphere (Gussenhoven et al., 1987), which can map along the equipotential magnetic field lines into the subauroral ionosphere in a poleward direction to cause SAPS (De Keyser, 1999). (2) Field-aligned currents (FACs) source mechanism: The ion pressure gradients of the ring current, which is caused by above-mentioned misalignment and/or the pitch angle scattering of precipitation (Yuan et al., 2016), will result in a fraction of downward Region 2 FACs to flow into the duskside subauroral ionosphere, where the conductivity is low due to lacking of electron precipitation (Heinemann et al., 1989). These FACs have to close through poleward Pederson currents with the Region 1 FACs, thus generating strong poleward electric fields (i.e., SAPS electric fields) in the low conductivity subauroral region (Anderson et al., 1993; Raeder et al., 2016). Other studies have also demonstrated that the location of SAPS is conjugate to the peak energy density of the ring current and the Region 2 FACs, and that the magnitude of SAPS velocity is approximately inversely proportional to the flux tube integrated Pedersen conductance (Zheng et al., 2008; H. Wang et al., 2008; He et al., 2014; Yu et al., 2015; Z. Wang et al., 2019). (3) Ionospheric feedback mechanism: The enhanced ion-neutral frictional heating associated with SAPS will accelerate the ion recombination rate, thus reduce the F-region density and create a large upward flow due to thermal expansion (Schunk et al., 1976; Anderson et al., 1991). This process will further reduce the already low subauroral conductivity and provide a feedback effect to amplify the strong electric fields (Anderson et al., 2001). (4) Substorm current wedge mechanism for SAPS and short-circuiting mechanism for SAID. Conventional theories normally involve relatively slow physical processes. However, Mishin et al. (2017) proposed that the broader SAPS and the narrower SAID channels could be separately generated by non-traditional mechanisms, since SAPS/SAID observations show very quick development (~ 10 min) shortly after substorm onset. Specifically, the prompt SAPSs response coincident with the westward traveling surge development in the nearby auroral region, which is the inherent part of the two-loop circuit of the substorm current wedge (Mishin et al., 2002; Sergeev et al., 2014; Kepko et al., 2015). This two-loop circuit builds up a large poleward electric field and demands closure of the Region 1 and Region 2 field-aligned currents via meridional currents, thus triggering fast ring current injections and SAPS on the dusk side (Mishin, 2016; Mishin et al., 2017). On the other hand, fast SAID response is suggested to be driven by the short-circuiting of the penetration of earthbound substorm hot plasma jets into the plasmasphere (Mishin et al., 2010; Mishin, 2013). Z. Wang et al. (2019) reported a rapid SAPS response to a localized and deep energetic particle injection during non-substorm time and suggested that the plasma pressure increase due to the injection is responsible for the localized SAPS enhancement. Taken in aggregate, these varied theoretical results indicate that more than one mechanism could be responsible for the formation and evolution of SAPS.

Besides observational case analyses, many statistical studies and modeling efforts have been made to characterize SAPS climatology, and its average spatial/temporal variation and activity dependence has been widely studied. Organizing principles of such studies include (1) Local time variation: The average geomagnetic latitude (MLAT) of SAPS tends to locate at the equatorward boundary of auroral precipitation around $60\text{--}65^\circ$ in the dusk and decreases linearly with respect to increasing MLT, reaching $50\text{--}55^\circ$ in the morning (Foster & Vo, 2002; Erickson et al., 2011). Also, SAPS tends to have largest

124 occurrence rate and peak flow velocity around 20 MLT that decreases toward dawn (Karlsson
125 et al., 1998; Foster & Vo, 2002; Erickson et al., 2011; Kunduri et al., 2017). (2) Geomag-
126 netic dependence: SAPS can be observed both during intense storms with flows exceed-
127 ing 1,500 m/s and time lags of 0–1.5 hours after southward turning of the interplane-
128 tary magnetic field (IMF), as well as during substorms with flows dropping to 100 m/s
129 and time lags of 0–2.5 hours after IMF southward turning (He et al., 2017; Kunduri et
130 al., 2018). Typically, SAPS tends to move equatorward and has a larger peak velocity
131 with respect to increasing geomagnetic activities (Kp, Dst, AE, and SYM/ASY-H in-
132 dices) (e.g., Karlsson et al., 1998; Foster & Vo, 2002; H. Wang et al., 2008; Erickson et
133 al., 2011; Kunduri et al., 2017). (3) Seasonal and hemispheric variation: Some studies
134 found that SAPS can be observed more frequently and have larger poleward electric fields
135 during the equinoxes in comparison to solstices (Karlsson et al., 1998; He et al., 2014).
136 However, some other studies indicated that SAPS peak velocities are larger in local winter
137 as compared to summer for both hemispheres (Koustov et al., 2006; H. Wang et al.,
138 2012; H. Wang & Lühr, 2013), and the Pederson currents and the electric fields are gen-
139 erally larger in the winter hemisphere (Kunduri et al., 2012). Furthermore, X. Zhang et
140 al. (2015) indicated that the drift velocities of SAID are generally larger in the North-
141 ern Hemisphere than the Southern Hemisphere in all MLT sectors.

142 Although significant progress has been obtained through these studies, current cli-
143 matological knowledge of the occurrence and variability of SAPS is still incomplete, and
144 there are some critical issues remaining to be addressed. These include: (1) What is the
145 statistical behavior of electron density and plasma temperature associated with SAPS?
146 Certain features of SAPS (e.g., zonal velocity, electric field, location, conductance) in-
147 vestigated in many prior studies have generally consistent results. Still, some counter-
148 examples exist in particular for ion temperature. For example, some storm-time case stud-
149 ies and numerical simulations have indicated that ion temperature around SAPS region
150 will be greatly enhanced due to frictional heating (e.g., Yeh & Foster, 1990; Anderson
151 et al., 1991; Moffett et al., 1998; Pintér et al., 2006; W. Wang et al., 2012; Erickson et
152 al., 2010; S.-R. Zhang et al., 2017). However, some statistical studies using DMSP mea-
153 surements indicated that the ion temperature around SAPS peak region shows no ap-
154 parent enhancement, or could even be depressed (H. Wang & Lühr, 2013; Q. Zhang et
155 al., 2020). Thus, how to interpret these conflicting results and re-evaluate the variabil-
156 ity of the plasma temperatures around SAPS region is of considerable interest (2) What
157 is the solar activity dependence of SAPS? The diurnal variation and geomagnetic depen-
158 dence of SAPS have been widely analyzed as mentioned above. Yet, very few studies have
159 focused on the solar cycle variation of SAPS due to limited coverage of observational databases.
160 He et al. (2014) analyzed DMSP 1987–2012 measurements and found that the narrow
161 SAID channel moves equatorward with larger widths during periods of high solar activ-
162 ities. However, it remains unknown whether the broader SAPS feature has a similar solar
163 cycle dependence, and what the solar activity dependence is of other pivotal param-
164 eters (i.e., electron density, ion temperature, electron temperature)? These are essential
165 open questions and need to be further addressed. (3) What is the possible influence of
166 the interplanetary magnetic field (IMF) orientation on SAPS? It is known that the aur-
167 oral convection pattern is strongly controlled by the magnitude and direction of the IMF
168 (e.g., Heppner & Maynard, 1987; Rich & Hairston, 1994; Weimer, 1995; Ruohoniemi &
169 Greenwald, 1996, 2005). However, there are few results in the literature concerning IMF
170 effects on SAPS morphology and dynamics. For example, He et al. (2017) found that
171 the lifetime of SAPS is linearly correlated with the duration of the southward IMF. Lin
172 et al. (2019) modeled the 2013 St. Patrick’s Day storm event and found that SAPS will
173 move equatorward with enhanced velocity and broader width when IMF B_z was becom-
174 ing more southward. Thus, it is still necessary to conduct a systematic statistical study
175 to verify this possible link further and to specify the relationship between IMF orienta-
176 tion and SAPS evolution.

177 Previously, Foster and Vo (2002) and Erickson et al. (2011) conducted two signif-
178 icant studies on SAPS by using Millstone Hill incoherent scatter radar data collected in
179 the subauroral ionosphere between May 1979–Jul 2000. They analyzed the average char-
180 acteristics of SAPS and summarized the variation pattern of SAPS with respect to MLT
181 and Kp (Dst). In this study, we extended these important early works to investigate in
182 depth the statistical behavior of SAPS by using Millstone Hill incoherent scatter radar
183 measurements between 1979–2019. The current work provides three major updates over
184 these prior studies: (1) We considerably extended the data coverage to four solar cycles,
185 and provided auroral equatorward boundary measurements alongside the Millstone Hill
186 observations to better distinguish auroral or subauroral flows in constructing reliable SAPS
187 dataset. (2) Besides SAPS itself, we also examined key features of electron density (N_e),
188 ion temperature (T_i), and electron temperature (T_e) in ionospheric regions located around
189 SAPS. (3) Besides local time and geomagnetic variations, we further investigated the sea-
190 sonal, solar cycle, as well as IMF dependencies of SAPS and associated plasma param-
191 eters. Results of our study provide partial information on the key questions described
192 above, and provide further information for clarifying the spatial and temporal variation
193 of SAPS. The rest of the paper is organized as follows. Section 2 describes the data and
194 methodology procedure. The statistical results and discussion are given in section 3. The
195 conclusions are presented in section 4.

196 2 Data and Method

197 The Millstone Hill incoherent scatter radar has been operated by the Massachusetts
198 Institute of Technology since 1960 and has provided valuable ionospheric measurements
199 with full altitude profiles, including but not limited to plasma convection, electron and
200 ion density, and electron and ion temperature information. The radar system is equipped
201 with a 68-m diameter fixed zenith antenna and a 46 m diameter fully steerable antenna
202 (MISA) with an extensive field-of-view. The MISA antenna was installed at Millstone
203 Hill in 1979 and provides extensive spatial and temporal coverage extending more than
204 30° in latitude, covering 100–1000 km in altitude, and spanning over 4 hours of local time
205 at F region heights (Foster & Vo, 2002; Erickson et al., 2011). Individual azimuth scans
206 also produce fine-scale plasma measurements with a typical temporal resolution of ~ 30 s
207 and an along-beam spatial resolution of ~ 100 –150 km. Over four decades of MISA avail-
208 ability, long-term observations through both regular yearly program and stormtime alert
209 experiments have built up a large database for auroral, subauroral, and midlatitude iono-
210 spheric studies over the North American sector (e.g., Yeh et al., 1991; Buonsanto et al.,
211 1992; Foster et al., 2005; L. P. Goncharenko et al., 2007; S.-R. Zhang & Holt, 2007). Within
212 these observations, SAPS flows readily appear as high-speed westward drifts in the dusk-
213 midnight midlatitude ionosphere equatorward of the auroral oval. In this study, we ex-
214 amined the radar azimuth scan measurements of ion velocity and associated plasma pa-
215 rameters during the years 1979–2019 to construct a SAPS data set and to further an-
216alyze SAPS and other related statistical features.

217 The previous technique for identifying SAPS occurrence was introduced in Foster
218 and Vo (2002) and Erickson et al. (2011). In this study, we further improved this tech-
219 nique and extended the data coverage as follows: (1) Specification of the equatorward
220 auroral boundary: The ion and electron energy flux measurements by precipitating par-
221 ticle spectrometer sensors (SSJ) onboard the DMSP satellites can provide high precision
222 and accurate auroral boundary determination. The DMSP SSJ-4 and SSJ-5 data dur-
223 ing 1982–2016 were used by Air Force Research Laboratory to create the Auroral Bound-
224 ary Index (ABI) data identifying the location of equatorward boundary along the satel-
225 lite path (Gussenhoven et al., 1981, 1983; Hardy et al., 2008). In this study, for a given
226 azimuth scan of the Millstone Hill incoherent scatter radar, a circular fitting for all avail-
227 able boundary locations within ± 60 min was applied to determine an integral bound-
228 ary distribution under MLT-MLAT coordinates. This choice was guided by many pre-

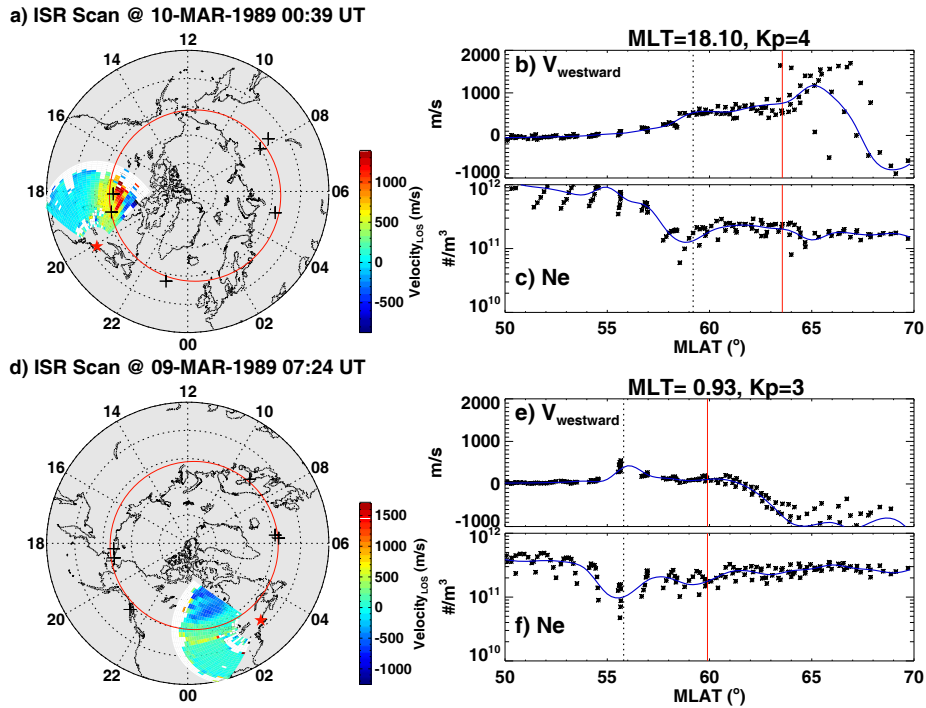


Figure 1. Observations of two SAPS events measured by the Millstone Hill incoherent scatter radar in 9-10 Mar 1989. (a) Line-of-sight plasma velocities for a full azimuth scan in the dusk sector under a polar view of MLT-MLAT coordinate. The concentric dashed circles are plotted in 10° interval, with the outermost ring representing 40° . The red circle represents the fitted equatorward boundary of the auroral oval with the DMSP satellite crossings marked by plus sign (see text for details). (b) Westward velocities and (c) electron densities as a function of geomagnetic latitude, with measurements individually shown by asterisks and collectively fitted by blue line. The red line represents the equatorward auroral boundary and the dotted line marks the identified SAPS peak location. The bottom panels (d-f) are the same as the upper ones, but represent a different azimuth scan near the midnight sector.

229 various studies which report that the shape of nighttime equatorward boundary of the au-
 230 roral oval can be approximately fitted by a circle (Gussenhoven et al., 1983; Hardy et
 231 al., 1989; Kunduri et al., 2017). If there is a data shortage for a given time or the fit-
 232 ting result is not good due to the lack of enough nighttime passes, then an alternative
 233 Kp-based auroral boundary model was used to implement the boundary determination
 234 (Hardy et al., 1987; Carbary, 2005). On average, the Kp-based auroral boundary model
 235 is used in 20% of cases. Considering that the actual boundary at a given time instance
 236 could be different from the statistical average of the model, the possibility cannot be ex-
 237 cluded that a fraction of the high-latitude portion of our SAPS datasets could be con-
 238 taminated by westward auroral convection in the dusk sector. (2) Computation of the
 239 westward component of the flow: The line-of-sight plasma $E \times B$ velocity at F region al-
 240 titudes was measured in each azimuth scan of the radar. Subsequently, the flow measure-
 241 ments were multiplied by a flow-angle correction factor using a cosine of the magnetic
 242 direction to calculate the true magnetically westward component. Such a procedure in-
 243 troduces relatively small errors for the predominantly magnetic westward SAPS direc-
 244 tion at subauroral altitudes; cf. Erickson et al. (2002). To reduce the errors induced by
 245 range discrepancies, we used measurements only in the F region between 300 km and 550
 246 km to extract the SAPS signature. (3) SAPS identification: SAPS was identified as a
 247 local peak westward flow that locates below the equatorward auroral boundary, or al-
 248 ternately identified as an inflection point enhancement on the equatorward slope of the
 249 convection cell in the dusk sector. The magnitude of SAPS peak velocity was required
 250 to be ≥ 100 m/s. On occasion, an associated main ionospheric trough of Ne depletion
 251 was used as auxiliary information to help specify SAPS location if the first flow crite-
 252 rion was met. As an example, Figure 1 shows two identified SAPS events in the dusk
 253 and midnight sector, respectively. The left panels show the line-of-sight velocities for a
 254 full azimuth scan and the fitted auroral equatorward boundary in the MLT-MLAT co-
 255 ordinates. The right panels show the latitudinal variation of the F-region plasma zonal
 256 velocities and Ne profiles. SAPS location can be visually identified from the 2D/1D ve-
 257 locity enhancement or inflection point as well as Ne depletion. Following these guide-
 258 lines, we generated a final data set of more than 1,500 scans containing SAPS out of $\sim 15,000$
 259 separate azimuth scans available from Millstone Hill during 1979–2019.

260 3 Results and Discussion

261 Figure 2a shows the temporal coverage and solar cycle variation of the constructed
 262 SAPS data set. In general, there were more SAPS events around solar maximum and
 263 declining phases than solar minimum. This could be partially due to the fact that ge-
 264 omagnetic activity is often increased during these periods. In particular, coronal mass
 265 ejection events occur more frequently in high solar activity years and recurrent geomag-
 266 netic activity associated with high speed streams occurs more frequently in the declin-
 267 ing phase of solar cycle. However, this yearly variation could also be largely impacted
 268 by the availability of original azimuth scan database that is shown in Figure 2c. We note
 269 that Millstone Hill experiments are often triggered due to prompt geomagnetic activity
 270 indications and thus are not randomly distributed in a synoptic manner with respect to
 271 time. Moreover, the measurement composition of different scan modes within each ex-
 272 periment is also highly variable. Only the fraction of Millstone Hill wide coverage az-
 273 imuth scans with low elevation are appropriate for deriving SAPS. These factors are par-
 274 tially responsible for the uneven distribution of SAPS data set.

275 Figure 2b and 2d display the seasonal variation of the constructed SAPS data set
 276 and original azimuth scan numbers, respectively. The percentage distribution of SAPS
 277 occurrence was also given. In order to evaluate the possible biases due to uneven data
 278 coverage, the results of our experiments can be approximately considered as a Binomial
 279 distribution, which describes the discrete probability distribution of the number of suc-

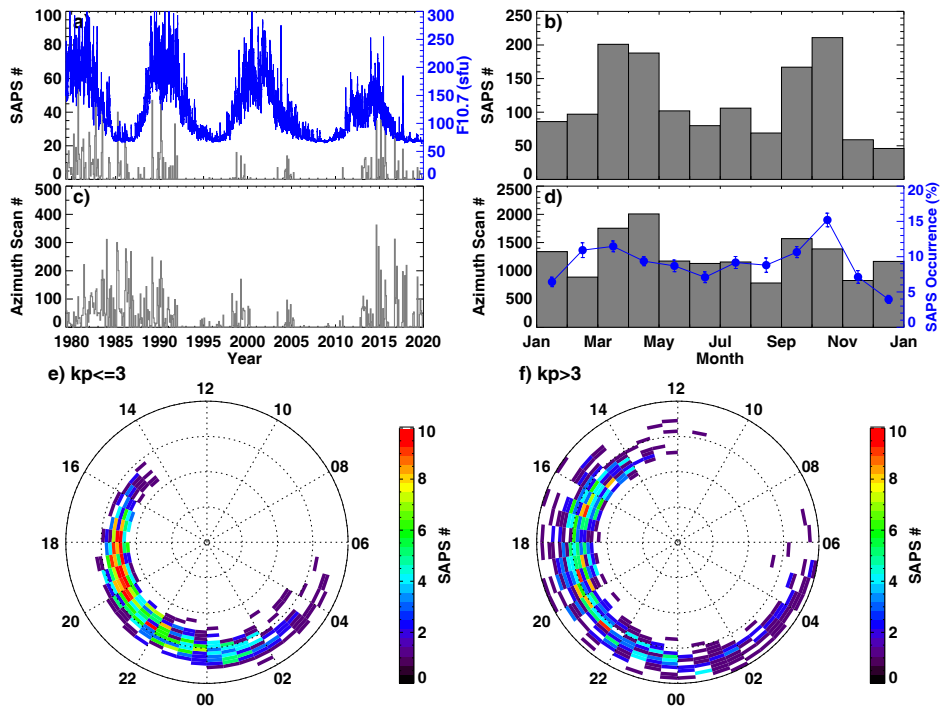


Figure 2. (a and b) Solar cycle and seasonal variation of the constructed SAPS data set. The temporal variation of $F10.7$ index is also plotted. (c and d) Solar cycle and seasonal distribution of the total database of wide coverage azimuth scan for detecting SAPS. The seasonal variation of SAPS occurrence rate is also shown in panel d. (e and f) Distribution of the constructed SAPS data set in the coordinates of magnetic local time and geomagnetic latitude under quiet ($K_p \leq 3$) and active ($K_p > 3$) geomagnetic conditions. The concentric circles are plotted in 10° interval with outermost one representing 50° MLAT.

280 cesses in a sequence of independent experiments. Thus, the uncertainty can be estimated
281 as follows:

$$\sigma = \sqrt{\frac{f \times (1 - f)}{N - 1}}, \quad (1)$$

282 where σ is the uncertainty, f is the occurrence rate, and N is the total number of az-
283 imuth scans for each given month. The seasonal variation of SAPS occurrence rate is be-
284 tween 5%–15% with two peaks occurring around the equinoxes that are barely affected
285 by the uncertainties. This could possibly relate to the Russell-McPherron effect that equino-
286 cial periods have increased geomagnetic activity with a higher-than-average IMF south-
287 ward component (Russell & McPherron, 1973). This seasonal pattern is consistent with
288 previous results (e.g., Karlsson et al., 1998; He et al., 2014), and we will further inves-
289 tigate the seasonal and solar cycle dependence of SAPS in the following subsections.

290 Figures 2e and 2f show the polar distribution of the SAPS data set in the MLT-
291 MLAT coordinates with a resolution of $0.5 \text{ hr} \times 1^\circ$ under quiet and active geomagnetic
292 conditions, respectively. Some typical characteristics of latitude, local time, and geomag-
293 netic preferences of SAPS can be summarized as: (1) SAPS peak tends to locate at the
294 equatorward auroral boundary around $60\text{--}65^\circ$ MLAT in the dusk, and gradually decreases
295 with increasing MLT; (2) SAPS has higher occurrence around dusk time than night time;
296 (3) SAPS peak location is mainly confined within 14–05 MLT during quiet time, with
297 elongation into both earlier and later MLTs as well as equatorward motion with enhanced
298 geomagnetic activity.

299 To proceed with statistical studies, we performed a superposed epoch analysis (SEA)
300 that is similar to those described in H. Wang et al. (2011) and H. Wang and Lühr (2013).
301 The MLAT of SAPS peak velocity was taken as the central point, around which the lat-
302 itudinal profiles of different plasma parameters (velocity, N_e , T_i , T_e) were stacked. The
303 average profiles were subsequently calculated, ranging from -10° to 10° off the SAPS peak
304 with a resolution of 0.5° . This method has the goal of investigating the relationship be-
305 tween these parameters as well as their variation patterns with respect to MLT, season,
306 geomagnetic activity, solar activity, and IMF orientation, respectively. Results are de-
307 scribed in following subsections.

308 3.1 Magnetic Local Time Variation

309 Figures 3a and 3b show the averaged Δ MLAT distribution of zonal plasma veloc-
310 ity derived from the superposed epoch analysis for different MLTs in 2-D and 1-D for-
311 mats, respectively. The specific values of SAPS-related plasma parameters are listed in
312 Table 1. In general, SAPS peak flows during different MLTs occur around central MLAT
313 of 0 as expected. However, there is a large difference between SAPS features in the dusk
314 ($17\text{--}21$ MLT) and midnight ($22\text{--}02$ MLT) sectors: the dusk-time SAPS channel has a higher
315 peak velocity (-728.3 m/s) and a broader latitudinal width ($\geq 5^\circ$), with the averaged
316 MLAT offsets of the equatorward auroral boundary being 3.1° . On the other hand, the
317 midnight SAPS channel is more tightly clustered with considerable reduction in width
318 by a factor of two, and the averaged MLAT offsets of the equatorward auroral bound-
319 ary, determined separately from DMSP observations, is 2.8° . The midnight SAPS peak
320 velocity (-373.5 m/s) is barely half of the dusk amplitude, and is approximately equal
321 to the average eastward corotation velocity at subauroral latitudes. These results sug-
322 gest that dusktime SAPS flow could overwhelm the corotation effect and transport iono-
323 spheric plasma both sunward and poleward to earlier MLTs, contributing to the forma-
324 tion of storm-enhanced density plumes (Foster, 1993; Kelley et al., 2004), also known as
325 the dusk effect (Mendillo, 2006). On the other hand, nighttime SAPS tends to counter-
326 act the corotation flow, and keeps plasma at a constant location in the inertial Sun-Earth
327 reference frame (constant MLT). This dusk-midnight difference of SAPS magnitude and

328 width is consistent with previous studies (Foster & Vo, 2002; Anderson, 2004; Erickson
329 et al., 2011; Kunduri et al., 2017).

330 Figure 3c and Figure 3d show the Δ MLAT-MLT distribution of electron density
331 associated with SAPS in 2-D and 1-D formats, respectively. Figure 3e shows the rela-
332 tive deviation of electron density with respect to its background values, obtained through
333 a eleven-point ($\sim 5^\circ$) smoothing average. It is known that the enhanced ion-neutral fric-
334 tional heating associated with SAPS will accelerate nonlinear ion loss processes and thus
335 facilitate formation of the midlatitude trough (Schunk et al., 1976; Rodger, 2008). How-
336 ever, we note in particular that the deepest trough occurs in the postmidnight sector around
337 00–02 MLT as can be seen from Figure 3c. The line plots in Figure 3e and Table 1 also
338 show that the midnight trough has more severe depletion (-20.7%) compared with that
339 of the dusktime trough (-16.4%). Previous results in the literature are contradictory
340 about the local time when the deepest trough are observed. For example, Tulunay and
341 Sayers (1971) reported that the deepest trough at the height of 550 km occurs near mid-
342 night by using Ariel 3 satellite data. Prölss (2007) reported that the largest electron den-
343 sity drops at the height of 350 km were observed around 18 MLT by using Dynamics Ex-
344 plorer 2 data, though this study only analyzed the trough events during 15–21 MLT. In
345 addition, Karpachev (2003) found that the northern hemisphere trough during winter
346 non-storm time ($Kp \leq 3$) in the 30–60°W longitudinal sector is slightly deeper in 18–19 LT
347 than 23–01 LT by using Cosmos satellite data at 500 km. These conflicting results may
348 be due to different spatial/temporal coverage and different criteria in identifying troughs,
349 and more future work is needed to address this problem further.

350 In results here, we report that the SAPS-related midlatitude trough at 300–550 km
351 altitude has more pronounced depletion in the postmidnight sector. Although based on
352 a specific subset of midlatitude trough events, this phenomenon is in agreement with that
353 indicated in Aa et al. (2020) in that the midlatitude trough in the Northern Hemisphere

Table 1. SAPS peak amplitude and associated plasma parameters for different MLTs, seasons, geomagnetic activity, solar activity, and IMF configurations. The Δ MLAT locations of equatorial auroral boundary (EAB) are shown in the rightmost column.

	Velocity (m/s)	Ne ($10^{11}/\text{m}^3$)		Ti (K)		Te (K)		EAB
	Peak	Peak	Δ Ne	Peak	Δ Ti	Peak	Δ Te	Δ MLAT
Dusk	-728.3	3.28	-16.4%	1595	4.9% (75)	2143	1.9% (42)	3.1°
Midnight	-373.5	2.82	-20.7%	1478	8.0% (110)	1780	5.2% (85)	2.8°
Dec Sol.	-549.1	1.79	-9.1%	1490	5.1% (72)	1976	6.1% (114)	3.3°
Equinox	-576.4	1.65	-20.9%	1603	6.1% (92)	2020	3.3% (65)	3.0°
Jun Sol.	-512.5	1.73	-13.2%	1518	4.2% (62)	2322	2.7% (61)	3.9°
kp ≤ 3	-444.9	1.84	-14.1%	1472	3.7% (53)	1875	1.6% (30)	3.5°
kp > 3	-672.4	1.56	-18.9%	1649	7.1% (109)	2220	3.4% (73)	2.9°
$F_{10.7 \leq 150}$	-630.1	1.20	-16.5%	1541	8.5% (120)	2038	2.4% (48)	3.2°
$F_{10.7 > 150}$	-513.1	2.04	15.7%	1564	4.1% (62)	2014	2.7% (53)	3.4°
+By, +Bz	-554.6	1.70	-13.0%	1462	3.3% (47)	2057	2.3% (46)	3.1°
+By, -Bz	-618.8	1.72	-14.9%	1501	5.5% (78)	2116	4.0% (81)	3.0°
-By, +Bz	-575.7	2.03	-15.2%	1488	2.9% (42)	1797	2.3% (40)	3.2°
-By, -Bz	-716.1	2.12	-15.8%	1545	2.0% (30)	2041	2.0% (40)	3.0°

usually exhibits a higher occurrence rate in the postmidnight sector than that of the evening sector. One possible explanation for this result is that the midnight plasma flow around SAPS region is significantly lower than that of dusktime, providing sufficient time for recombination to produce a deeper depletion (Voiculescu & Nygrén, 2007). Around this local time, a convection flow configuration, referred to as the Harang reversal, is often observed, which is a result of the overlap between the Region-2 upward and downward FACs (e.g., Zou, Lyons, Wang, et al., 2009; Zou, Lyons, Nicolls, et al., 2009; Gkioulidou et al., 2009). The high-latitude return flows bifurcate at 01-02 MLT and thus the flow stagnation point between the high-latitude convection and corotation extends to this local time as well.

Figures 3f–3h and Figures 3i–3k show the MLT variation of ion temperature and electron temperature associated with SAPS, respectively. Both the ion and electron temperatures exhibit moderate enhancement around SAPS region compared to the background trend. This is consistent with observations from the Dynamics Explorer-2 satellite which show that ion and electron temperature within SAPS-related troughs will be strongly elevated (Moffett et al., 1998). The temperature increment is larger in the midnight sector (T_i : 8.0% (~ 110 K) and T_e : 5.2% (~ 85 K)) than that in the dusk sector (T_i : 4.9% (~ 75 K) and T_e : 1.9% (~ 42 K)). The temperature enhancement are inversely proportional to the electron density decrease within the trough. However, there might be a large altitudinal gradient of the ion temperature since H. Wang and Lühr (2013) reported that the ion temperature around SAPS region at 800 km was reduced $\sim 30\%$. Heelis et al. (1993) found that frictional heating can quickly increase the ion temperature to a constant level over a broad altitudinal region between 300 km and 500 km, which is approximately consistent with the current range of Millstone Hill radar measurements. This result also indicates that a new thermal equilibrium between ions and neutrals can be effectively attained. At higher altitudes above 600 km, however, it takes much longer time to increase the ion temperature to a new equilibrium since ion-neutral collisions are much smaller and not as effective at thermal transfer as at lower altitudes. Furthermore, enhanced ion temperature and frictional heating at lower altitudes will result in a large vertical pressure gradient and cause thermal expansion and plasma upward flow. Thus, compared with lower altitudes, frictional heating is less efficient in the topside ionosphere. For these reasons, H. Wang and Lühr (2013) proposed a mechanism in which ion temperature at 800 km is more likely to initially respond to adiabatic cooling associated with plasma expansion from lower altitudes. However, as time progresses, it is expected that thermal conduction and local frictional heating would eventually increase the topside ion temperature in this scenario. Future work is still needed to further study SAPS-related ion temperature variation in the topside ionosphere.

In general, electron temperature in the ionosphere is also determined by the thermal balance between heating and cooling processes. Besides daytime photoelectron heating by solar extreme ultraviolet radiation, it is known that the downward energy and heat transfer from the ring current along magnetic field lines during geomagnetically disturbed periods will cause a subauroral electron temperature enhancement, which usually occurs in association with the midlatitude trough in the nighttime topside ionosphere (e.g., Evans, 1970; Kozyra et al., 1986; Watanabe et al., 1989; Fok, Kozyra, Warren, & Brace, 1991; Afonin et al., 1997; Prölss, 2006; W. Wang et al., 2006). Furthermore, Coulomb collisions with ions provide an important energy loss mechanism for topside ionospheric electrons (Schunk & Nagy, 2000). In the SAPS region, characterized by intense heating and ion upwelling during storm time, energy exchange between the electrons and ions forms the primary cooling processes for thermal electrons in the $F2$ layer. Lower electron density will therefore tend to result in higher electron temperatures because of the greater thermal energy available per particle, and the cooling process will be less efficient due to reduced Coulomb coupling with ions (Schunk & Nagy, 1978; Moffett & Quegan, 1983). Taken in aggregate, the relative enhancement of electron temperature in the SAPS region will therefore be more pronounced around midnight due to more profound trough

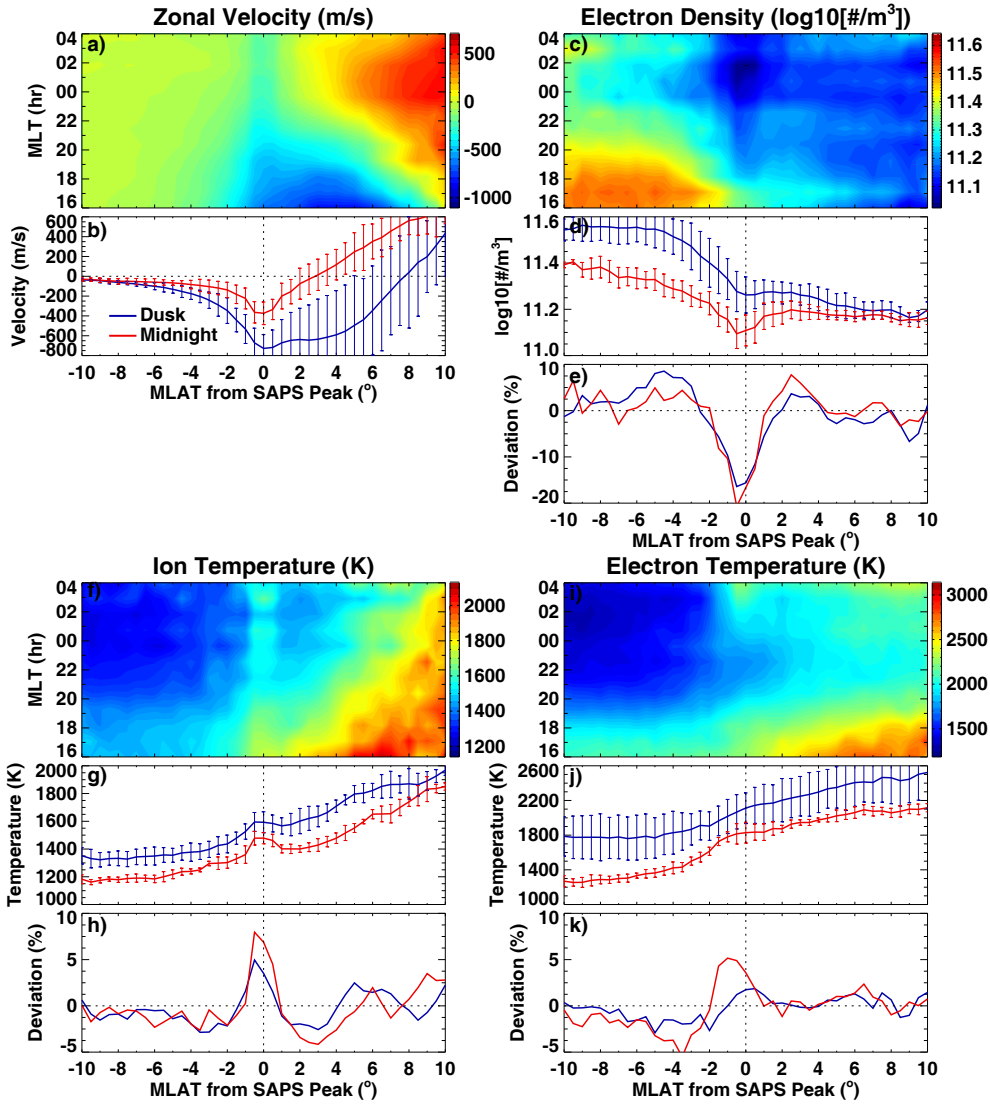


Figure 3. Local time variation of the superposed epoch analysis of SAPS related plasma parameters: zonal plasma velocity (a and b), electron density (c–e), ion temperature (f–h), and electron temperature (i–k), respectively. The key MLAT of “0” represents the location of SAPS peak velocity. The top and middle panels of each group are the 2-D and 1-D distribution. The bottom panels of each group show the percentile deviation of N_e , T_i , and T_e with respect to background values, respectively. The blue lines represent the variation patterns around the dusk (17–21 MLT), and the red lines represent those around the midnight (22–02 MLT). The exact amplitudes are recorded in Table 1.

depletion than that occurring in dusk sectors. This Te - Ne correlation associated with SAPS will be further addressed later.

3.2 Seasonal Variation

Figures 4a–4b and 4c–4e display the averaged Δ MLAT distribution of SAPS-related plasma velocity and electron density for different seasons in 2-D and 1-D formats, respectively. There is a slight winter-summer asymmetry in that the SAPS peak velocity has larger values in winter than summer, with the exact values being recorded in Table 1. Many studies have found that the SAPS velocity is inversely proportional to the flux-tube integrated Pedersen conductivity in the subauroral region, which is primarily controlled by solar illumination (e.g., Zheng et al., 2008; He et al., 2014; Yu et al., 2015). Thus, the smaller conductivity in winter due to insufficient illumination will lead to an enhanced SAPS electric field and flow velocity to maintain the subauroral current continuity. This seasonal asymmetry is also reported in previous studies (e.g., Koustov et al., 2006; H. Wang et al., 2012; H. Wang & Lühr, 2013). However, it is worth noting that this seasonal difference is within uncertainty levels (~ 100 – 200 m/s) for this study, and it could also be affected by uneven data distribution and variation of solar flux. Future simulation work is still needed to further specify this issue.

The SAPS peak velocity is slightly larger around equinoctial months than local winter, though the difference is quite small (~ 30 m/s). The SAPS-related midlatitude trough also exhibits relatively larger depletion around equinoxes (-20.9%) than December solstice (-9.1%). Karlsson et al. (1998) found that the strength of the subauroral electric field has maximum values close to the equinoxes and minimum values around the summer solstice. He et al. (2014) also found that SAID events can be more frequently observed during equinoxes than solstices. This feature may be related to enhanced geomagnetic activity and ionospheric convection flow around equinoxes. In particular, equinoctial periods have increased solar wind driving conditions with a higher-than-average IMF southward component (Russell & McPherron, 1973), and field-aligned ionospheric conductivity is relatively low when the nightside auroral zones of both hemispheres are simultaneously in the darkness around equinoxes (Lyatsky et al., 2001). Both effects will result in an enhanced SAPS velocity with more substantial frictional heating and deeper trough structure. This phenomenon is also consistent with that indicated in Aa et al. (2020), in that the nighttime midlatitude trough has a higher occurrence rate around equinoxes than local winter.

Figures 4f–4h and 4i–4k show the averaged Δ MLAT distribution of SAPS-related ion and electron temperature for different seasons, respectively. For ion temperature, the relative deviation (~ 4 – 6%) is almost seasonally independent. For electron temperature, on the other hand, the SAPS-related enhancement in the December solstice is 6.1% (114 K), while the temperature enhancement during equinoxes is 3.3% (65 K) and is almost negligible in the June solstice. As the background temperature during June solstice is higher than other seasons, relative increase in temperature for the same amount of energy input will likely to be lower. Our results are contextually consistent with previous studies. Evans (1973) found that the seasonal variation of the heat flux flow into the ionosphere from the plasmasphere can reach an order of magnitude, and the lowest heat fluxes occur in summer and highest fluxes in winter. Similarly, Fok, Kozyra, Warren, and Brace (1991) quantitatively confirmed that the downward electron heat flux from the plasmasphere in winter is comparable to magnetospheric heat flux and is larger than during other seasons. Besides heating sources from the magnetosphere, Richards and Torr (1986) indicated that there is a strong inter-hemispheric thermal coupling between conjugate ionospheres at midlatitude, and solar illumination in the sunlit summer hemisphere can make a considerable contribution to heat the conjugate winter hemisphere immediately. All of the mechanisms above can result in a larger increase of electron temperature in winter than in the absence of a sunlit conjugate region.

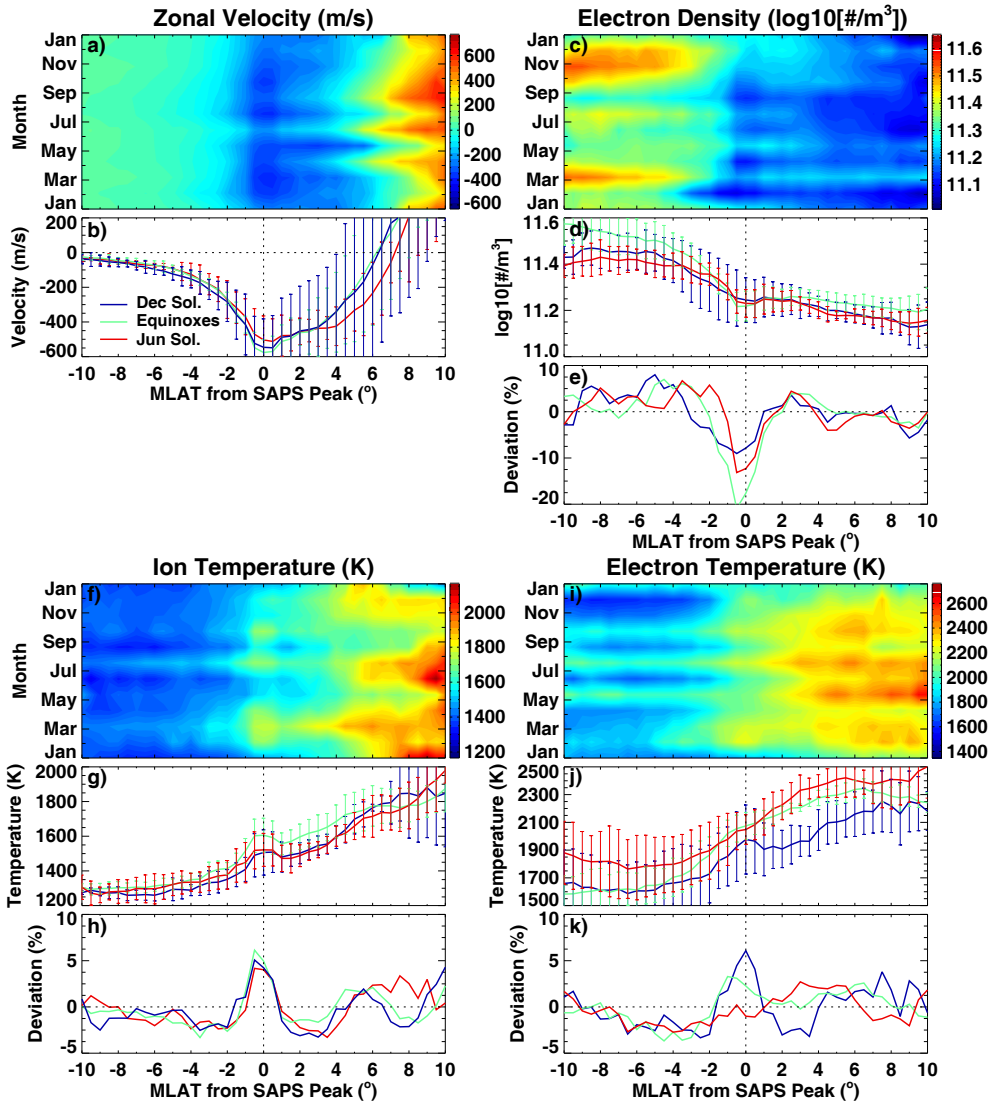


Figure 4. The same as Figure 3, but for seasonal variation. The blue, green, and red lines represent the variation pattern around December solstice (November, December, January, and February), equinoxes (March, April, September, and October), and June solstices (May, June, July, and August), respectively.

3.3 Geomagnetic Activity Dependence

Figures 5a–5b and 5c–5e display the averaged Δ MLAT variation of SAPS-related plasma velocity and electron density for different geomagnetic activity levels, respectively. Many previous studies have indicated that both SAPS velocity and associated ion vertical flow velocity will increase with respect to increasing geomagnetic activity (e.g., Foster & Vo, 2002; Erickson et al., 2011; H. Wang & Lühr, 2013; Kunduri et al., 2017), and the midlatitude trough becomes deeper with increasing geomagnetic activity (e.g., Collis & Haggstrom, 1988; Karpachev et al., 1996; Werner & Prölss, 1997; Prölss, 2007; Aa et al., 2020). In the current study, the blue lines represent the quiet time variation pattern with $K_p \leq 3$, while the red lines represent disturbed geomagnetic conditions with $K_p > 3$. It can be seen from both Figure 4 and Table 1 that the disturbed conditions are associated with higher SAPS peak velocity (-672.4 m/s) and deeper trough depletion (-18.9%) than quiet time conditions (-444.9 m/s and -14.1%), respectively. This again confirmed that the increased frictional heating and expansion within the stormtime SAPS region would accelerate the recombination rate and the trough formation.

Figures 5f–5h and 5i–5k show the averaged Δ MLAT distribution of SAPS-related ion and electron temperatures for different geomagnetic activity levels, respectively. Both the ion and electron temperatures exhibit larger enhancement around SAPS region during disturbed geomagnetic conditions that are almost two times of temperature enhancements during quiet conditions. This feature is consistent with that indicated in previous studies (Kozyra et al., 1986; Fok, Kozyra, Warren, & Brace, 1991; Moffett et al., 1998; Prölss, 2006).

3.4 Solar Activity Dependence

Figures 6a–6b and Figures 6c–6e show the averaged Δ MLAT variation of SAPS-related plasma velocity and electron density for different solar activity levels, respectively. The blue lines represent the variation pattern during low solar activity periods ($F_{10.7} \leq 150$), while the red lines represent those during high solar activity periods ($F_{10.7} > 150$). It can be seen that SAPS has a larger peak value (-630.1 m/s) around low solar activity periods than that around high solar activity periods (-513.1 m/s). This negative correlation between SAPS flow and solar activity is reasonable, as Robinson and Vondrak (1984) and Hardy et al. (1987) indicated that the contribution to the height-integrated ionospheric Pedersen conductivity from solar radiation approximately equals to $0.88\sqrt{F_{10.7}\cos\chi}$, where χ is the solar zenith angle. Thus, the weaker Pedersen conductivity around solar minimum will naturally lead to an increased SAPS electric field and flow velocity, as well as an enhanced ion vertical flow. In addition, the co-rotating interaction region during the declining phase of a solar cycle could induce persistent geomagnetic perturbations. This makes the low solar activity years constitute a large number of SAPS events with medium to high level K_p values, which also helps to maintain the SAPS magnitude at a high level statistically.

Moreover, He et al. (2014) indicated that the narrow SAID channel moves equatorward during high solar activity periods. This is in agreement with that mentioned in Le et al. (2017) and Karpachev (2019) that the position of midlatitude trough will move slightly equatorward from low solar activity to high solar activity periods. In our results, the SAPS-related midlatitude trough exhibits almost identical percentile depletion among low and high solar activity periods. Figure 6e shows that the background electron density in high solar activity periods is nearly two times of that in low solar activity, because the enhanced solar extreme ultraviolet radiation associated with higher $F_{10.7}$ will increase the ionization production rate. Thus, it can be deduced that the trough depth, which equals to the product of background density times percentile deviation, should be more significant in high solar activity periods. This is consistent with that mentioned in Aa et al. (2020).

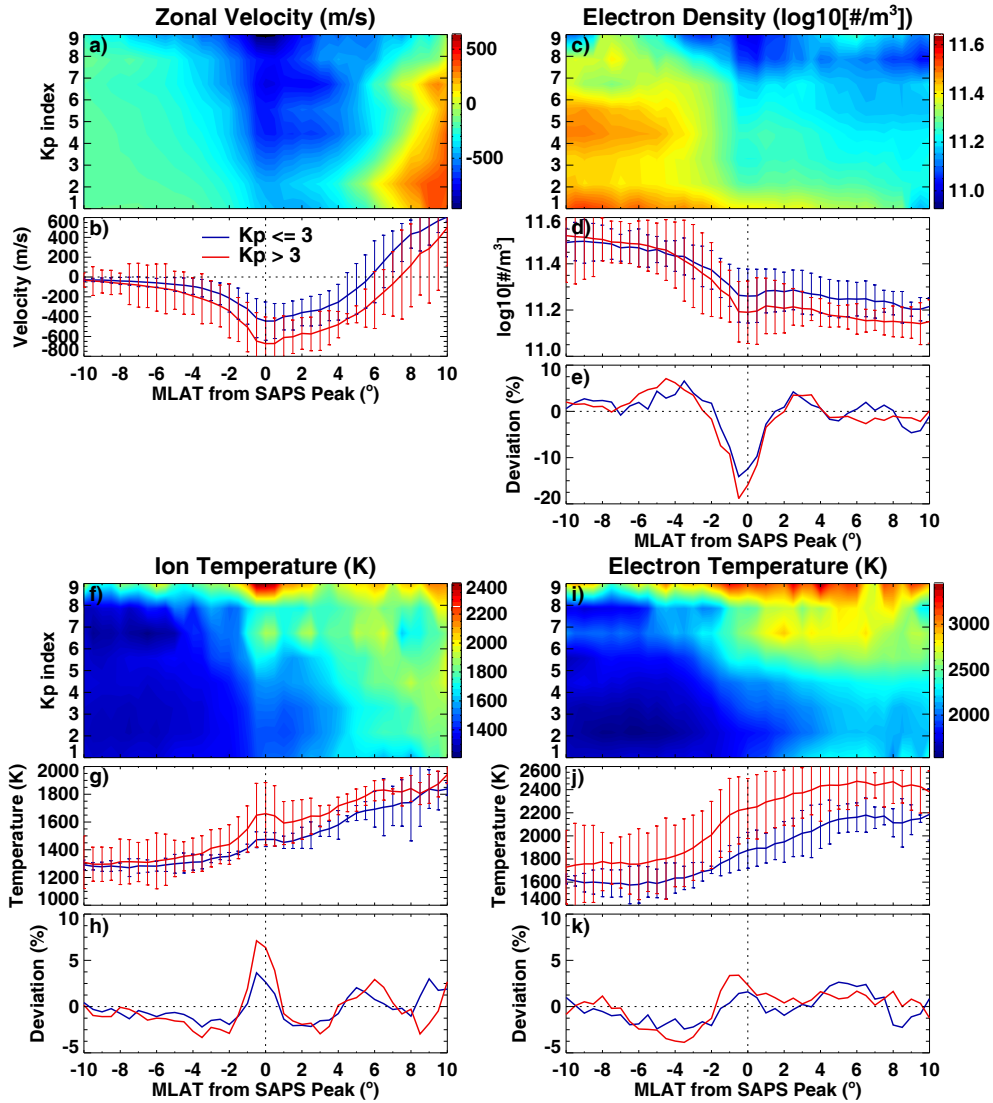


Figure 5. The same as Figure 3, but for different geomagnetic activities. The blue lines represent the variation pattern for $K_p \leq 3$, while the red lines represent those for $K_p > 3$.

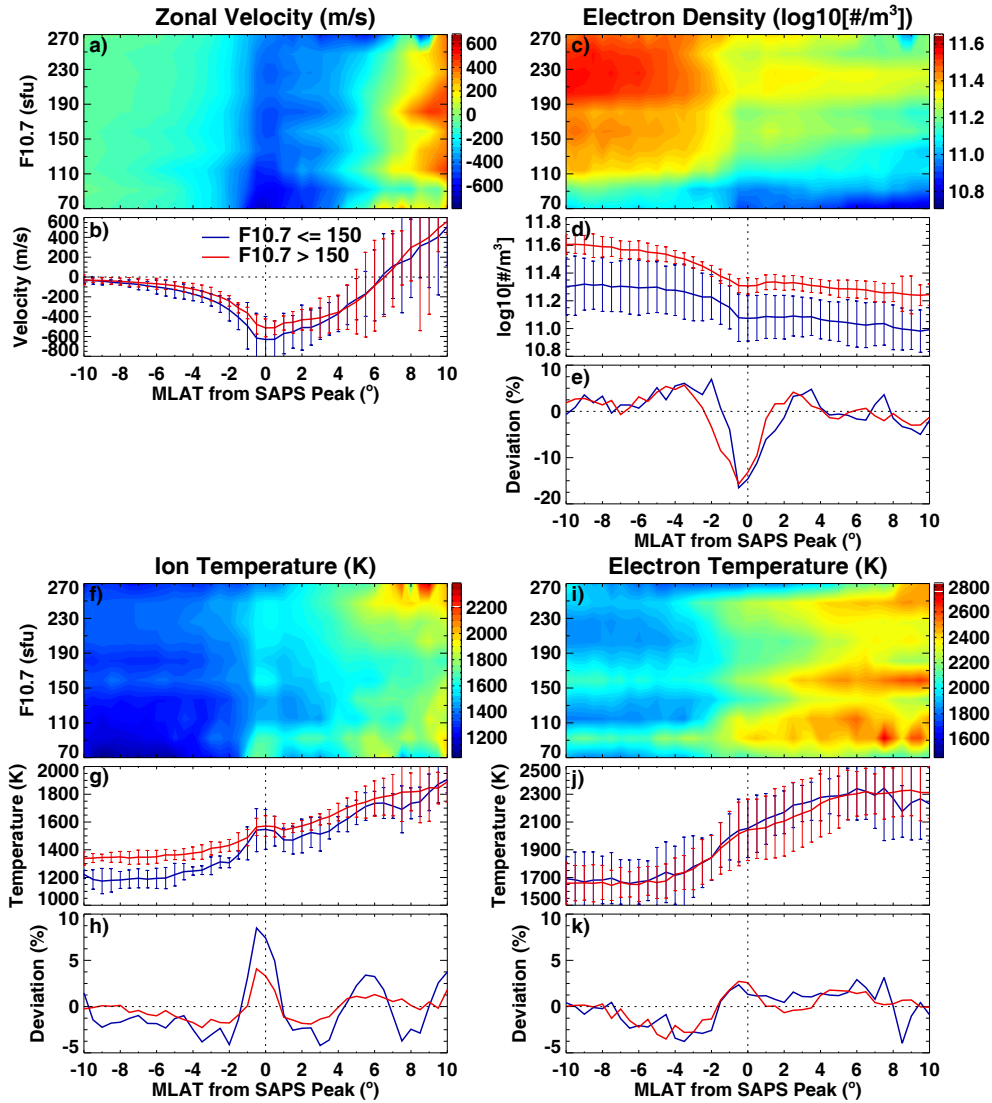


Figure 6. The same as Figure 3, but for different solar activities. The blue lines represent the variation pattern for $F_{10.7} \leq 150$, while the red lines represent those for $F_{10.7} > 150$.

511 Figures 6f–6h and 6i–6k show the averaged Δ MLAT variation of SAPS-related ion
 512 and electron temperature for different solar activity levels, respectively. For ion temper-
 513 ature, low solar activity results exhibit larger enhancement associated with SAPS com-
 514 pared with those during high solar activity periods, which is similar to the plasma flow
 515 results. It is important to note that frictional heating depends on both ion-neutral ve-
 516 locity difference and ion density, and therefore the detailed solar cycle variation of SAPS-
 517 related T_i and its inter-relationship with frictional heating and electron density might
 518 be complicated and involve both ionospheric and thermospheric conditions. Specific sim-
 519 ulations are needed to further address this issue in the future. For electron temperature,
 520 the absolute values and the relative enhancements between low and high solar activity
 521 periods in our results are approximately the same. This is consistent with observation
 522 results from Fok, Kozyra, and Brace (1991) and simulation results from Kozyra et al.
 523 (1990), both of which indicated that magnetospheric heat flux and electron densities both
 524 vary by an order of magnitude between solar maximum and minimum. For a given level
 525 of magnetic activity, the net result is to maintain similar electron temperature enhance-
 526 ments within the solar cycle.

527 3.5 Interplanetary Magnetic Field Dependence

528 Figures 7a–7b show the averaged Δ MLAT variation of SAPS-related zonal plasma
 529 velocity in 2-D and 1-D formats for different IMF clock angles in the solar wind. We note
 530 that the IMF data used for clock angle derivation was from OMNI datasets at 1 AU with
 531 time shifting to the nose of the Earth's bow shock. The clock angle was estimated based
 532 on 1-hour interval IMF data. It can be seen that both SAPS flow and ion vertical flow
 533 are much stronger when the IMF clock angle is between -180° and -90° (i.e., negative
 534 B_y and negative B_z). For IMF B_z dependence, other studies indicate that SAPS will
 535 move equatorward with a larger magnitude when IMF B_z becomes stronger southward,
 536 a condition often associated with enhanced geomagnetic activity and extended convec-
 537 tion pattern (Horvath & Lovell, 2016; Lin et al., 2019). For IMF B_y dependence, it is
 538 known that the main effect of B_y is to change the shape and orientation of the two-cell
 539 convection pattern, in particular when B_z is negative (Heelis, 1984; Heppner & Maynard,
 540 1987; Weimer, 1995). In the Northern Hemisphere, the dusk cell is more crescent-shaped
 541 for negative B_y and more round for positive B_y , while the dependence of the dawn cell
 542 is the reverse (Ruohoniemi & Greenwald, 1996, 2005). Therefore, under the condition
 543 of negative B_y and negative B_z , the sunward returning flow in the vicinity of the whole
 544 evening–midnight sector is predominantly westward since it is dominated by the more
 545 crescent-shaped dusk cell. This background trend will facilitate SAPS formation and iden-
 546 tification through higher westward speed over wider MLT regions, similar to a “down-
 547 stream acceleration” process. On the contrary, if B_y is positive, the background convec-
 548 tion flow around midnight is predominantly eastward, and the neutral wind flow pattern
 549 will also be influenced with a strong eastward zonal wind at subauroral latitudes (McCormac
 550 et al., 1985; Thayer et al., 1987). This neutral wind friction tends to prevent sunward
 551 plasma flow from gaining high velocity, similar to an “upstream acceleration” process.
 552 Thus, our results of the SAPS dependence on IMF are understandable. Moreover, there
 553 is a hemispheric asymmetry of B_y effects on the convection pattern in the Southern Hemi-
 554 sphere (Papitashvili et al., 1994; Leonard et al., 1995), which means that the condition
 555 for strong SAPS flow should be more favored with positive B_y and negative B_z . This
 556 point is partially supported by the results given by Karlsson et al. (1998) that the strongest
 557 poleward electric fields associated with SAPS are seen exclusively for negative B_y in the
 558 Northern Hemisphere and positive B_y in the Southern Hemisphere.

559 Figures 7c–7e show the averaged Δ MLAT variation of SAPS-related electron density
 560 for different IMF clock angles in the solar wind. It can be seen that the deepest trough
 561 occurs around $\pm 180^\circ$ of southward IMF. This is expected, since it is reported that the
 562 trough depth will increase with increasing geomagnetic activity due to enhanced disso-
 563 ciative recombination associated with strong frictional heating within SAPS (e.g., Col-

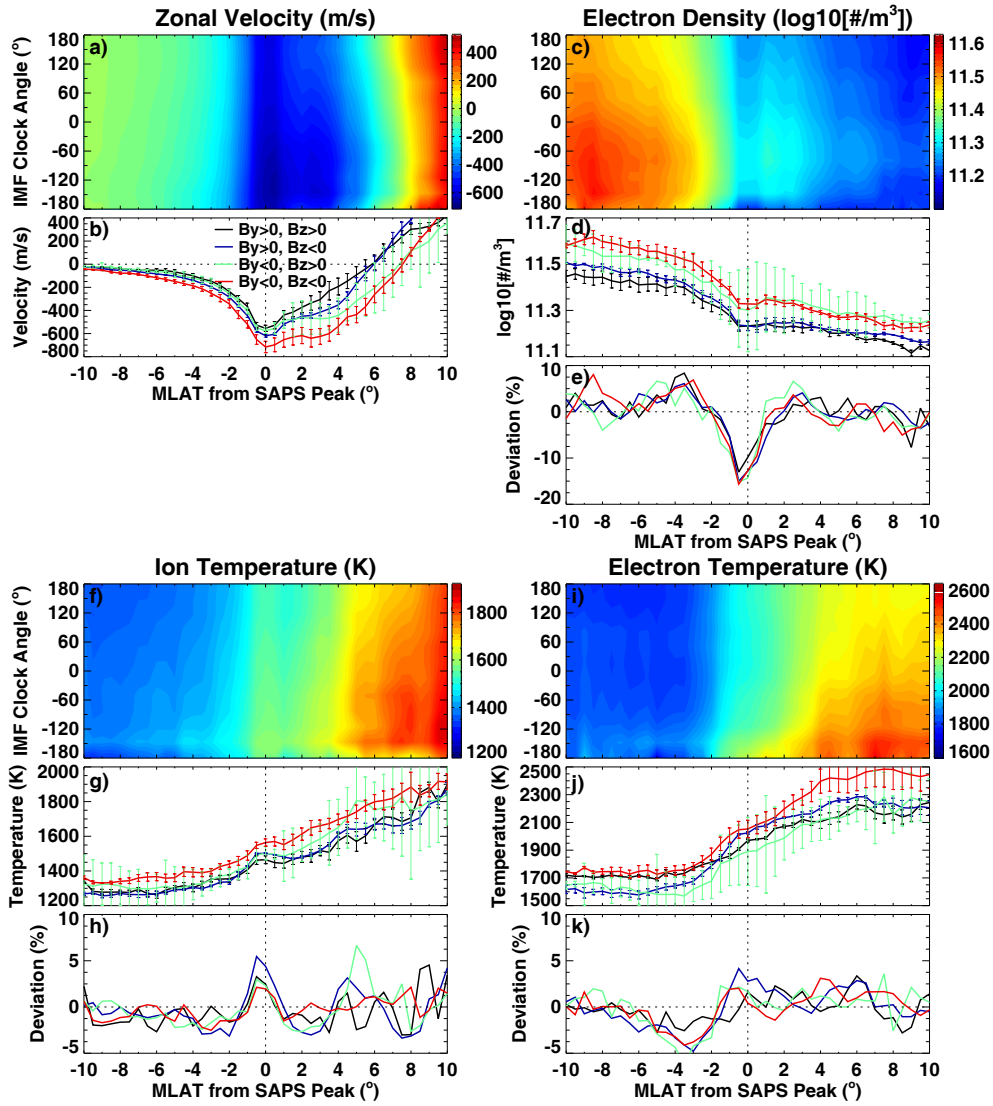


Figure 7. The same as Figure 3, but for different interplanetary magnetic field (IMF) clock angles. In the 1-D plot, four different orientation of IMF B_y and B_z components are shown by different combinations of colors and line styles.

lis & Haggstrom, 1988; Karpachev et al., 1996; Prölss, 2007; Aa et al., 2020). Moreover, the relative deviation of Ne is slightly larger under negative By and negative Bz than other conditions, which is similar to the SAPS distribution reported here. Another point worth noting is that the overall level of electron density is generally lower with positive By and is higher with negative By . One possible explanation is related with the thermosphere wind circulation patterns through collisional interactions with the convecting ions. As mentioned above, the thermosphere wind circulation pattern at mid-to-high latitudes also has an IMF dependence similar to ions: specifically, for positive (negative) By , the size of the dusk (dawn) circulation cell and its neutral wind speed will increase (e.g., McCormac et al., 1985; Thayer et al., 1987; Hernandez et al., 1991; Richmond et al., 2003). Furthermore, around the midnight sector in the Northern Hemisphere, a strong and positive By will cause stronger eastward zonal wind at high latitudes as well as stronger equatorward winds at lower latitudes due to clockwise diversion driven by Coriolis force, which will amplify the stormtime equatorward surge of thermospheric meridional wind and lead to an equatorward progression of neutral disturbances with reduction of O/N_2 ratio, causing the background electron density to decrease (Rees et al., 1986; Immel et al., 1997; L. Goncharenko et al., 2006; Förster et al., 2008). On the other hand, ion drag is a significant force for modifying neutral winds in the low density region around SAPS (Ferdousi et al., 2019), and enhanced westward neutral wind was found to peak around the same latitude as SAPS flow (H. Wang et al., 2011, 2012). The Coriolis force on the westward wind drives a poleward wind disturbance and can sometimes establish a poleward wind to prevent the storm time equatorward surge (S.-R. Zhang et al., 2015), thus raising the O/N_2 ratio and background electron density. This condition will be more favored with larger SAPS under negative By as mentioned before.

Figures 7f–7h and 7i–7k show the averaged $\Delta MLAT$ variation of SAPS-related ion and electron temperature for different IMF clock angles, respectively. Similar to the plasma velocity, both ion and electron temperature have generally larger values when the IMF clock angle is between -180° and -90° though their relative deviation fluctuates between 40–80 K exhibiting no clear IMF dependence. S.-R. Zhang et al. (2016) analyzed the long-term cooling trends of ionospheric ion temperature at Sondrestrom and found that more negative Bz corresponds to Ti reduction in the topside ionosphere during nighttime, possibly due to adiabatic cooling. This may partially inhibit the Ti enhancement effect associated with stronger geomagnetic activity though further study is still needed to quantify the relative contribution of this mechanism.

3.6 Joint heat flow analysis of SAPS region Ne and Te

A joint analysis of the combined quantity $Ne \times Te$ is important in understanding the characteristics of heat flow around the SAPS region. It is known that in the F region and topside ionosphere, the thermal electron heating rate is proportional to thermal electron densities, while the dominant electron cooling process is Coulomb collisions with ambient ions, with a cooling rate proportional to Ne^2 (and the difference between Te and Ti) (Schunk & Nagy, 1978). Thus, many studies have reported negatively correlated Ne and Te relationships under a quasi-steady state of thermal equilibrium (e.g., S.-R. Zhang & Holt, 2004; S.-R. Zhang et al., 2004), with the heat content term of $Ne \times Te$ likely related to $1/Ne$. Figure 8 shows a scatter plot comparison between $Ne \times Te$ and $1/Ne$ from our study with very good correlation ($R=-0.93$). Results indicate that $Ne \times Te$ is essentially determined by Ne , and Te changes in response to the variation of Ne . This also means that the above-mentioned thermally quasi-steady state is valid for our SAPS data with no large external heating to ionospheric electrons from sources such as soft particle precipitation or field-aligned heat conduction from higher altitudes. Under this assumption, a quantitative relationship between Ne and Te at 300–550 km heights can be approximately derived for SAPS regions from our results as:

$$Te = 10^{\alpha \times \log(Ne) + \beta}, \quad (2)$$

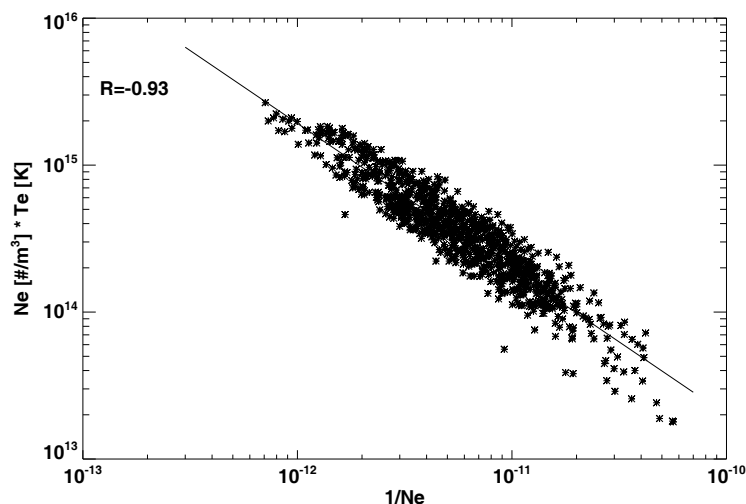


Figure 8. A scatter plot showing the comparison between $1/Ne$ and $Ne \times Te$ around SAPS.

615 where α and β equal to -0.0085 and 3.39 , respectively. The uncertainties for these two
 616 coefficients are 0.002 and 0.126 , respectively. This result is new, and should be further
 617 expanded by future coupled ionosphere, plasmasphere, and magnetospheric modeling stud-
 618 ies.

619 4 Conclusions

620 This paper presents a comprehensive statistical study of the subauroral polariza-
 621 tion stream as well as related electron density, ion temperature, and electron temper-
 622 ature by using long-term measurements of Millstone Hill incoherent scatter radar over
 623 North American sector during 1979–2019. A superposed epoch analysis technique was
 624 used to investigate the distribution patterns of these parameters with respect to MLT,
 625 season, geomagnetic activity, solar activity, and IMF orientation, respectively. The sta-
 626 tistical results in this study not only confirmed some previously-established character-
 627 istics but also proposed new insights on SAPS, such as its solar activity and IMF depen-
 628 dencies.

629 The main results that further confirmed previously published ones are as follows:

630 1. SAPS has MLT variation with larger magnitude and broader width around dusk
 631 than midnight, seasonal asymmetry with higher peak velocity in winter than summer,
 632 and geomagnetic dependence with larger velocity during active periods than quiet time.

633 2. SAPS is usually associated with a midlatitude trough of 15–20% Ne depletion,
 634 and the trough depth exhibits an increasing trend with increasing Kp value.

635 3. The subauroral ion and electron temperature exhibit 3–8% (50–120 K) enhance-
 636 ment associated with SAPS, and both have larger enhancement during geomagnetically
 637 active periods. The ion temperature is determined by the altitude-dependent contribu-
 638 tion from SAPS-related frictional heating and local heat conduction/advection. The elec-
 639 tron temperature is influenced by the thermal interaction between downward heat trans-
 640 fer from ring current and local Coulomb cooling, and lower Ne tends to make the heat-

641 ing (cooling) process more (less) efficient in generating more significant electron temper-
642 ature enhancement.

643 The new findings on SAPS features are summarized as follows:

644 1. The average SAPS detection rate among our database is 5%–15% with two peaks
645 occurring around equinoxes, likely due to enhanced geomagnetic activities during equinoc-
646 tial periods. SAPS tends to have larger velocity in low solar activity than high solar ac-
647 tivity periods, which could be partially attributed to weaker height-integrated Pedersen
648 conductivity around solar minimum.

649 2. SAPS has a dependence on IMF orientation, which tend to have larger veloc-
650 ity when the IMF clock angle is between -180° and -90° (i.e., negative B_y and neg-
651 ative B_z). This phenomenon might be collectively interpreted by the B_z -related geo-
652 magnetic dependence of SAPS, as well as the B_y -related dependence of plasma convec-
653 tion and neutral wind patterns.

654 3. The SAPS-related midlatitude trough has clear MLT and seasonal preference.
655 It has the largest depletion in the postmidnight sector around 00-02 MLT, probably re-
656 sults from extended subauroral plasma stagnation due to the reduced SAPS that is close
657 to the counteracting corotation flow. The trough depth is larger around equinoxes than
658 other seasons, likely due to slightly increased SAPS number and magnitude associated
659 with enhanced geomagnetic activities around equinoxes.

660 4. The ion and electron temperature enhancement around SAPS peak is generally
661 more pronounced during midnight than dusk. Conditions for ion temperature enhance-
662 ment are more favored during low solar activity periods, while the electron temperature
663 enhancement is almost constant within solar cycle.

664 5. SAPS thermal content $T_e \times N_e$ is consistent with thermal equilibrium, is strongly
665 dependent on $1/N_e$, and therefore T_e exhibits negative correlation with respect to N_e .
666 This result could indicate that external heat input to the ionosphere in SAPS regions
667 through thermal conduction from the plasmasphere is unlikely to be substantial, but this
668 needs to be further explored with future modeling studies.

Acknowledgments

669 Millstone Hill incoherent scatter radar observation and analysis are part of the US NSF
 670 Geospace Facility program under a cooperative agreement AGS-1952737 with Massachusetts
 671 Institute of Technology. The same NSF program supports Madrigal Database (<http://openmadrigal.org>)
 672 which provides all Millstone Hill radar data used in this work. SRZ and AJC acknowl-
 673 edge the AFOSR support for the MURI Project FA9559-16-1-0364; and AJC, SRZ and
 674 LPG acknowledge the ONR Grant N00014-17-1-2186. The F10.7 and IMF data is ac-
 675 quired from NASA/GSFC's Space Physics Data Facility's OMNIWeb service (<https://cdaweb.gsfc.nasa.gov/>).
 676 Kp indices are downloaded from Kyoto world data center for Geomagnetism (<http://wdc.kugi.kyoto->
 677 [u.ac.jp/](http://wdc.kugi.kyoto-u.ac.jp/)). The DMSP SSJ/4 and SSJ/5 particle detectors were designed and calibrated
 678 by Dave Hardy of the Air Force Research Laboratory, and the Auroral Boundary Index
 679 (ABI) was downloaded from Madrigal Database (<http://cedar.openmadrigal.org>), which
 680 was also provided by the Air Force Research Laboratory, Kirtland Air Force Base, New
 681 Mexico.
 682

References

- 683
- 684 Aa, E., Zou, S., Erickson, P. J., Zhang, S.-R., & Liu, S. (2020). Statistical analy-
 685 sis of the main ionospheric trough using swarm in situ measurements. *Journal*
 686 *of Geophysical Research: Space Physics*, *125*(3), e2019JA027583. doi: 10.1029/
 687 2019JA027583
- 688 Afonin, V. V., Bassolo, V. S., Smilauer, J., & Lemaire, J. F. (1997, February). Mo-
 689 tion and erosion of the nightside plasmopause region and of the associated
 690 subauroral electron temperature enhancement: Cosmos 900 observations. *Jour-*
 691 *nal of Geophysical Research*, *102*(A2), 2093-2104. doi: 10.1029/96JA02497
- 692 Anderson, P. C. (2004, Jun). Subauroral electric fields and magnetospheric convec-
 693 tion during the April, 2002 geomagnetic storms. *Geophysical Research Letters*,
 694 *31*(11), L11801. doi: 10.1029/2004GL019588
- 695 Anderson, P. C., Carpenter, D. L., Tsuruda, K., Mukai, T., & Rich, F. J. (2001,
 696 Dec). Multisatellite observations of rapid subauroral ion drifts (SAID). *Jour-*
 697 *nal of Geophysical Research: Space Physics*, *106*(A12), 29585-29600. doi:
 698 10.1029/2001JA000128
- 699 Anderson, P. C., Hanson, W. B., Heelis, R. A., Craven, J. D., Baker, D. N., &
 700 Frank, L. A. (1993, Apr). A proposed production model of rapid subauroral
 701 ion drifts and their relationship to substorm evolution. *Journal of Geophysical*
 702 *Research*, *98*(A4), 6069-6078. doi: 10.1029/92JA01975
- 703 Anderson, P. C., Heelis, R. A., & Hanson, W. B. (1991, Apr). The ionospheric
 704 signatures of rapid subauroral ion drifts. *Journal of Geophysical Research*,
 705 *96*(A4), 5785-5792. doi: 10.1029/90JA02651
- 706 Buonsanto, M. J., Foster, J. C., & Sipler, D. P. (1992, Feb). Observations
 707 From Millstone Hill During the Geomagnetic Disturbances of March and
 708 April 1990. *Journal of Geophysical Research*, *97*(A2), 1225-1243. doi:
 709 10.1029/91JA02428
- 710 Califf, S., Li, X., Wolf, R. A., Zhao, H., Jaynes, A. N., Wilder, F. D., . . . Red-
 711 mon, R. (2016, Jun). Large-amplitude electric fields in the inner magneto-
 712 sphere: Van Allen Probes observations of subauroral polarization streams.
 713 *Journal of Geophysical Research: Space Physics*, *121*(6), 5294-5306. doi:
 714 10.1002/2015JA022252
- 715 Carbary, J. F. (2005, Oct). A Kp-based model of auroral boundaries. *Space*
 716 *Weather*, *3*(10), S10001. doi: 10.1029/2005SW000162
- 717 Clausen, L. B. N., Baker, J. B. H., Ruohoniemi, J. M., Greenwald, R. A., Thomas,
 718 E. G., Shepherd, S. G., . . . Sazykin, S. (2012, May). Large-scale observations
 719 of a subauroral polarization stream by midlatitude SuperDARN radars: In-
 720 stantaneous longitudinal velocity variations. *Journal of Geophysical Research*,
 721 *117*(A5), A05306. doi: 10.1029/2011JA017232

- 722 Collis, P. N., & Haggstrom, I. (1988). Plasma convection and auroral precipi-
 723 tation processes associated with the main ionospheric trough at high lati-
 724 tudes. *Journal of Atmospheric and Terrestrial Physics*, *50*, 389-404. doi:
 725 10.1016/0021-9169(88)90024-4
- 726 De Keyser, J. (1999, Jun). Formation and evolution of subauroral ion drifts in the
 727 course of a substorm. *Journal of Geophysical Research*, *104*(A6), 12339-12350.
 728 doi: 10.1029/1999JA900109
- 729 Ebihara, Y., Nishitani, N., Kikuchi, T., Ogawa, T., Hosokawa, K., Fok, M. C., &
 730 Thomsen, M. F. (2009, Jan). Dynamical property of storm time subauroral
 731 rapid flows as a manifestation of complex structures of the plasma pressure in
 732 the inner magnetosphere. *Journal of Geophysical Research*, *114*(A1), A01306.
 733 doi: 10.1029/2008JA013614
- 734 Erickson, P. J., Beroz, F., & Miskin, M. Z. (2011, Mar). Statistical characterization
 735 of the American sector subauroral polarization stream using incoherent scatter
 736 radar. *Journal of Geophysical Research: Space Physics*, *116*, A00J21. doi:
 737 10.1029/2010JA015738
- 738 Erickson, P. J., Foster, J. C., & Holt, J. M. (2002, April). Inferred electric field
 739 variability in the polarization jet from Millstone Hill E region coherent scatter
 740 observations. *Radio Science*, *37*(2), 1027. doi: 10.1029/2000RS002531
- 741 Erickson, P. J., Goncharenko, L. P., Nicolls, M. J., Ruohoniemi, M., & Kelley,
 742 M. C. (2010, March). Dynamics of North American sector ionospheric
 743 and thermospheric response during the November 2004 superstorm. *Jour-
 744 nal of Atmospheric and Solar-Terrestrial Physics*, *72*(4), 292-301. doi:
 745 10.1016/j.jastp.2009.04.001
- 746 Erickson, P. J., Matsui, H., Foster, J. C., Torbert, R. B., Ergun, R. E., Khotyaint-
 747 sev, Y. V., ... Magnes, W. (2016, Jul). Multipoint MMS observations of
 748 fine-scale SAPS structure in the inner magnetosphere. *Geophysical Research
 749 Letters*, *43*(14), 7294-7300. doi: 10.1002/2016GL069174
- 750 Evans, J. V. (1970, January). Midlatitude ionospheric temperatures during three
 751 magnetic storms in 1965. *Journal of Geophysical Research*, *75*(25), 4803. doi:
 752 10.1029/JA075i025p04803
- 753 Evans, J. V. (1973, January). Seasonal and sunspot cycle variations of F Region
 754 electron temperatures and protonospheric heat fluxes. *Journal of Geophysical
 755 Research*, *78*(13), 2344. doi: 10.1029/JA078i013p02344
- 756 Ferdousi, B., Nishimura, Y., Maruyama, N., & Lyons, L. R. (2019, March). Subau-
 757 roral Neutral Wind Driving and Its Feedback to SAPS During the 17 March
 758 2013 Geomagnetic Storm. *Journal of Geophysical Research: Space Physics*,
 759 *124*(3), 2323-2337. doi: 10.1029/2018JA026193
- 760 Fok, M. C., Kozyra, J. U., & Brace, L. H. (1991, February). Solar cycle variation
 761 in the subauroral electron temperature enhancement: Comparison of AE-C
 762 and DE 2 satellite observations. *Journal of Geophysical Research*, *96*(A2),
 763 1861-1866. doi: 10.1029/90JA02377
- 764 Fok, M. C., Kozyra, J. U., Warren, M. F., & Brace, L. H. (1991, June). Seasonal
 765 variations in the subauroral electron temperature enhancement. *Journal of
 766 Geophysical Research*, *96*(A6), 9773-9780. doi: 10.1029/91JA00791
- 767 Förster, M., Rentz, S., Köhler, W., Liu, H., & Haaland, S. E. (2008, June). IMF
 768 dependence of high-latitude thermospheric wind pattern derived from CHAMP
 769 cross-track measurements. *Annales Geophysicae*, *26*(6), 1581-1595. doi:
 770 10.5194/angeo-26-1581-2008
- 771 Foster, J. C. (1993, February). Storm time plasma transport at middle and high
 772 latitudes. *Journal of Geophysical Research*, *98*(A2), 1675-1690. doi: 10.1029/
 773 92JA02032
- 774 Foster, J. C., & Burke, W. J. (2002). SAPS: A new categorization for sub-auroral
 775 electric fields. *EOS Transactions*, *83*(36), 393. doi: 10.1029/2002EO000289
- 776 Foster, J. C., Coster, A. J., Erickson, P. J., Holt, J. M., Lind, F. D., Rideout, W.,

- 777 ... Rich, F. J. (2005, Sep). Multiradar observations of the polar tongue of
778 ionization. *Journal of Geophysical Research (Space Physics)*, *110*(A9), A09S31.
779 doi: 10.1029/2004JA010928
- 780 Foster, J. C., Erickson, P. J., Coster, A. J., Thaller, S., Tao, J., Wygant, J. R., &
781 Bonnell, J. W. (2014, February). Storm time observations of plasmasphere ero-
782 sion flux in the magnetosphere and ionosphere. *Geophysical Research Letters*,
783 *41*(3), 762-768. doi: 10.1002/2013GL059124
- 784 Foster, J. C., Rideout, W., Sandel, B., Forrester, W. T., & Rich, F. J. (2007,
785 Mar). On the relationship of SAPS to storm-enhanced density. *Jour-
786 nal of Atmospheric and Solar-Terrestrial Physics*, *69*(3), 303-313. doi:
787 10.1016/j.jastp.2006.07.021
- 788 Foster, J. C., & Vo, H. B. (2002, Dec). Average characteristics and activity depen-
789 dence of the subauroral polarization stream. *Journal of Geophysical Research:
790 Space Physics*, *107*(A12), 1475. doi: 10.1029/2002JA009409
- 791 Galperin, Y., Ponomarov, Y., & Zosinova, A. (1974). Plasma convection in polar
792 ionosphere. *Annales de Geophysique*, *30*(1-7).
- 793 Gkioulidou, M., Wang, C.-P., Lyons, L. R., & Wolf, R. A. (2009, July). Formation
794 of the Harang reversal and its dependence on plasma sheet conditions: Rice
795 convection model simulations. *Journal of Geophysical Research :Space Physics*,
796 *114*(A7), A07204. doi: 10.1029/2008JA013955
- 797 Goldstein, J., Burch, J. L., Sandel, B. R., Mende, S. B., Brandt, P. C., & Hairston,
798 M. R. (2005, Mar). Coupled response of the inner magnetosphere and iono-
799 sphere on 17 April 2002. *Journal of Geophysical Research*, *110*(A3), A03205.
800 doi: 10.1029/2004JA010712
- 801 Goldstein, J., Sandel, B. R., Thomsen, M. F., Spasojević, M., & Reiff, P. H. (2004,
802 Mar). Simultaneous remote sensing and in situ observations of plasmaspheric
803 drainage plumes. *Journal of Geophysical Research*, *109*(A3), A03202. doi: 10
804 .1029/2003JA010281
- 805 Goncharenko, L., Salah, J., Crowley, G., Paxton, L. J., Zhang, Y., Coster, A., ...
806 Taran, V. (2006, March). Large variations in the thermosphere and iono-
807 sphere during minor geomagnetic disturbances in April 2002 and their associ-
808 ation with IMF B_y . *Journal of Geophysical Research*, *111*(A3), A03303. doi:
809 10.1029/2004JA010683
- 810 Goncharenko, L. P., Foster, J. C., Coster, A. J., Huang, C., Aponte, N., & Pax-
811 ton, L. J. (2007, Jul). Observations of a positive storm phase on September
812 10, 2005. *Journal of Atmospheric and Solar-Terrestrial Physics*, *69*(10-11),
813 1253-1272. doi: 10.1016/j.jastp.2006.09.011
- 814 Gussenhoven, M. S., Hardy, D. A., & Burke, W. J. (1981, Feb). DMSP/F2 electron
815 observations of equatorward auroral boundaries and their relationship to mag-
816 netospheric electric fields. *Journal of Geophysical Research*, *86*(A2), 768-778.
817 doi: 10.1029/JA086iA02p00768
- 818 Gussenhoven, M. S., Hardy, D. A., & Heinemann, N. (1983, Jul). Systematics of
819 the equatorward diffuse auroral boundary. *Journal of Geophysical Research*,
820 *88*(A7), 5692-5708. doi: 10.1029/JA088iA07p05692
- 821 Gussenhoven, M. S., Hardy, D. A., & Heinemann, N. (1987, Apr). The equator-
822 ward boundary of auroral ion precipitation. *Journal of Geophysical Research*,
823 *92*(A4), 3273-3283. doi: 10.1029/JA092iA04p03273
- 824 Hardy, D. A., Gussenhoven, M. S., & Brautigam, D. (1989, Jan). A statistical model
825 of auroral ion precipitation. *Journal of Geophysical Research*, *94*(A1), 370-392.
826 doi: 10.1029/JA094iA01p00370
- 827 Hardy, D. A., Gussenhoven, M. S., Raistrick, R., & McNeil, W. J. (1987, Novem-
828 ber). Statistical and functional representations of the pattern of auroral energy
829 flux, number flux, and conductivity. *Journal of Geophysical Research*, *92*(A11),
830 12275-12294. doi: 10.1029/JA092iA11p12275
- 831 Hardy, D. A., Holeman, E. G., Burke, W. J., Gentile, L. C., & Bounar, K. H. (2008,

- 832 Jun). Probability distributions of electron precipitation at high magnetic lat-
833 itudes. *Journal of Geophysical Research*, *113*(A6), A06305. doi: 10.1029/
834 2007JA012746
- 835 He, F., Zhang, X., & Chen, B. (2014, Jun). Solar cycle, seasonal, and diurnal vari-
836 ations of subauroral ion drifts: Statistical results. *Journal of Geophysical Re-*
837 *search: Space Physics*, *119*(6), 5076-5086. doi: 10.1002/2014JA019807
- 838 He, F., Zhang, X., Wang, W., Liu, L., Ren, Z., Yue, X., . . . Wang, H. (2018, Apr).
839 Large-Scale Structure of Subauroral Polarization Streams During the Main
840 Phase of a Severe Geomagnetic Storm. *Journal of Geophysical Research: Space*
841 *Physics*, *123*(4), 2964-2973. doi: 10.1002/2018JA025234
- 842 He, F., Zhang, X., Wang, W., & Wan, W. (2017, Nov). Different Evolution Patterns
843 of Subauroral Polarization Streams (SAPS) During Intense Storms and Quiet
844 Time Substorms. *Geophysical Research Letters*, *44*(21), 10,796-10,804. doi:
845 10.1002/2017GL075449
- 846 Heelis, R. A. (1984, May). The effects of interplanetary magnetic field orientation on
847 dayside high-latitude ionospheric convection. *Journal of Geophysical Research*,
848 *89*(A5), 2873-2880. doi: 10.1029/JA089iA05p02873
- 849 Heelis, R. A., Bailey, G. J., Sellek, R., Moffett, R. J., & Jenkins, B. (1993, Decem-
850 ber). Field-aligned drifts in subauroral ion drift events. *Journal of Geophysical*
851 *Research*, *98*(A12), 21493-21500. doi: 10.1029/93JA02209
- 852 Heinemann, N. C., Gussenhoven, M. S., Hardy, D. A., Rich, F. J., & Yeh, H. C.
853 (1989, Oct). Electron/ion precipitation differences in relation to region 2 field-
854 aligned currents. *Journal of Geophysical Research*, *94*(A10), 13593-13600. doi:
855 10.1029/JA094iA10p13593
- 856 Hoppner, J. P., & Maynard, N. C. (1987, May). Empirical high-latitude electric field
857 models. *Journal of Geophysical Research*, *92*(A5), 4467-4490. doi: 10.1029/
858 JA092iA05p04467
- 859 Hernandez, G., McCormac, F. G., & Smith, R. W. (1991, April). Austral thermo-
860 spheric wind circulation and interplanetary magnetic field orientation. *Journal*
861 *of Geophysical Research*, *96*(A4), 5777-5783. doi: 10.1029/90JA02458
- 862 Horvath, I., & Lovell, B. C. (2016, Feb). Structured subauroral polarization streams
863 and related auroral undulations occurring on the storm day of 21 January
864 2005. *Journal of Geophysical Research: Space Physics*, *121*(2), 1680-1695. doi:
865 10.1002/2015JA022057
- 866 Huang, C.-S., & Foster, J. C. (2007, Nov). Correlation of the subauroral polariza-
867 tion streams (SAPS) with the Dst index during severe magnetic storms. *Jour-*
868 *nal of Geophysical Research: Space Physics*, *112*(A11), A11302. doi: 10.1029/
869 2007JA012584
- 870 Immel, T. J., Craven, J. D., & Frank, L. A. (1997, April). Influence of IMF B_y
871 on large-scale decreases of O column density at middle latitudes. *Jour-*
872 *nal of Atmospheric and Solar-Terrestrial Physics*, *59*, 725-737. doi:
873 10.1016/S1364-6826(96)00099-5
- 874 Karlsson, T., Marklund, G. T., Blomberg, L. G., & Mälkki, A. (1998, Mar). Subau-
875 roral electric fields observed by the Freja satellite: A statistical study. *Journal*
876 *of Geophysical Research*, *103*(A3), 4327-4342. doi: 10.1029/97JA00333
- 877 Karpachev, A. T. (2003). The dependence of the main ionospheric trough shape
878 on longitude, altitude, season, local time, and solar and magnetic activity. *Ge-*
879 *omagnetism and Aeronomy*, *43*(2), 239-251.
- 880 Karpachev, A. T. (2019). Variations in the Winter Troughs' Position With Local
881 Time, Longitude, and Solar Activity in the Northern and Southern Hemi-
882 spheres. *Journal of Geophysical Research: Space Physics*, *124*(10), 8039-8055.
883 doi: 10.1029/2019JA026631
- 884 Karpachev, A. T., Deminov, M. G., & Afonin, V. V. (1996, Jan). Model of the
885 mid-latitude ionospheric trough on the base of Cosmos-900 and Intercosmos-
886 19 satellites data. *Advances in Space Research*, *18*(6), 221-230. doi:

- 887 10.1016/0273-1177(95)00928-0
 888 Kelley, M. C., Vlasov, M. N., Foster, J. C., & Coster, A. J. (2004, Octo-
 889 ber). A quantitative explanation for the phenomenon known as storm-
 890 enhanced density. *Geophysical Research Letters*, *31*(19), L19809. doi:
 891 10.1029/2004GL020875
- 892 Kepko, L., McPherron, R. L., Amm, O., Apatenkov, S., Baumjohann, W., Birn, J.,
 893 ... Sergeev, V. (2015, July). Substorm Current Wedge Revisited. *Space Sci*
 894 *Review*, *190*(1-4), 1-46.
- 895 Koustov, A. V., Drayton, R. A., Makarevich, R. A., McWilliams, K. A., St-Maurice,
 896 J. P., Kikuchi, T., & Frey, H. U. (2006, Jul). Observations of high-velocity
 897 SAPS-like flows with the King Salmon SuperDARN radar. *Annales Geophysi-*
 898 *caae*, *24*(6), 1591-1608. doi: 10.5194/angeo-24-1591-2006
- 899 Kozyra, J. U., Brace, L. H., Cravens, T. E., & Nagy, A. F. (1986, October). A
 900 statistical study of the subauroral electron temperature enhancement using
 901 Dynamics Explorer-2 Langmuir probe observations. *Journal of Geophysical*
 902 *Research*, *91*(A10), 11270-11280. doi: 10.1029/JA091iA10p11270
- 903 Kozyra, J. U., Valladares, C. E., Carlson, H. C., Buonsanto, M. J., & Slater, D. W.
 904 (1990, August). A theoretical study of the seasonal and solar cycle variations
 905 of stable Auroa Red arcs. *Journal of Geophysical Research*, *95*(A8), 12219-
 906 12234. doi: 10.1029/JA095iA08p12219
- 907 Kunduri, B. S. R., Baker, J. B. H., Ruohoniemi, J. M., Clausen, L. B. N., Gro-
 908 ccott, A., Thomas, E. G., ... Talaat, E. R. (2012, Aug). An examination of
 909 inter-hemispheric conjugacy in a subauroral polarization stream. *Journal of*
 910 *Geophysical Research*, *117*(A8), A08225. doi: 10.1029/2012JA017784
- 911 Kunduri, B. S. R., Baker, J. B. H., Ruohoniemi, J. M., Nishitani, N., Oksavik, K.,
 912 Erickson, P. J., ... Miller, E. S. (2018, Sep). A New Empirical Model of
 913 the Subauroral Polarization Stream. *Journal of Geophysical Research: Space*
 914 *Physics*, *123*(9), 7342-7357. doi: 10.1029/2018JA025690
- 915 Kunduri, B. S. R., Baker, J. B. H., Ruohoniemi, J. M., Thomas, E. G., Shepherd,
 916 S. G., & Sterne, K. T. (2017, Jun). Statistical characterization of the large-
 917 scale structure of the subauroral polarization stream. *Journal of Geophysical*
 918 *Research: Space Physics*, *122*(6), 6035-6048. doi: 10.1002/2017JA024131
- 919 Landry, R. G., & Anderson, P. C. (2018, Apr). An Auroral Boundary-Oriented
 920 Model of Subauroral Polarization Streams (SAPS). *Journal of Geophysical Re-*
 921 *search: Space Physics*, *123*(4), 3154-3169. doi: 10.1002/2017JA024921
- 922 Le, H., Yang, N., Liu, L., Chen, Y., & Zhang, H. (2017). The latitudinal structure
 923 of nighttime ionospheric TEC and its empirical orthogonal functions model
 924 over North American sector. *Journal of Geophysical Research: Space Physics*,
 925 *122*(1), 963-977. doi: 10.1002/2016JA023361
- 926 Lejosne, S., & Mozer, F. S. (2017, Sep). Subauroral Polarization Streams (SAPS)
 927 Duration as Determined From Van Allen Probe Successive Electric Drift
 928 Measurements. *Geophysical Research Letters*, *44*(18), 9134-9141. doi:
 929 10.1002/2017GL074985
- 930 Leonard, J. M., Pinnock, M., Rodger, A. S., Dudeney, J. R., Greenwald, R. A., &
 931 Baker, K. B. (1995, July). Ionospheric plasma convection in the southern
 932 hemisphere. *Journal of Atmospheric and Terrestrial Physics*, *57*, 889-897. doi:
 933 10.1016/0021-9169(94)00070-5
- 934 Lin, D., Wang, W., Scales, W. A., Pham, K., Liu, J., Zhang, B., ... Maimaiti, M.
 935 (2019, Jul). SAPS in the 17 March 2013 Storm Event: Initial Results From the
 936 Coupled Magnetosphere-Ionosphere-Thermosphere Model. *Journal of Geophys-*
 937 *ical Research: Space Physics*, *124*(7), 6212-6225. doi: 10.1029/2019JA026698
- 938 Lyatsky, W., Newell, P. T., & Hamza, A. (2001, Jan). Solar illumination as cause of
 939 the equinoctial preference for geomagnetic activity. *Geophysical Research Let-*
 940 *ters*, *28*(12), 2353-2356. doi: 10.1029/2000GL012803
- 941 Makarevich, R. A., Kellerman, A. C., Bogdanova, Y. V., & Koustov, A. V. (2009,

- 942 Apr). Time evolution of the subauroral electric fields: A case study during
 943 a sequence of two substorms. *Journal of Geophysical Research*, *114*(A4),
 944 A04312. doi: 10.1029/2008JA013944
- 945 McCormac, F. G., Killeen, T. L., Gombosi, E., Hays, P. B., & Spencer, N. W. (1985,
 946 April). Configuration of the high-latitude thermosphere neutral circulation for
 947 IMF B_y negative and positive. *Geophysical Research Letters*, *12*(4), 155-158.
 948 doi: 10.1029/GL012i004p00155
- 949 Mendillo, M. (2006, December). Storms in the ionosphere: Patterns and processes
 950 for total electron content. *Reviews of Geophysics*, *44*(4), RG4001. doi: 10
 951 .1029/2005RG000193
- 952 Mishin, E. V. (2013, Sep). Interaction of substorm injections with the subauroral
 953 geospace: 1. Multispacecraft observations of SAID. *Journal of Geophysical Re-
 954 search: Space Physics*, *118*(9), 5782-5796. doi: 10.1002/jgra.50548
- 955 Mishin, E. V. (2016, Jul). SAPS onset timing during substorms and the westward
 956 traveling surge. *Geophysical Research Letters*, *43*(13), 6687-6693. doi: 10.1002/
 957 2016GL069693
- 958 Mishin, E. V., Foster, J. C., Potekhin, A. P., Rich, F. J., Schlegel, K., Yumoto, K.,
 959 ... Friedel, R. (2002, December). Global ULF disturbances during a storm-
 960 time substorm on 25 September 1998. *Journal of Geophysical Research (Space
 961 Physics)*, *107*(A12), 1486. doi: 10.1029/2002JA009302
- 962 Mishin, E. V., Nishimura, Y., & Foster, J. (2017, Aug). SAPS/SAID revisited:
 963 A causal relation to the substorm current wedge. *Journal of Geophysical Re-
 964 search: Space Physics*, *122*(8), 8516-8535. doi: 10.1002/2017JA024263
- 965 Mishin, E. V., Puhl-Quinn, P. A., & Santolik, O. (2010, Apr). SAID: A turbulent
 966 plasmaspheric boundary layer. *Geophysical Research Letters*, *37*(7), L07106.
 967 doi: 10.1029/2010GL042929
- 968 Moffett, R. J., Ennis, A. E., Bailey, G. J., Heelis, R. A., & Brace, L. H. (1998,
 969 April). Electron temperatures during rapid subauroral ion drift events. *An-
 970 nales Geophysicae*, *16*(4), 450-459. doi: 10.1007/s00585-998-0450-x
- 971 Moffett, R. J., & Quegan, S. (1983). The mid-latitude trough in the electron
 972 concentration of the ionospheric F-layer - A review of observations and mod-
 973 elling. *Journal of Atmospheric and Terrestrial Physics*, *45*, 315-343. doi:
 974 10.1016/S0021-9169(83)80038-5
- 975 Muldrew, D. B. (1965). F-Layer Ionization Troughs Deduced from Alou-
 976 ette Data. *Journal of Geophysical Research*, *70*(11), 2635-2650. doi:
 977 10.1029/JZ070i011p02635
- 978 Nagano, H., Nishitani, N., & Hori, T. (2015, Aug). Occurrence characteristics and
 979 lowest speed limit of subauroral polarization stream (SAPS) observed by the
 980 SuperDARN Hokkaido East radar. *Earth, Planets, and Space*, *67*, 126. doi:
 981 10.1186/s40623-015-0299-7
- 982 Oksavik, K., Greenwald, R. A., Ruohoniemi, J. M., Hairston, M. R., Paxton, L. J.,
 983 Baker, J. B. H., ... Barnes, R. J. (2006, Jun). First observations of the
 984 temporal/spatial variation of the sub-auroral polarization stream from the Su-
 985 perDARN Wallops HF radar. *Geophysical Research Letters*, *33*(12), L12104.
 986 doi: 10.1029/2006GL026256
- 987 Papitashvili, V. O., Belov, B. A., Faermark, D. S., Feldstein, Y. I., Golyshev, S. A.,
 988 Gromova, L. I., & Levitin, A. E. (1994, July). Electric potential patterns in
 989 the northern and southern polar regions parameterized by the interplanetary
 990 magnetic field. *Journal of Geophysical Research*, *99*(A7), 13251-13262. doi:
 991 10.1029/94JA00822
- 992 Parkinson, M. L., Pinnock, M., Wild, J. A., Lester, M., Yeoman, T. K., Milan, S. E.,
 993 ... Kikuchi, T. (2005, Jun). Interhemispheric asymmetries in the occurrence of
 994 magnetically conjugate sub-auroral polarisation streams. *Annales Geophysicae*,
 995 *23*(4), 1371-1390. doi: 10.5194/angeo-23-1371-2005
- 996 Pintér, B., Thom, S. D., Balthazor, R., Vo, H., & Bailey, G. J. (2006, Oct).

- 997 Modeling subauroral polarization streams equatorward of the plasmopause
 998 footprints. *Journal of Geophysical Research*, *111*(A10), A10306. doi:
 999 10.1029/2005JA011457
- 1000 Prölss, G. W. (2006, August). Subauroral electron temperature enhancement in the
 1001 nighttime ionosphere. *Annales Geophysicae*, *24*(7), 1871-1885. doi: 10.5194/
 1002 angeo-24-1871-2006
- 1003 Prölss, G. W. (2007, Mar). The equatorward wall of the subauroral trough in the af-
 1004 ternoon/evening sector. *Annales Geophysicae*, *25*(3), 645-659. doi: 10.5194/
 1005 angeo-25-645-2007
- 1006 Raeder, J., Cramer, W. D., Jensen, J., Fuller-Rowell, T., Maruyama, N., Toffo-
 1007 letto, F., & Vo, H. (2016, Nov). Sub-Auroral Polarization Streams: A
 1008 complex interaction between the magnetosphere, ionosphere, and thermo-
 1009 sphere. In *Journal of physics conference series* (Vol. 767, p. 012021). doi:
 1010 10.1088/1742-6596/767/1/012021
- 1011 Rees, D., Fuller-Rowell, T. J., Gordon, R., Smith, M. F., Maynard, N. C., Heppner,
 1012 J. P., ... Killeen, T. L. (1986, January). A theoretical and empirical study of
 1013 the response of the high latitude thermosphere to the sense of the “Y” compo-
 1014 nent of the interplanetary magnetic field. *Planet. Space Sci.*, *34*(1), 1-40. doi:
 1015 10.1016/0032-0633(86)90100-5
- 1016 Rich, F. J., & Hairston, M. (1994, March). Large-scale convection patterns observed
 1017 by DMSP. *Journal of Geophysical Research*, *99*(A3), 3827-3844. doi: 10.1029/
 1018 93JA03296
- 1019 Richards, P. G., & Torr, D. G. (1986, August). Thermal coupling of conjugate iono-
 1020 spheres and the tilt of the earth’s magnetic field. *Journal of Geophysical Re-
 1021 search*, *91*(A8), 9017-9022. doi: 10.1029/JA091iA08p09017
- 1022 Richmond, A. D., LathuillèRe, C., & Vennerstroem, S. (2003, February). Winds
 1023 in the high-latitude lower thermosphere: Dependence on the interplane-
 1024 tary magnetic field. *Journal of Geophysical Research*, *108*(A2), 1066. doi:
 1025 10.1029/2002JA009493
- 1026 Robinson, R. M., & Vondrak, R. R. (1984, June). Measurements of E region ioniza-
 1027 tion and conductivity produced by solar illumination at high latitudes. *Journal
 1028 of Geophysical Research*, *89*(A6), 3951-3956. doi: 10.1029/JA089iA06p03951
- 1029 Rodger, A. S. (2008, Jan). The mid-latitude trough—Revisited. *Washington DC
 1030 American Geophysical Union Geophysical Monograph Series*, *181*, 25-33. doi:
 1031 10.1029/181GM04
- 1032 Ruohoniemi, J. M., & Greenwald, R. A. (1996, October). Statistical patterns
 1033 of high-latitude convection obtained from Goose Bay HF radar observa-
 1034 tions. *Journal of Geophysical Research*, *101*(A10), 21743-21764. doi:
 1035 10.1029/96JA01584
- 1036 Ruohoniemi, J. M., & Greenwald, R. A. (2005, September). Dependencies of high-
 1037 latitude plasma convection: Consideration of interplanetary magnetic field,
 1038 seasonal, and universal time factors in statistical patterns. *Journal of Geophys-
 1039 ical Research*, *110*(A9), A09204. doi: 10.1029/2004JA010815
- 1040 Russell, C. T., & McPherron, R. L. (1973, Jan). Semiannual variation of geo-
 1041 omagnetic activity. *Journal of Geophysical Research*, *78*(1), 92. doi:
 1042 10.1029/JA078i001p00092
- 1043 Schunk, R. W., Banks, P. M., & Raitt, W. J. (1976). Effects of electric fields and
 1044 other processes upon the nighttime high-latitude F layer. *Journal of Geophys-
 1045 ical Research*, *81*(19), 3271. doi: 10.1029/JA081i019p03271
- 1046 Schunk, R. W., & Nagy, A. F. (1978, August). Electron temperatures in the F
 1047 region of the ionosphere: theory and observation. *Reviews of Geophysics and
 1048 Space Physics*, *16*, 355-399. doi: 10.1029/RG016i003p00355
- 1049 Schunk, R. W., & Nagy, A. F. (2000). *Ionospheres: physics, plasma physics, and
 1050 chemistry*. Cambridge University Press.
- 1051 Sergeev, V. A., Nikolaev, A. V., Tsyganenko, N. A., Angelopoulos, V., Runov, A. V.,

- 1052 Singer, H. J., & Yang, J. (2014, February). Testing a two-loop pattern of the
1053 substorm current wedge (SCW2L). *Journal of Geophysical Research (Space*
1054 *Physics)*, *119*(2), 947-963. doi: 10.1002/2013JA019629
- 1055 Spiro, R. W., Heelis, R. A., & Hanson, W. B. (1978, September). Ion convection and
1056 the formation of the mid-latitude F region ionization trough. *Journal of Geo-*
1057 *physical Research*, *83*(A9), 4255-4264. doi: 10.1029/JA083iA09p04255
- 1058 Spiro, R. W., Heelis, R. A., & Hanson, W. B. (1979, Aug). Rapid subauroral ion
1059 drifts observed by Atmosphere Explorer C. *Geophysical Research Letters*, *6*(8),
1060 657-660. doi: 10.1029/GL006i008p00657
- 1061 Thayer, J. P., Killeen, T. L., McCormac, F. G., Tschan, C. R., Ponthieu, J. J., &
1062 Spencer, N. W. (1987, December). Thermospheric neutral wind signatures
1063 dependent on the east-west component of the interplanetary magnetic field for
1064 Northern and Southern Hemispheres as measured from Dynamics Explorer-2.
1065 *Annales Geophysicae*, *5*, 363-368.
- 1066 Tulunay, Y. K., & Sayers, J. (1971, Nov). Characteristics of the mid-latitude
1067 trough as determined by the electron density experiment on Ariel III.
1068 *Journal of Atmospheric and Terrestrial Physics*, *33*(11), 1737-1761. doi:
1069 10.1016/0021-9169(71)90221-2
- 1070 Voiculescu, M., & Nygrén, T. (2007). IMF effect on ionospheric trough occurrence at
1071 equinoxes. *Advances in Space Research*, *40*(12), 1935-1940. doi: 10.1016/j.asr
1072 .2007.04.108
- 1073 Wang, H., & Lühr, H. (2013, Sep). Seasonal variation of the ion upflow in the
1074 topside ionosphere during SAPS (subauroral polarization stream) periods.
1075 *Annales Geophysicae*, *31*(9), 1521-1534. doi: 10.5194/angeo-31-1521-2013
- 1076 Wang, H., Lühr, H., Häusler, K., & Ritter, P. (2011, Mar). Effect of subauroral
1077 polarization streams on the thermosphere: A statistical study. *Journal of Geo-*
1078 *physical Research*, *116*(A3), A03312. doi: 10.1029/2010JA016236
- 1079 Wang, H., Lühr, H., & Ma, S. (2012, Apr). The relation between subauroral po-
1080 larization streams, westward ion fluxes, and zonal wind: Seasonal and hemi-
1081 spheric variations. *Journal of Geophysical Research*, *117*(A4), A04323. doi:
1082 10.1029/2011JA017378
- 1083 Wang, H., Ridley, A. J., Lühr, H., Liemohn, M. W., & Ma, S. Y. (2008, Dec). Sta-
1084 tistical study of the subauroral polarization stream: Its dependence on the
1085 cross-polar cap potential and subauroral conductance. *Journal of Geophysical*
1086 *Research: Space Physics*, *113*(A12), A12311. doi: 10.1029/2008JA013529
- 1087 Wang, W., Burns, A. G., & Killeen, T. L. (2006, November). A numerical study of
1088 the response of ionospheric electron temperature to geomagnetic activity. *Jour-*
1089 *nal of Geophysical Research*, *111*(A11), A11301. doi: 10.1029/2006JA011698
- 1090 Wang, W., Talaat, E. R., Burns, A., Emery, B., Hsieh, S., Lei, J., & Xu, J. (2012,
1091 Jul). Thermosphere and ionosphere response to subauroral polarization
1092 streams (SAPS): Model simulations. *Journal of Geophysical Research*,
1093 *117*(A7), A07301. doi: 10.1029/2012JA017656
- 1094 Wang, Z., Zou, S., Shepherd, S. G., Liang, J., Gjerloev, J. W., Ruohoniemi, J. M.,
1095 ... Wygant, J. R. (2019, March). Multi-instrument Observations of Mesoscale
1096 Enhancement of Subauroral Polarization Stream Associated With an Injec-
1097 tion. *Journal of Geophysical Research: Space Physics*, *124*(3), 1770-1784. doi:
1098 10.1029/2019JA026535
- 1099 Watanabe, S., Oyama, K.-I., & Abe, T. (1989, November). Electron temperature
1100 structure around mid latitude ionospheric trough. *Planet. Space Sci.*, *37*(11),
1101 1453-1460. doi: 10.1016/0032-0633(89)90115-3
- 1102 Weimer, D. R. (1995, October). Models of high-latitude electric potentials derived
1103 with a least error fit of spherical harmonic coefficients. *Journal of Geophysical*
1104 *Research*, *100*(A10), 19595-19608. doi: 10.1029/95JA01755
- 1105 Werner, S., & Prölss, G. W. (1997). The position of the ionospheric trough as a
1106 function of local time and magnetic activity. *Advances in Space Research*,

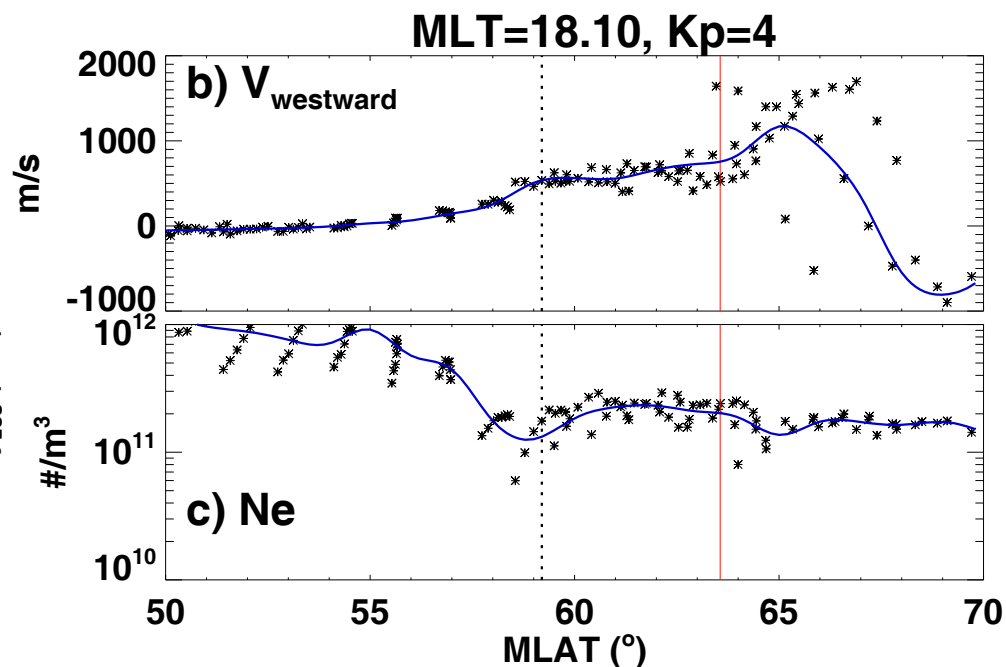
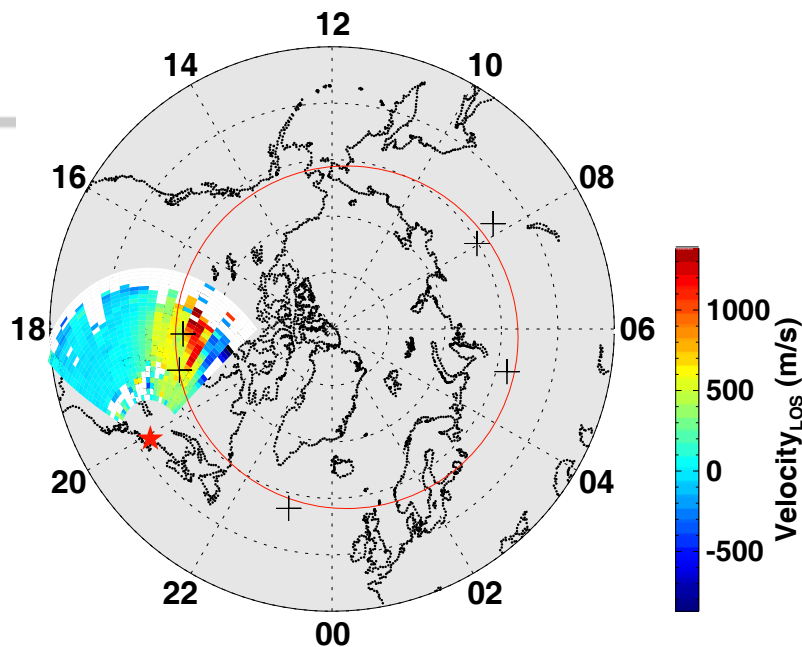
- 1107 20(9), 1717-1722. doi: 10.1016/S0273-1177(97)00578-4
- 1108 Yeh, H. C., & Foster, J. C. (1990, June). Storm time heavy ion outflow at mid-
1109 latitude. *Journal of Geophysical Research*, 95(A6), 7881-7891. doi: 10.1029/
1110 JA095iA06p07881
- 1111 Yeh, H. C., Foster, J. C., Rich, F. J., & Swider, W. (1991, Apr). Storm time electric
1112 field penetration observed at mid-latitude. *Journal of Geophysical Research*,
1113 96(A4), 5707-5721. doi: 10.1029/90JA02751
- 1114 Yu, Y., Jordanova, V., Zou, S., Heelis, R., Ruohoniemi, M., & Wygant, J. (2015,
1115 Mar). Modeling subauroral polarization streams during the 17 March 2013
1116 storm. *Journal of Geophysical Research: Space Physics*, 120(3), 1738-1750.
1117 doi: 10.1002/2014JA020371
- 1118 Yuan, Z., Xiong, Y., Qiao, Z., Li, H., Huang, S., Wang, D., . . . Wang, J. (2016,
1119 Feb). A subauroral polarization stream driven by field-aligned currents asso-
1120 ciated with precipitating energetic ions caused by EMIC waves: A case study.
1121 *Journal of Geophysical Research: Space Physics*, 121(2), 1696-1705. doi:
1122 10.1002/2015JA021804
- 1123 Zhang, Q., Liu, Y., Zhang, Q.-H., Xing, Z., Wang, Y., & Ma, Y. (2020, Mar). Sta-
1124 tistical study of ion upflow associated with subauroral polarization streams
1125 (SAPS) at substorm time. *Journal of Geophysical Research: Space Physics*,
1126 125(7), e2019JA027163. doi: 10.1029/2019JA027163
- 1127 Zhang, S.-R., Erickson, P. J., Foster, J. C., Holt, J. M., Coster, A. J., Makela, J. J.,
1128 . . . Kerr, R. B. (2015, July). Thermospheric poleward wind surge at mid-
1129 latitudes during great storm intervals. *Geophysical Research Letters*, 42(13),
1130 5132-5140. doi: 10.1002/2015GL064836
- 1131 Zhang, S.-R., Erickson, P. J., Zhang, Y., Wang, W., Huang, C., Coster, A. J., . . .
1132 Kerr, R. (2017, Jan). Observations of ion-neutral coupling associated with
1133 strong electrodynamic disturbances during the 2015 St. Patrick's Day storm.
1134 *Journal of Geophysical Research: Space Physics*, 122(1), 1314-1337. doi:
1135 10.1002/2016JA023307
- 1136 Zhang, S.-R., & Holt, J. M. (2004, January). Ionospheric plasma temperatures dur-
1137 ing 1976-2001 over Millstone Hill. *Advances in Space Research*, 33(6), 963-969.
1138 doi: 10.1016/j.asr.2003.07.012
- 1139 Zhang, S.-R., & Holt, J. M. (2007, Jun). Ionospheric climatology and variability
1140 from long-term and multiple incoherent scatter radar observations: Climatol-
1141 ogy in eastern American sector. *Journal of Geophysical Research*, 112(A6),
1142 A06328. doi: 10.1029/2006JA012206
- 1143 Zhang, S.-R., Holt, J. M., Erickson, P. J., Goncharenko, L. P., Nicolls, M. J., Mc-
1144 Cready, M., & Kelly, J. (2016, September). Ionospheric ion temperature
1145 climate and upper atmospheric long-term cooling. *Journal of Geophysical
1146 Research: Space Physics*, 121(9), 8951-8968. doi: 10.1002/2016JA022971
- 1147 Zhang, S.-R., Holt, J. M., Zaluca, A. M., & Amory-Mazaudier, C. (2004, Novem-
1148 ber). Midlatitude ionospheric plasma temperature climatology and empirical
1149 model based on Saint Santin incoherent scatter radar data from 1966 to 1987.
1150 *Journal of Geophysical Research: Space Physics*, 109(A11), A11311. doi:
1151 10.1029/2004JA010709
- 1152 Zhang, X., He, F., Wang, W., & Chen, B. (2015, Jun). Hemispheric asymmetry
1153 of subauroral ion drifts: Statistical results. *Journal of Geophysical Research:
1154 Space Physics*, 120(6), 4544-4554. doi: 10.1002/2015JA021016
- 1155 Zheng, Y., Brandt, P. C., Lui, A. T. Y., & Fok, M.-C. (2008, Apr). On iono-
1156 spheric trough conductance and subauroral polarization streams: Simu-
1157 lation results. *Journal of Geophysical Research*, 113(A4), A04209. doi:
1158 10.1029/2007JA012532
- 1159 Zou, S., Lyons, L. R., Nicolls, M. J., Heinselman, C. J., & Mende, S. B. (2009, De-
1160 cember). Nightside ionospheric electrodynamics associated with substorms:
1161 PFISR and THEMIS ASI observations. *Journal of Geophysical Research:*

- 1162 *Space Physics*, 114(A12), A12301. doi: 10.1029/2009JA014259
- 1163 Zou, S., Lyons, L. R., Wang, C. P., Boudouridis, A., Ruohoniemi, J. M., Anderson,
- 1164 P. C., ... Devlin, J. C. (2009). On the coupling between the Harang reversal
- 1165 evolution and substorm dynamics: A synthesis of SuperDARN, DMSP,
- 1166 and IMAGE observations. *Journal of Geophysical Research: Space Physics*,
- 1167 114(A1), A01205. doi: 10.1029/2008JA013449
- 1168 Zou, S., Moldwin, M. B., Ridley, A. J., Nicolls, M. J., Coster, A. J., Thomas, E. G.,
- 1169 & Ruohoniemi, J. M. (2014, Oct). On the generation/decay of the storm-
- 1170 enhanced density plumes: Role of the convection flow and field-aligned ion
- 1171 flow. *Journal of Geophysical Research: Space Physics*, 119(10), 8543-8559. doi:
- 1172 10.1002/2014JA020408
- 1173 Zou, S., Ridley, A. J., Moldwin, M. B., Nicolls, M. J., Coster, A. J., Thomas, E. G.,
- 1174 & Ruohoniemi, J. M. (2013, December). Multi-instrument observations of SED
- 1175 during 24-25 October 2011 storm: Implications for SED formation processes.
- 1176 *Journal of Geophysical Research (Space Physics)*, 118(12), 7798-7809. doi:
- 1177 10.1002/2013JA018860

Figure 1.

Author Manuscript

a) ISR Scan @ 10-MAR-1989 00:39 UT



d) ISR Scan @ 09-MAR-1989 07:24 UT

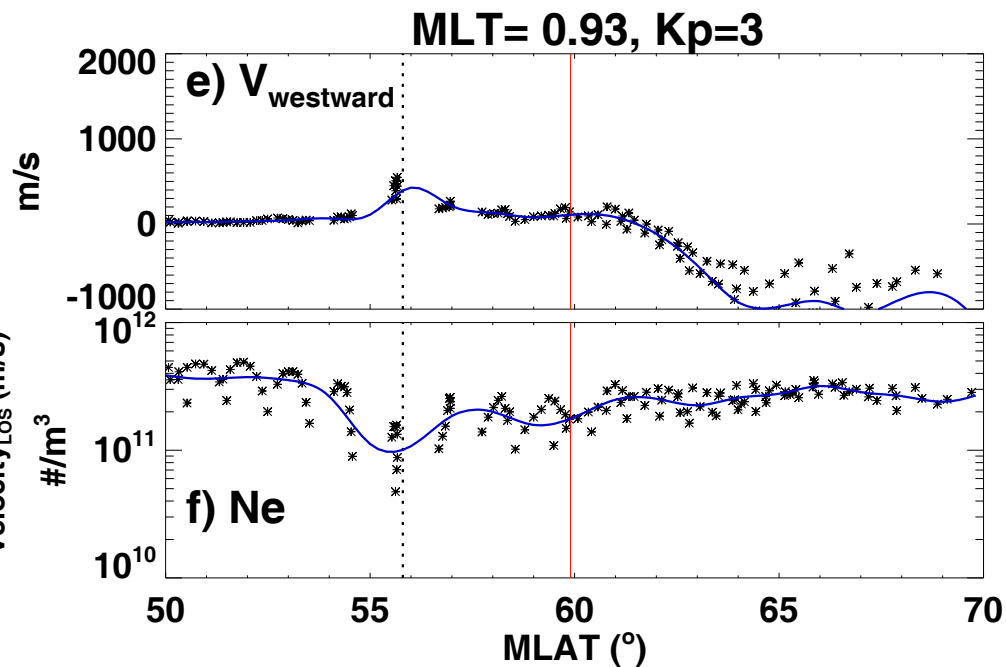
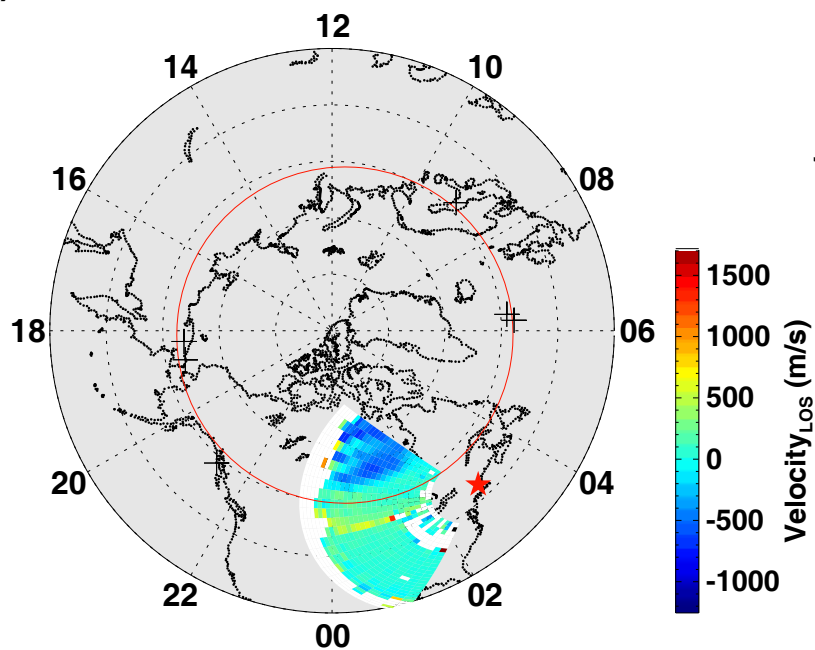
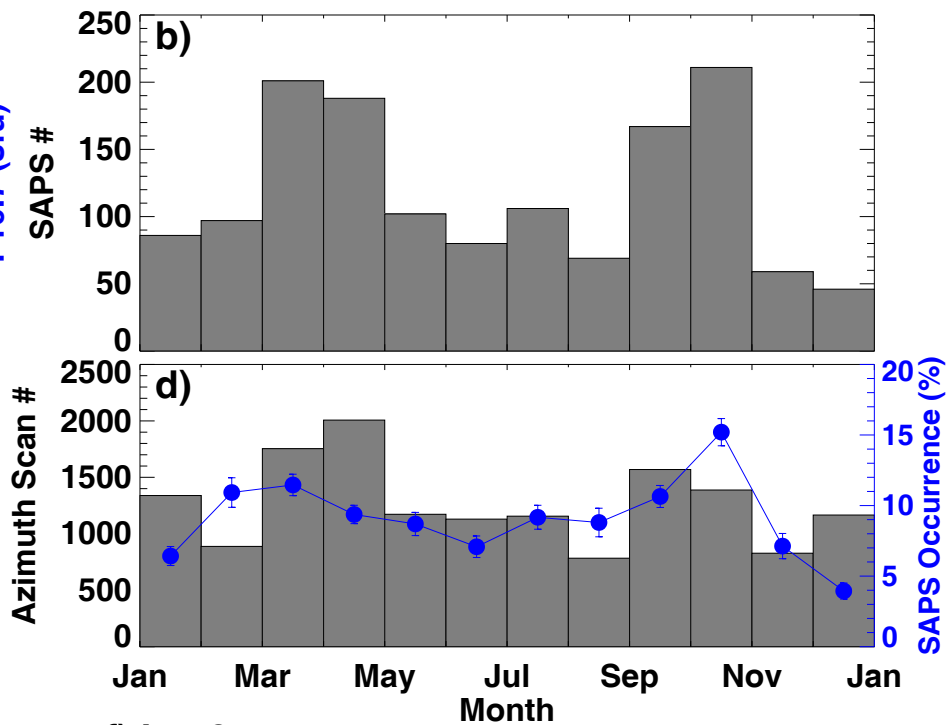
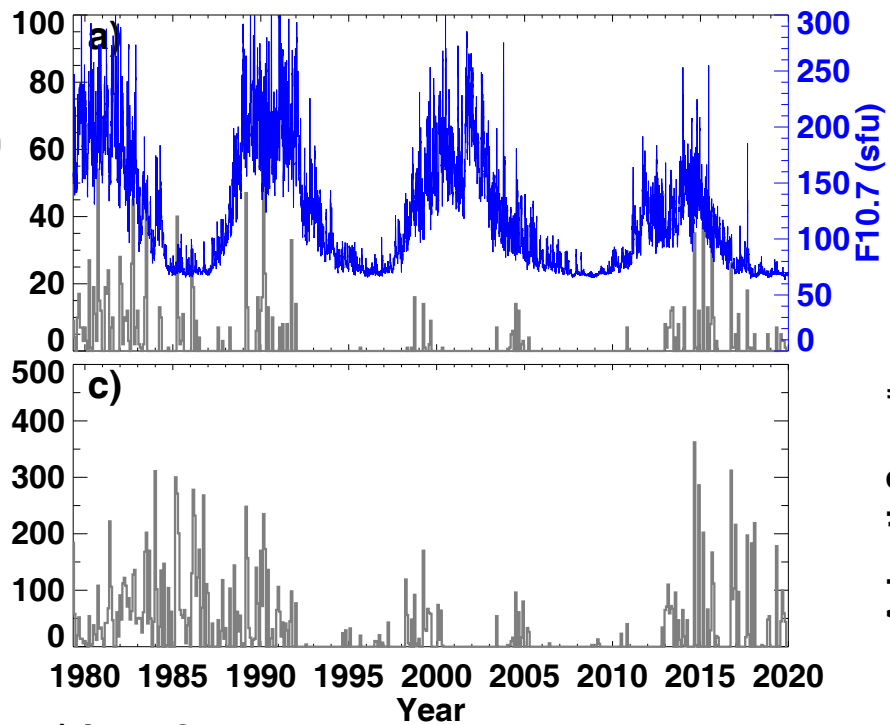
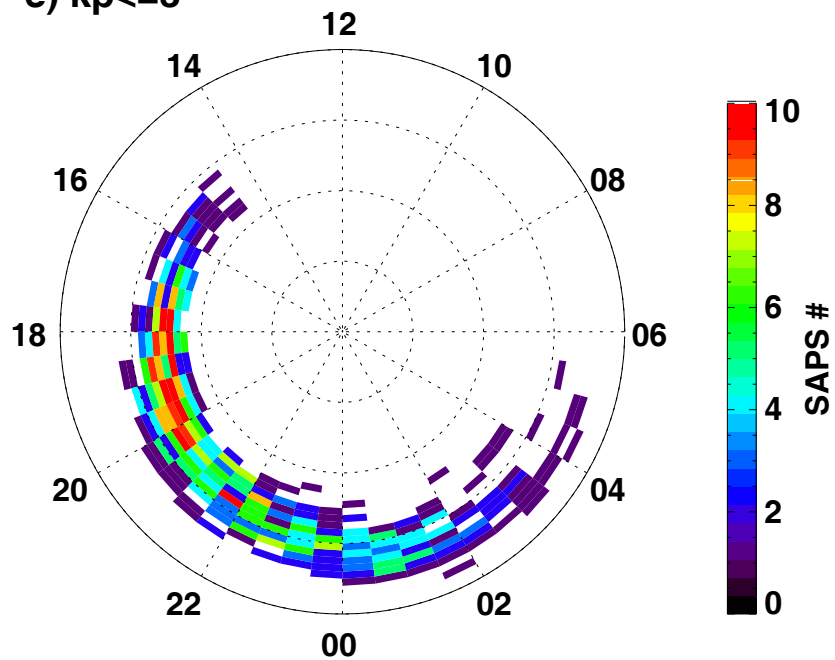


Figure 2.

Author Manuscript



e) $kp \leq 3$



f) $kp > 3$

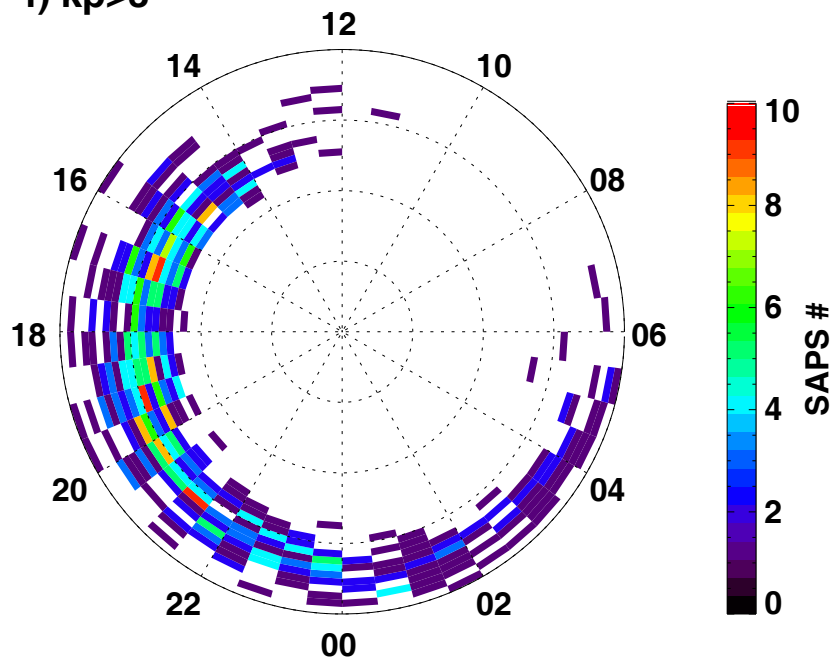


Figure 3.

Author Manuscript

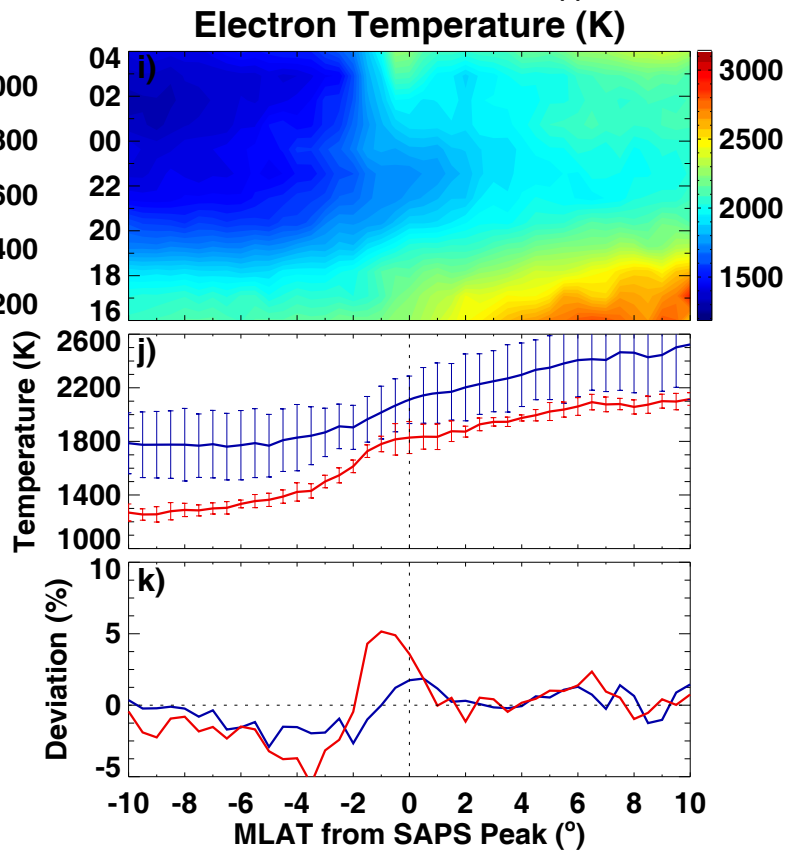
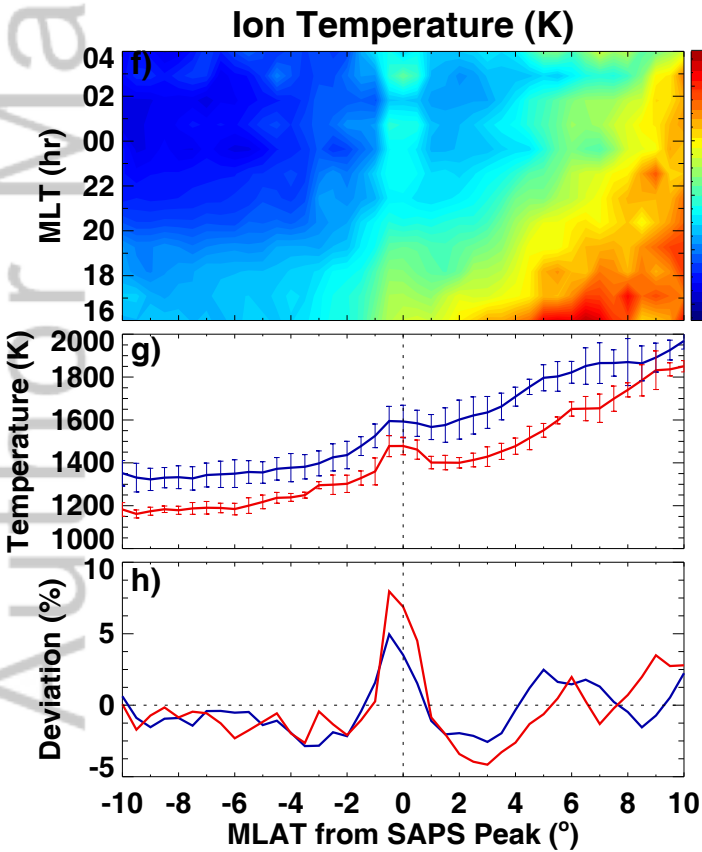
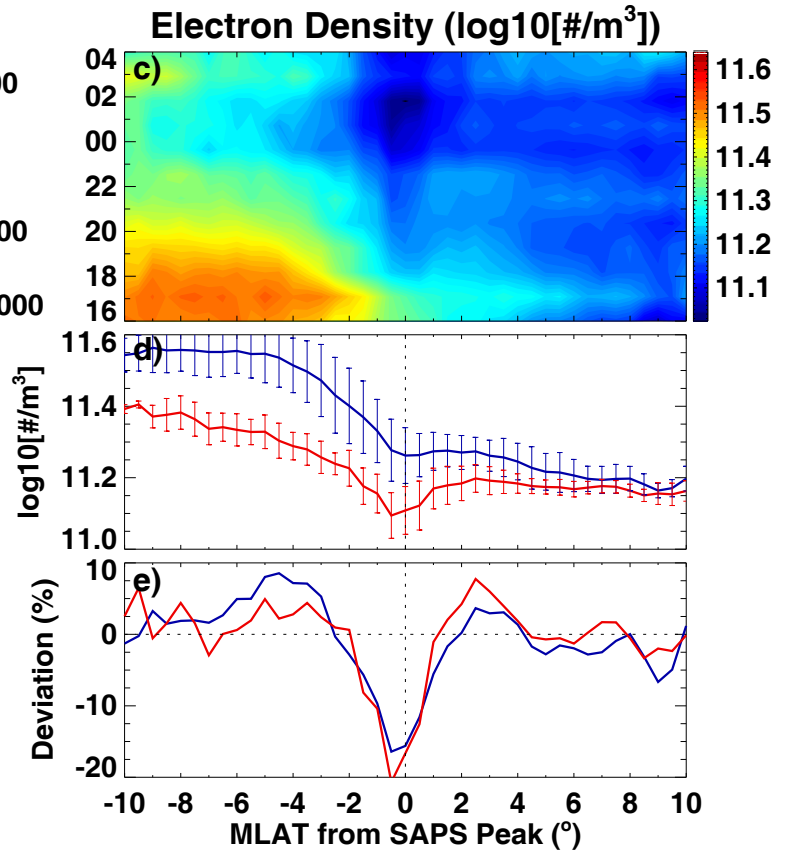
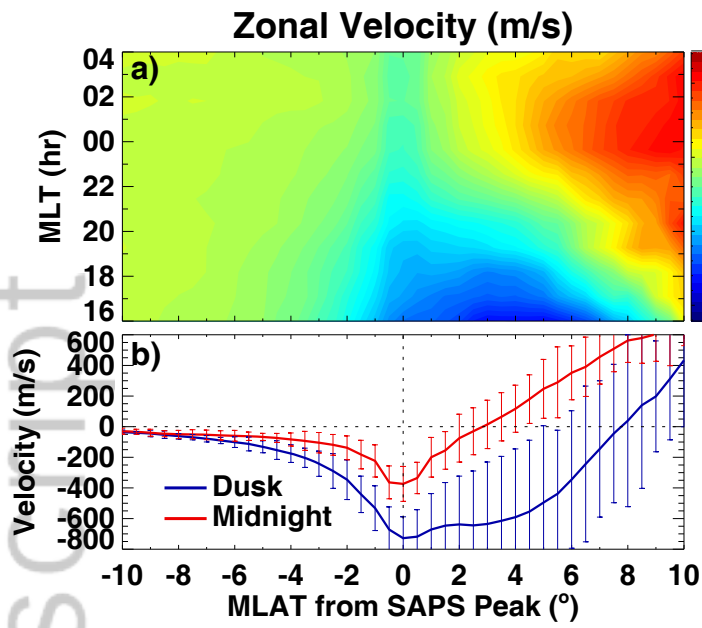


Figure 4.

Author Manuscript

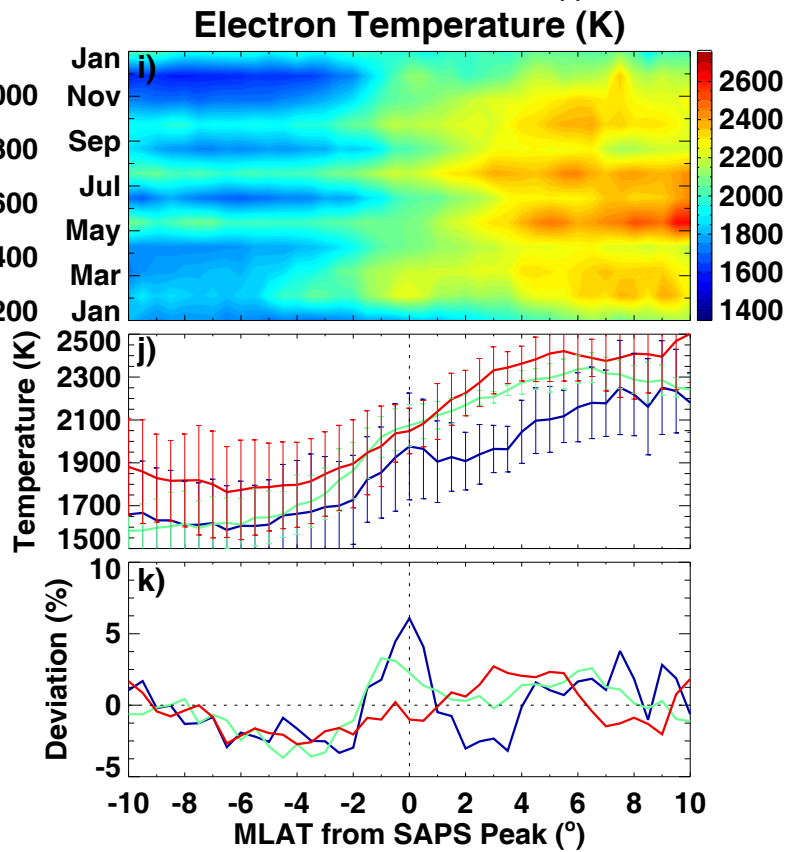
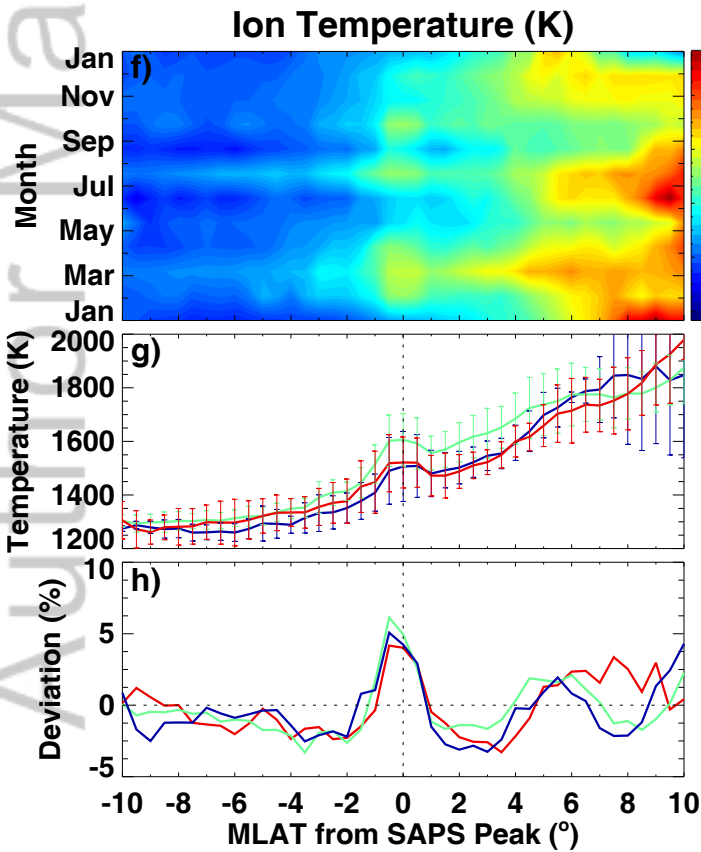
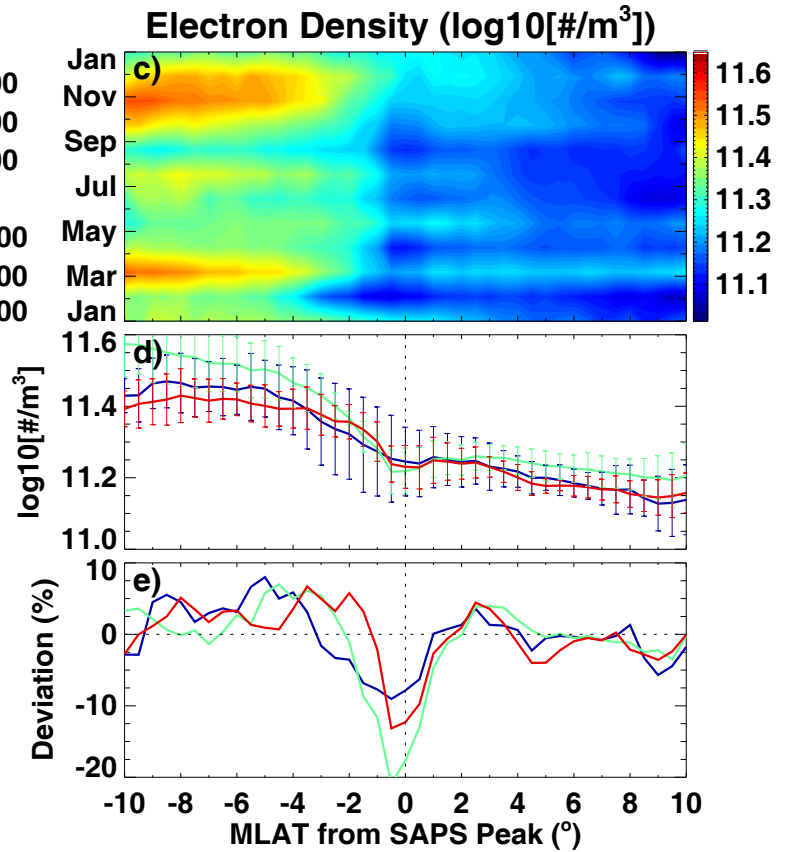
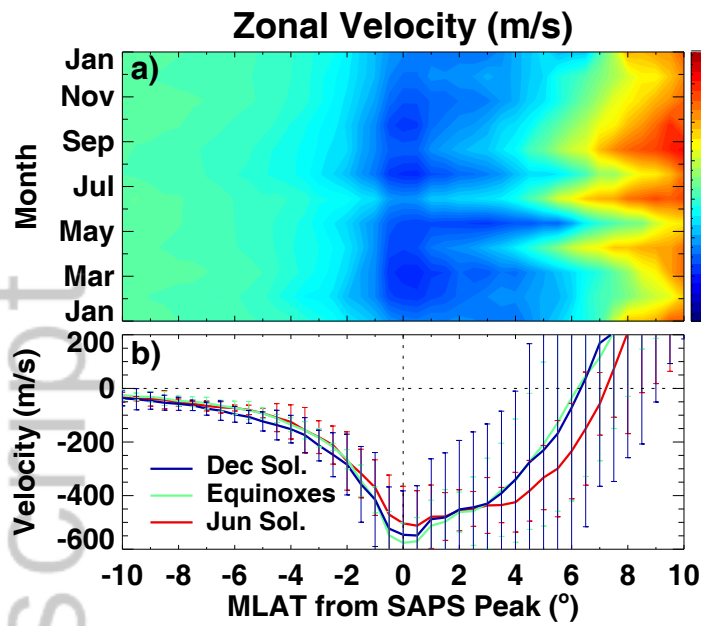
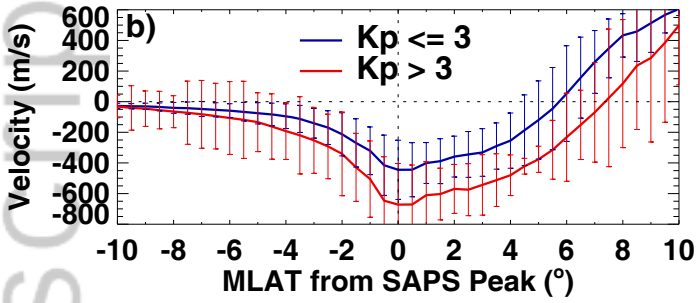
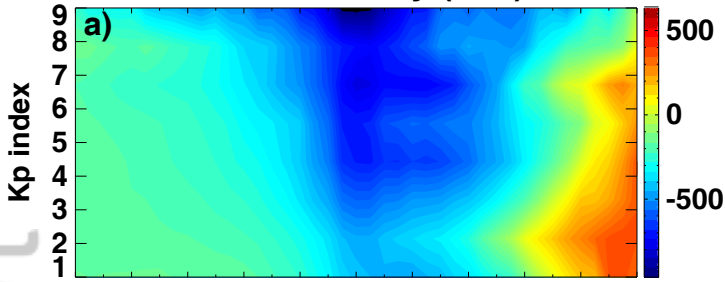


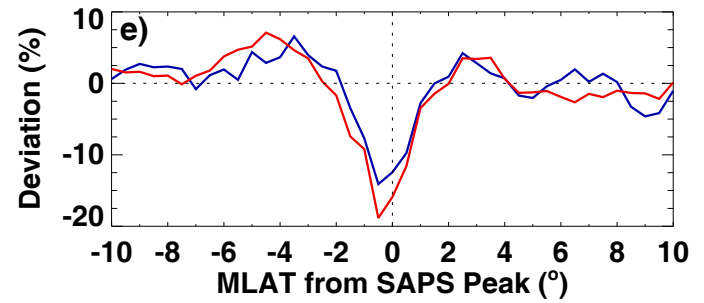
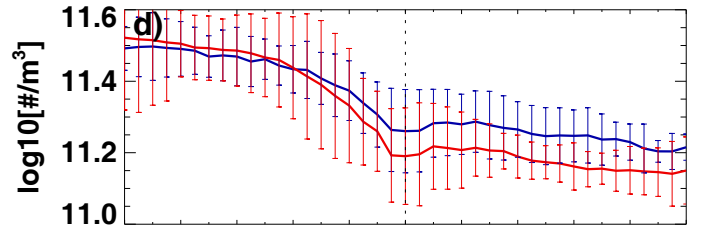
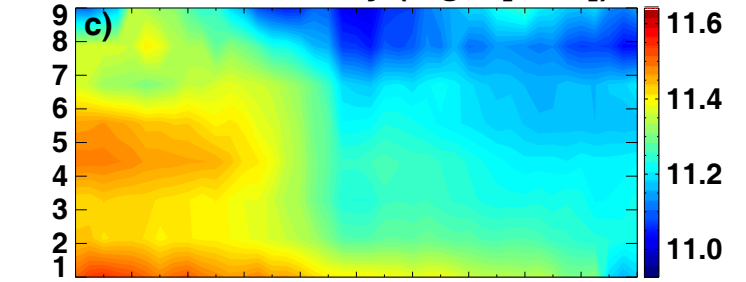
Figure 5.

Author Manuscript

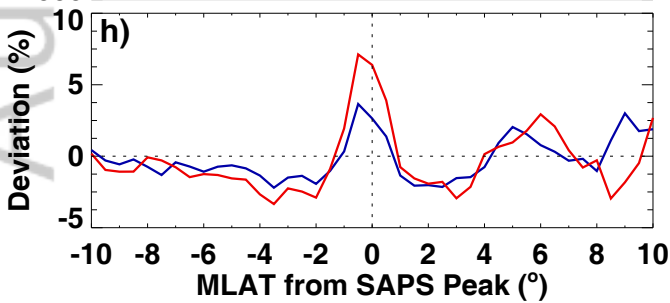
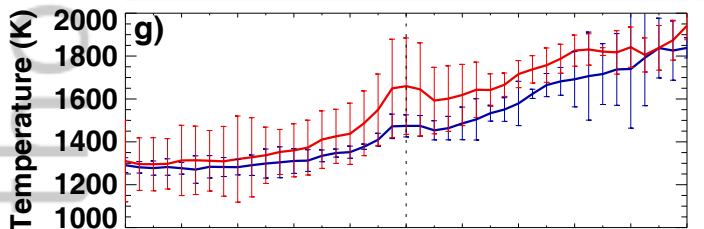
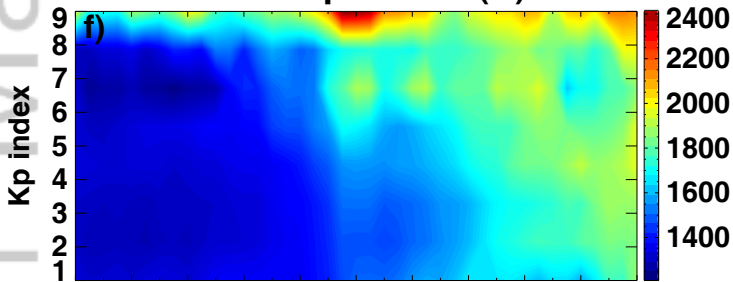
Zonal Velocity (m/s)



Electron Density (log10[#/m³])



Ion Temperature (K)



Electron Temperature (K)

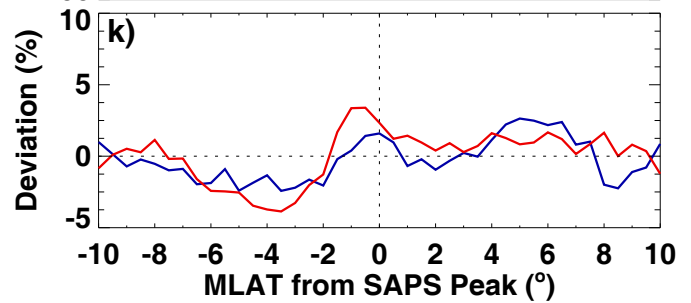
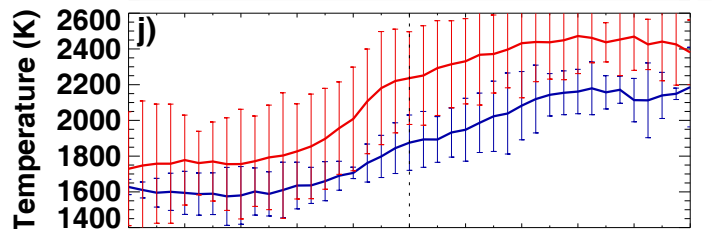
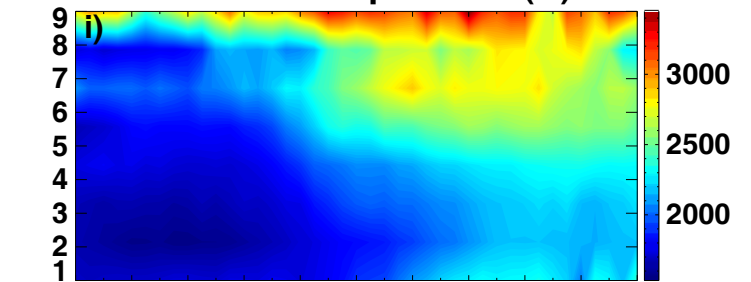
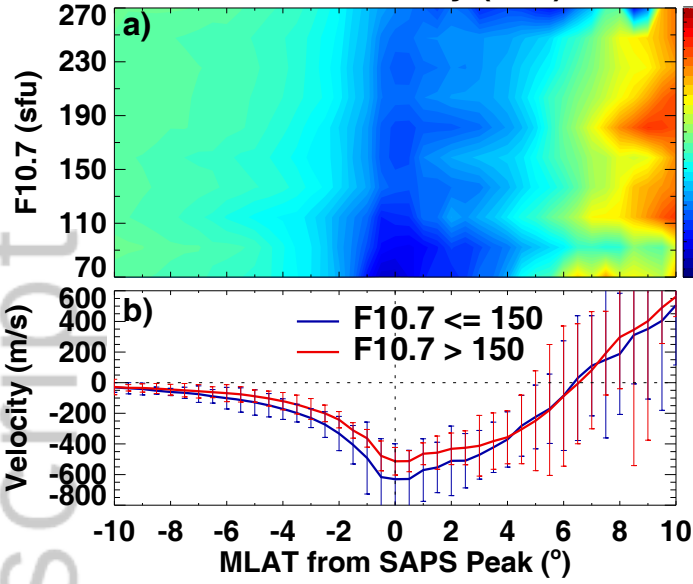


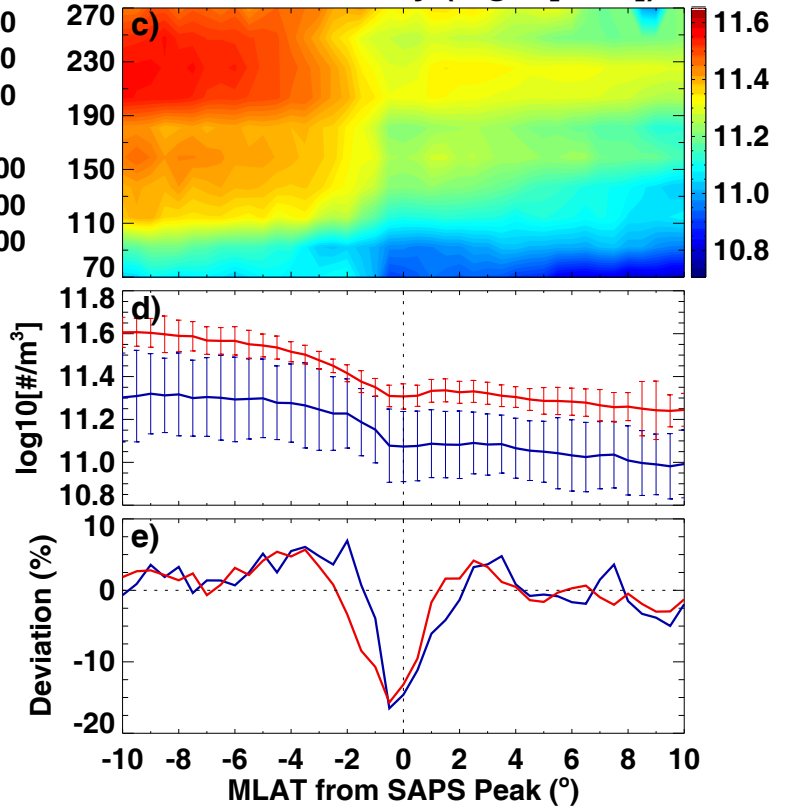
Figure 6.

Author Manuscript

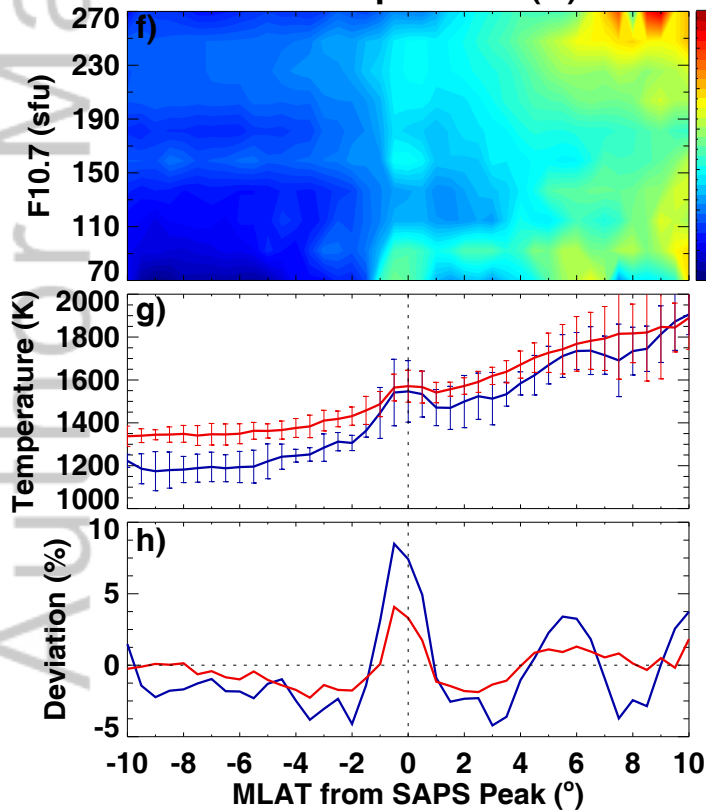
Zonal Velocity (m/s)



Electron Density ($\log_{10}[\#/m^3]$)



Ion Temperature (K)



Electron Temperature (K)

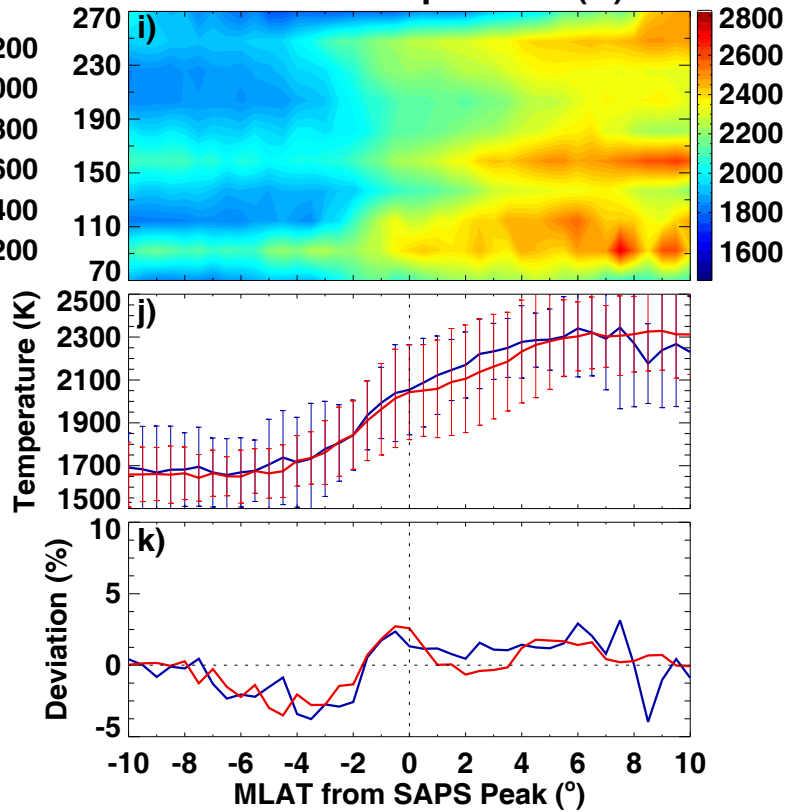


Figure 7.

Author Manuscript

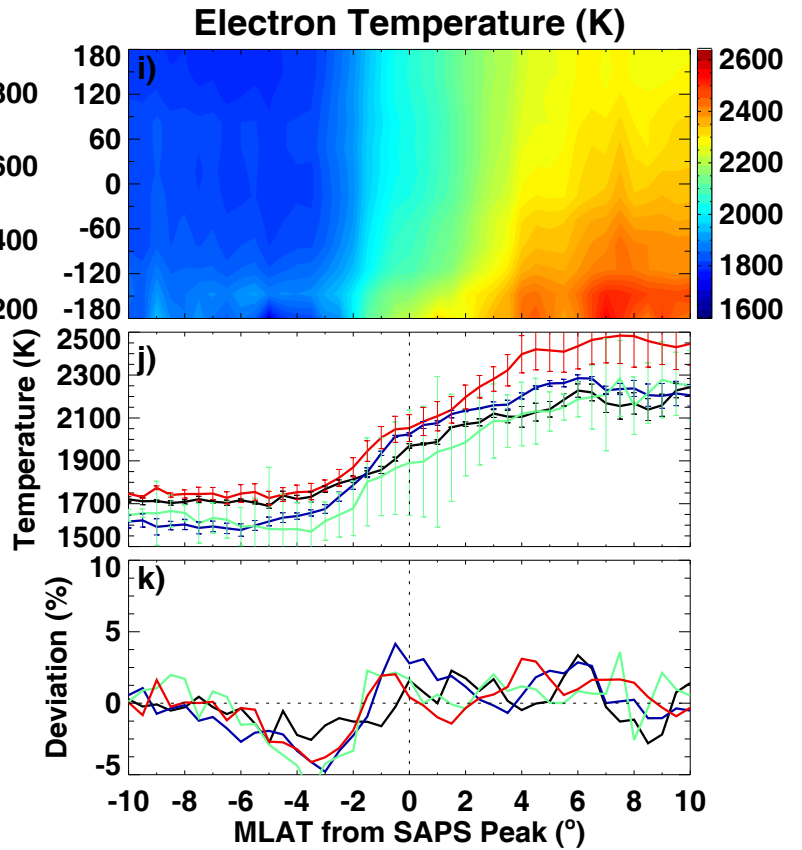
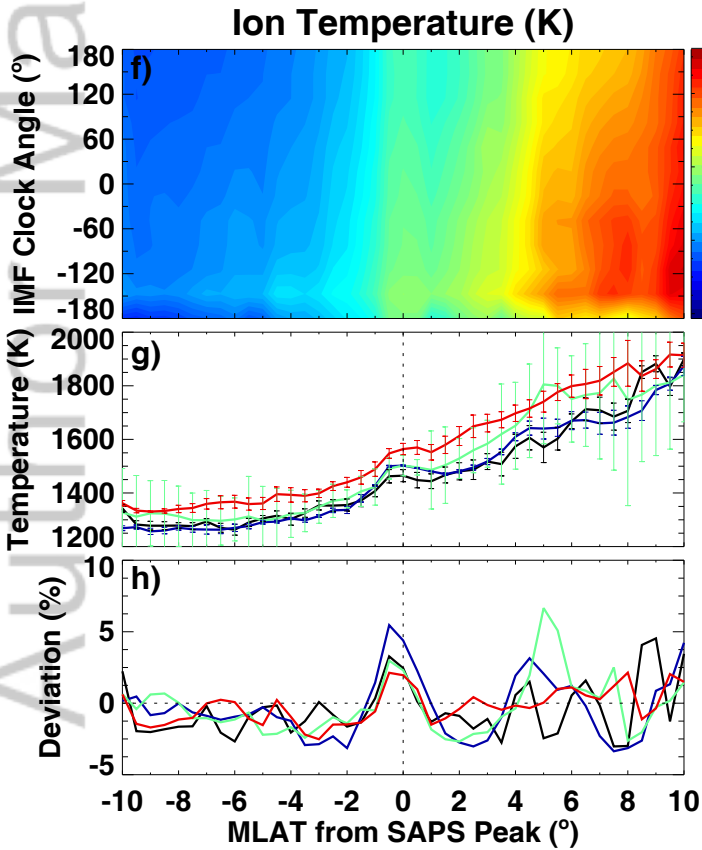
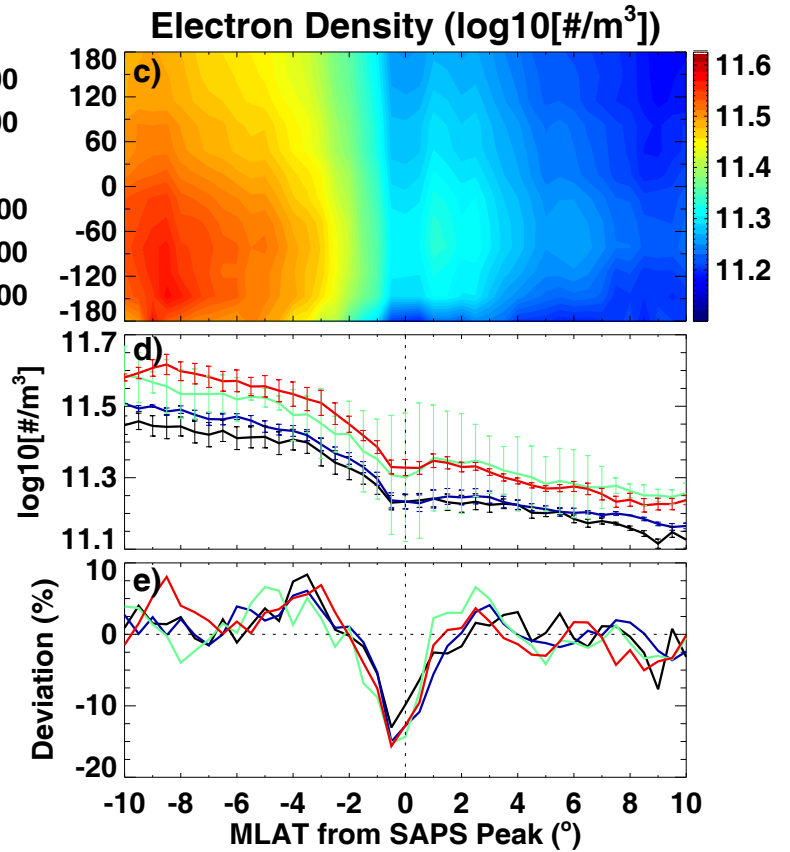
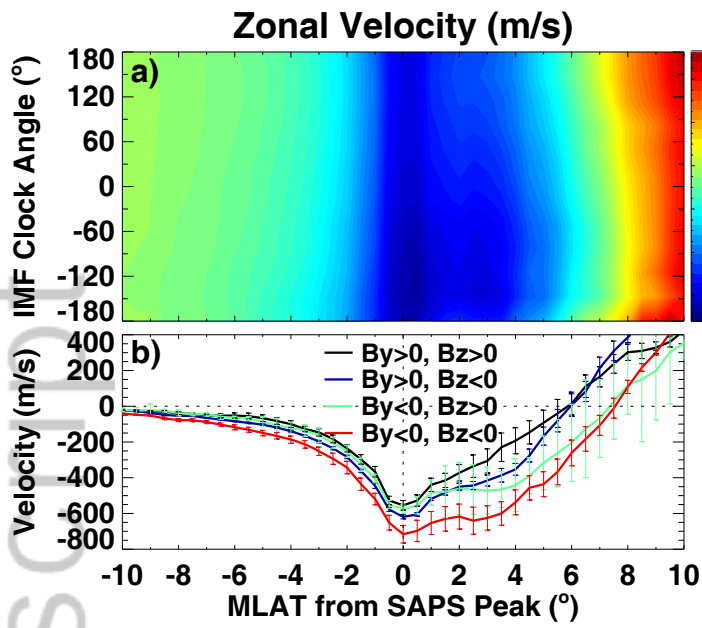
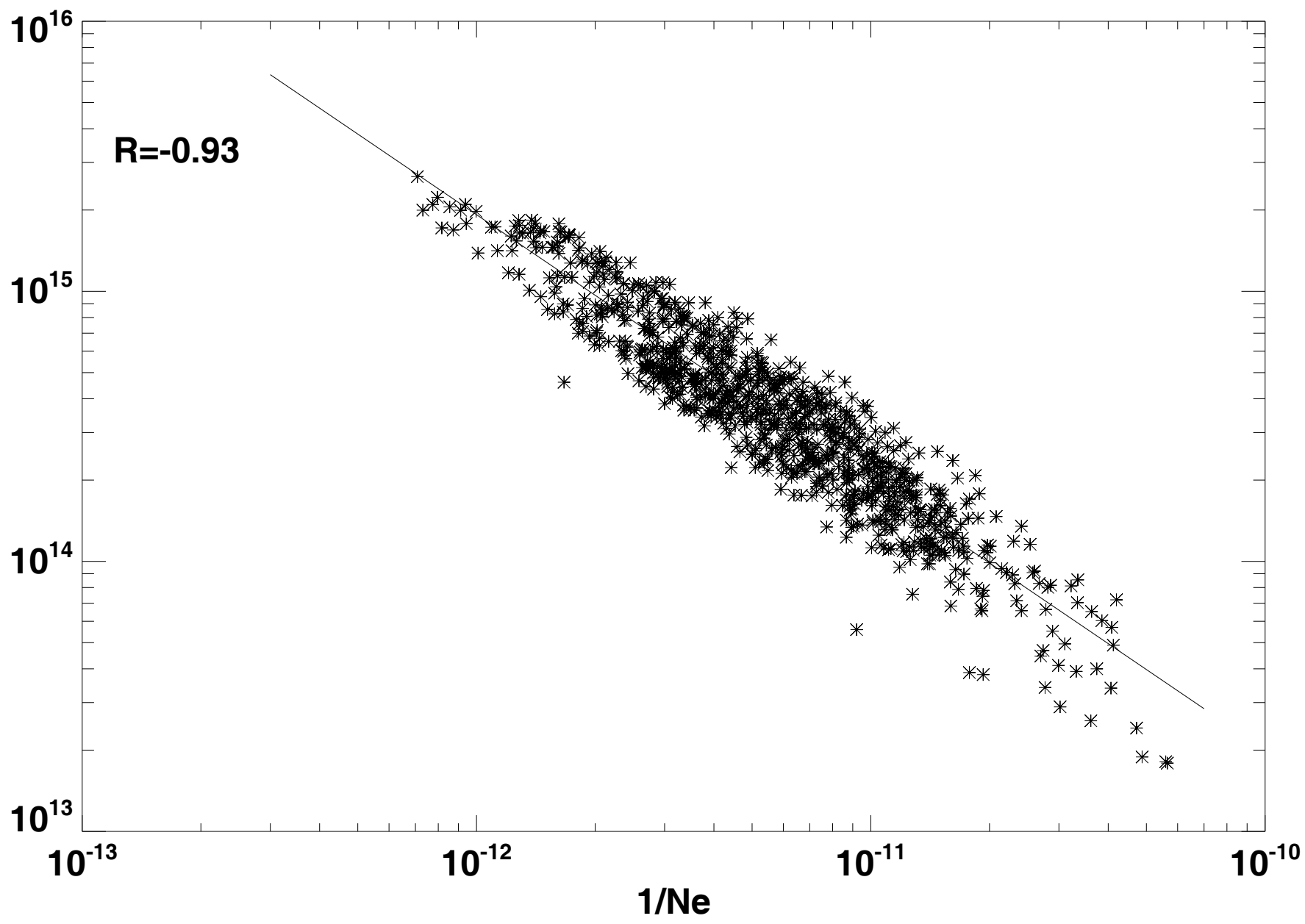
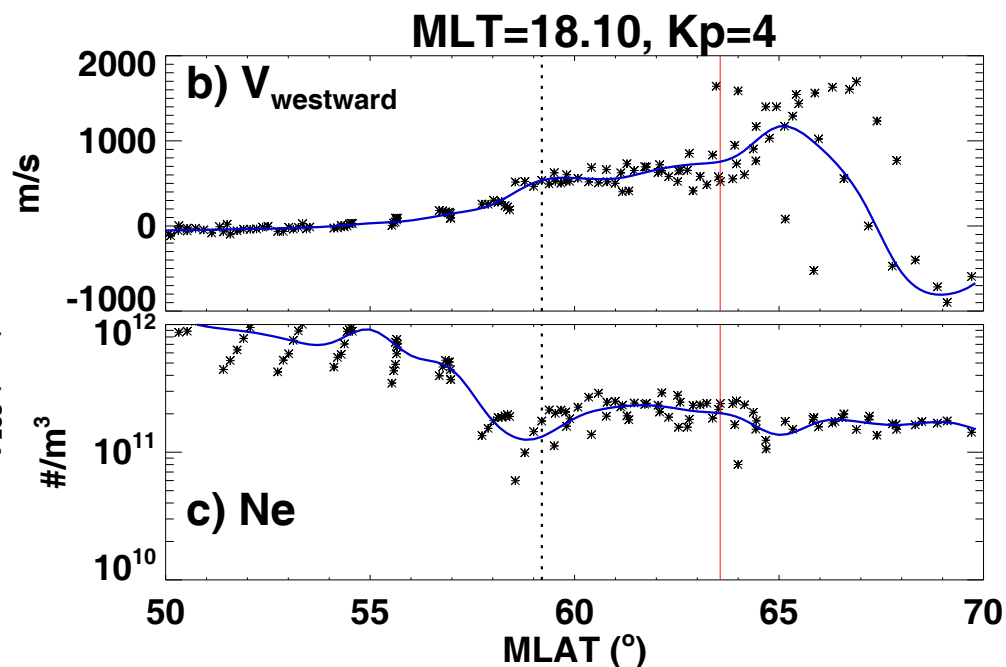
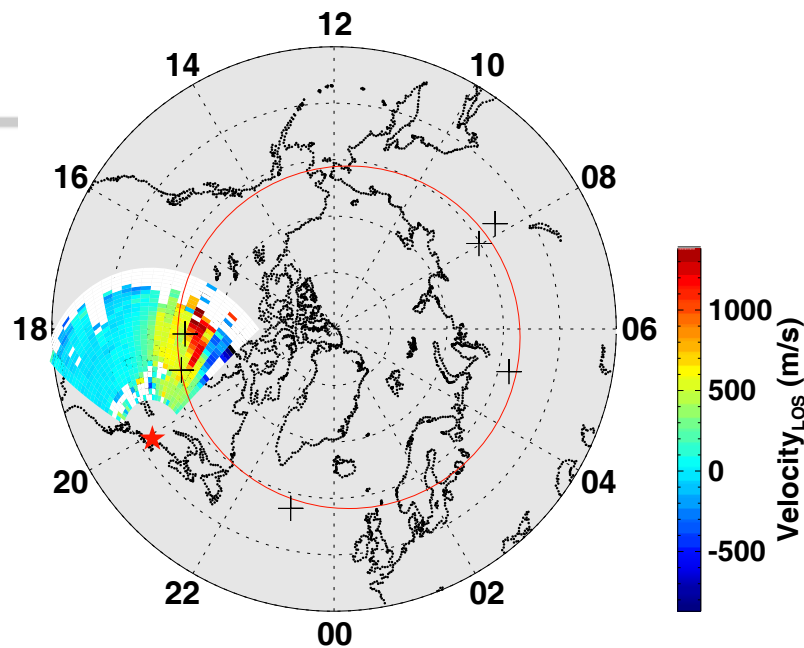


Figure 8.

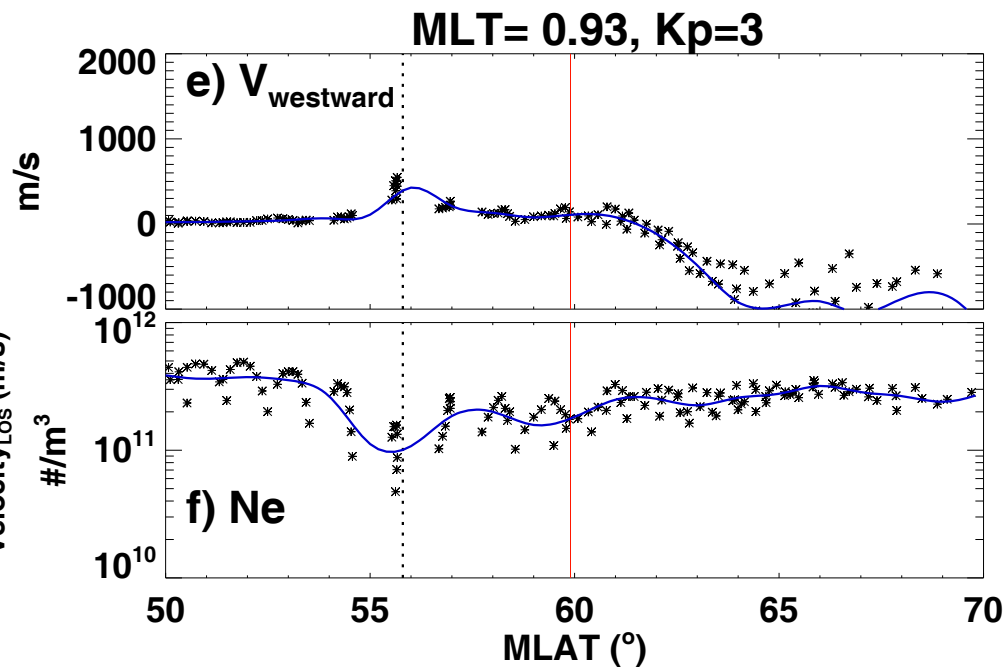
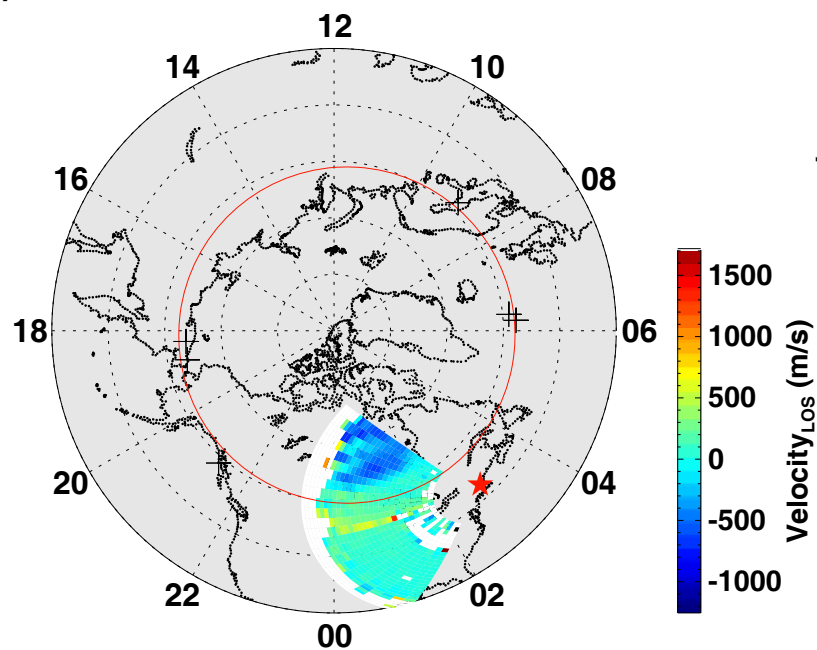
Author Manuscript

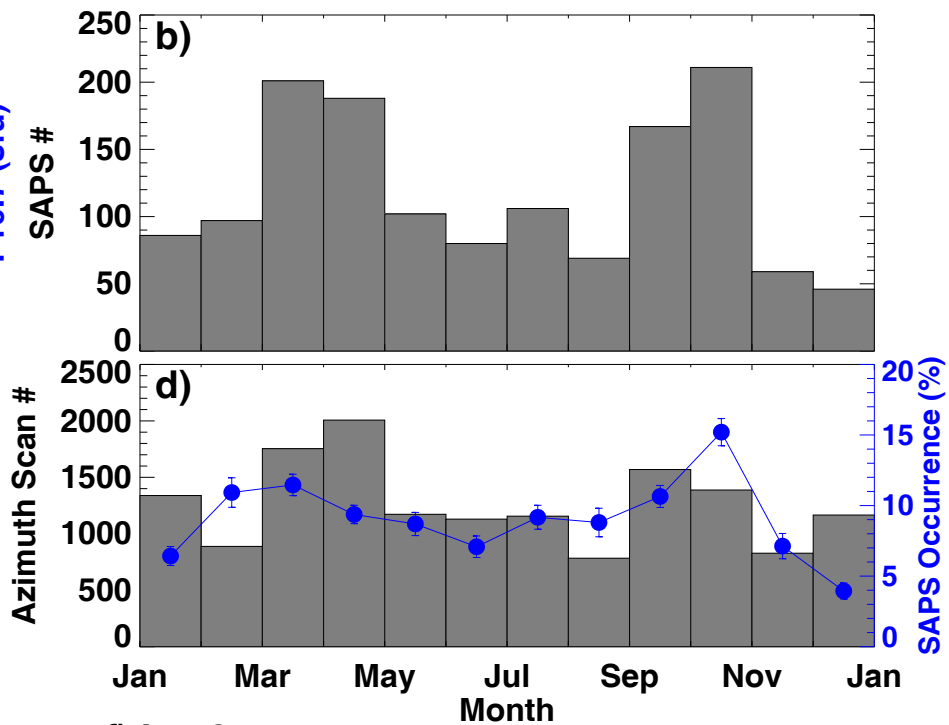
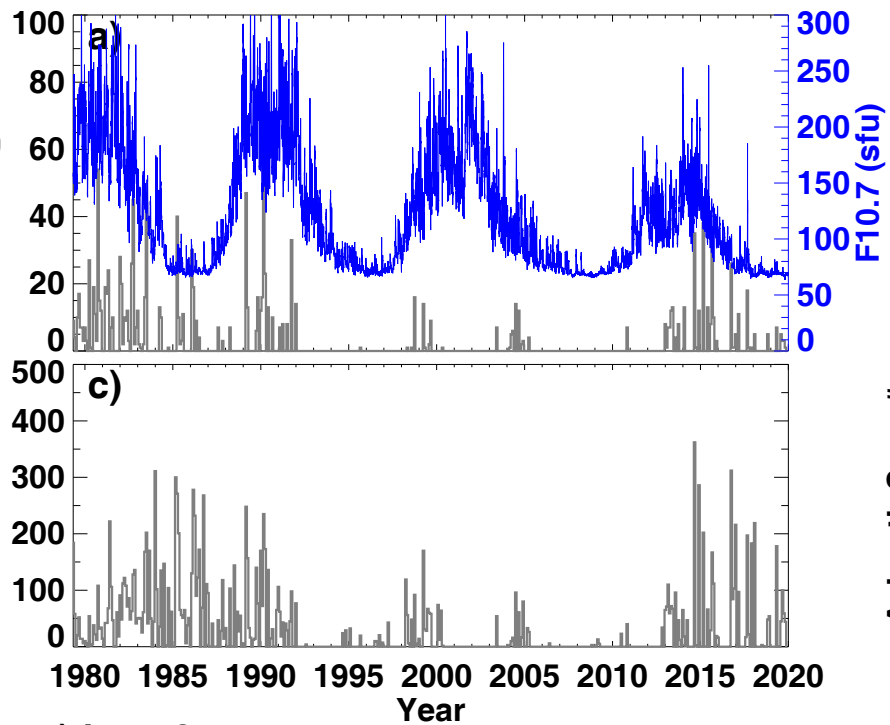


a) ISR Scan @ 10-MAR-1989 00:39 UT

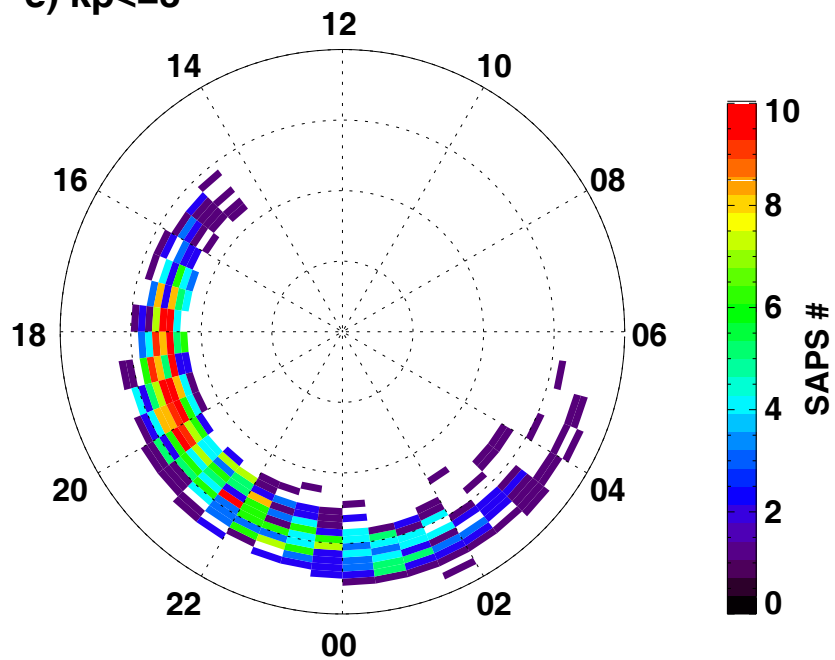


d) ISR Scan @ 09-MAR-1989 07:24 UT

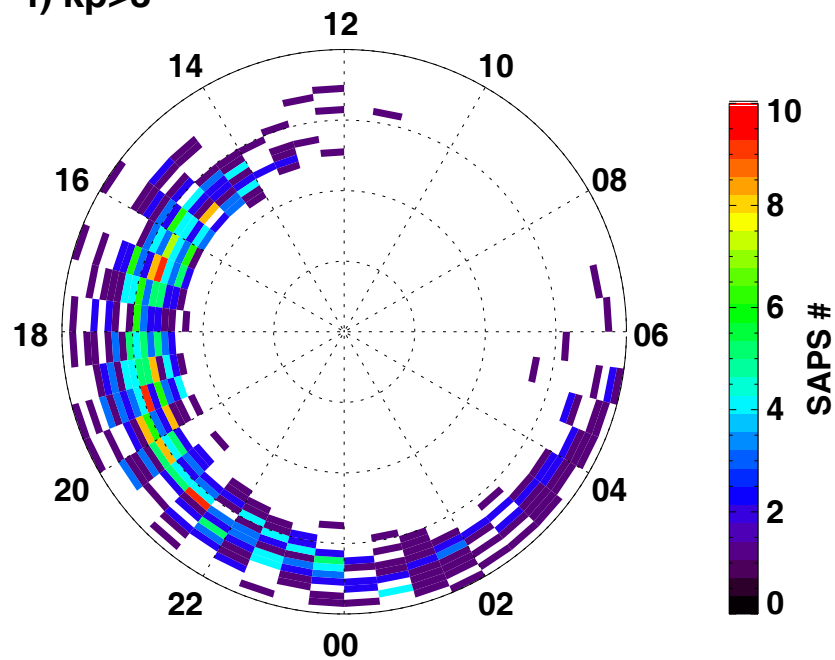


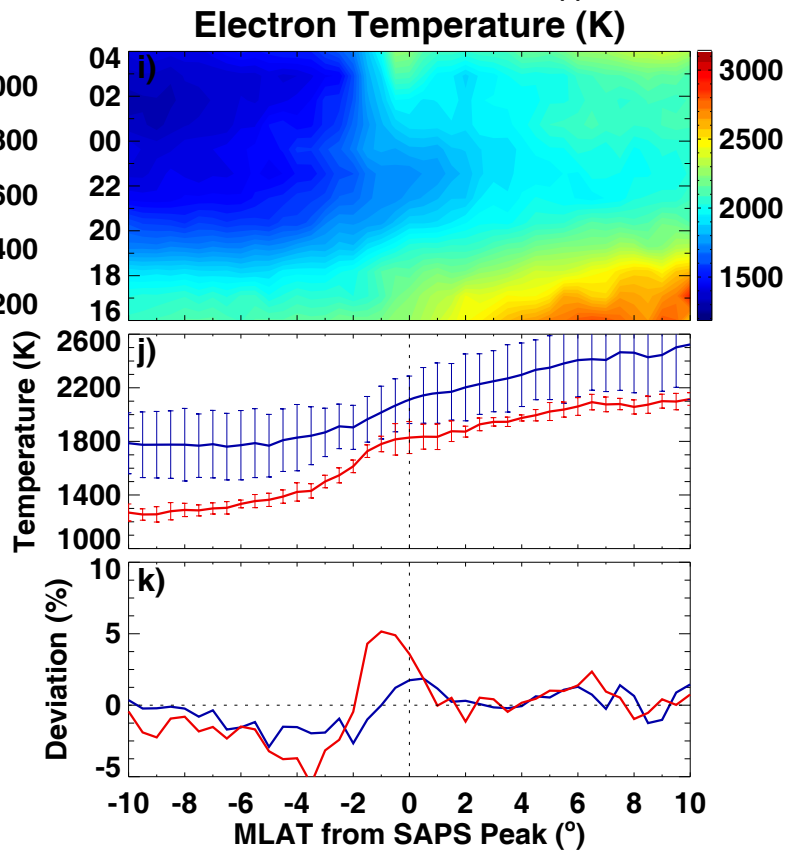
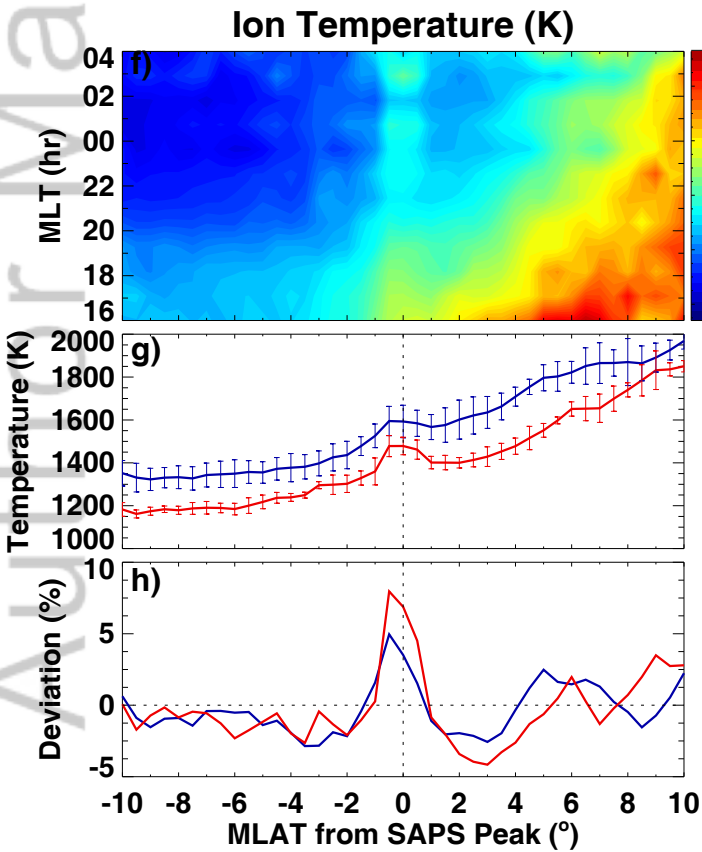
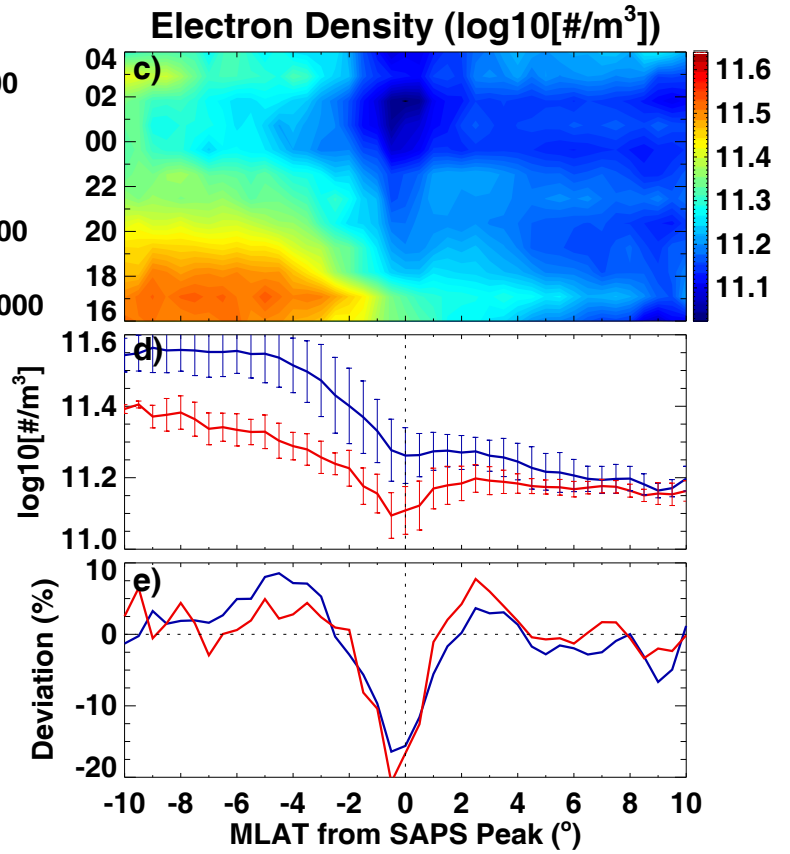
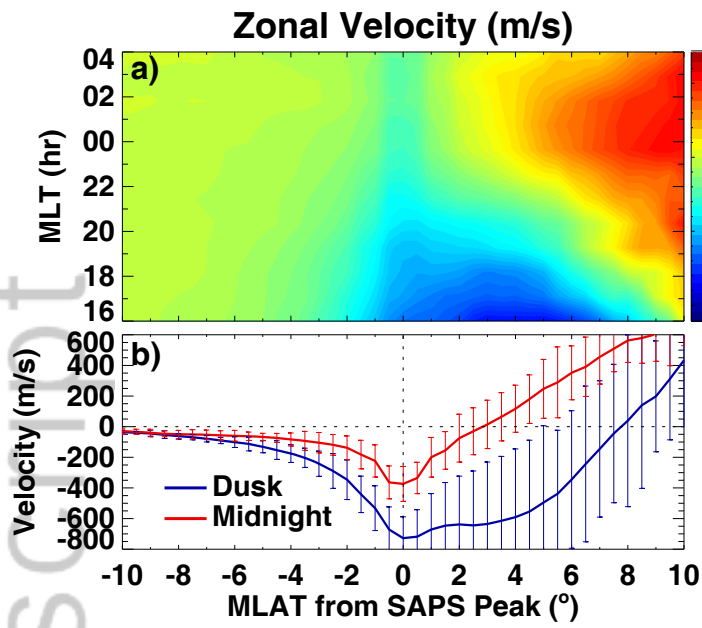


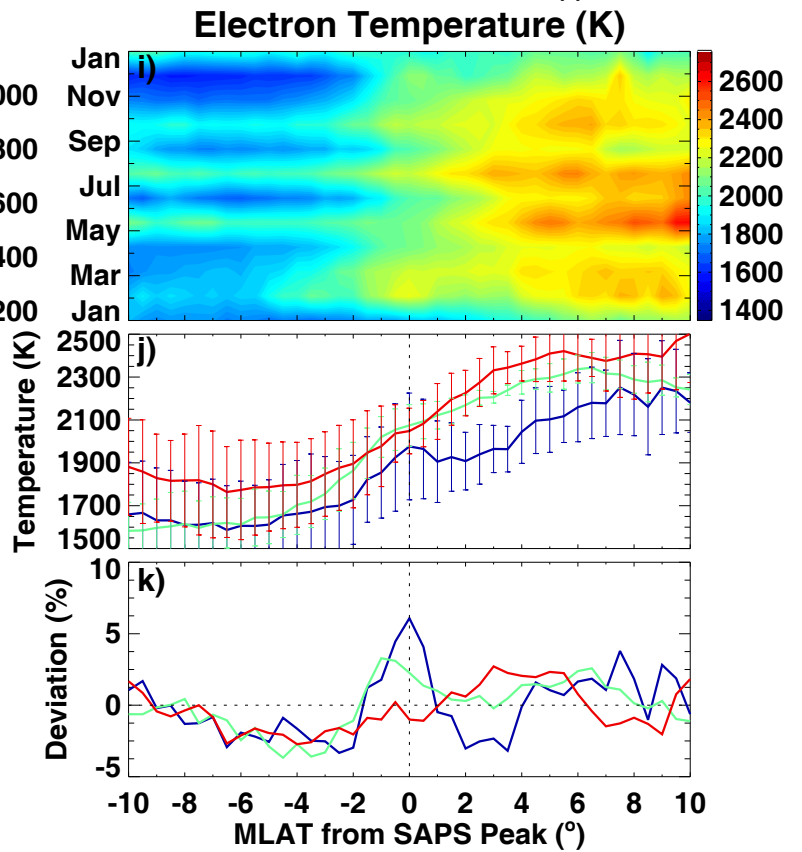
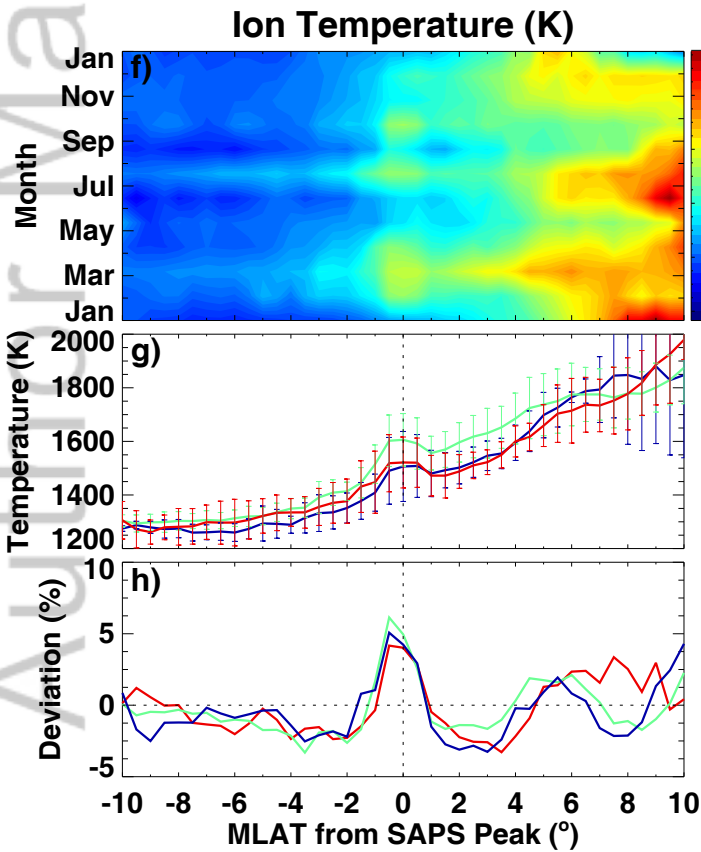
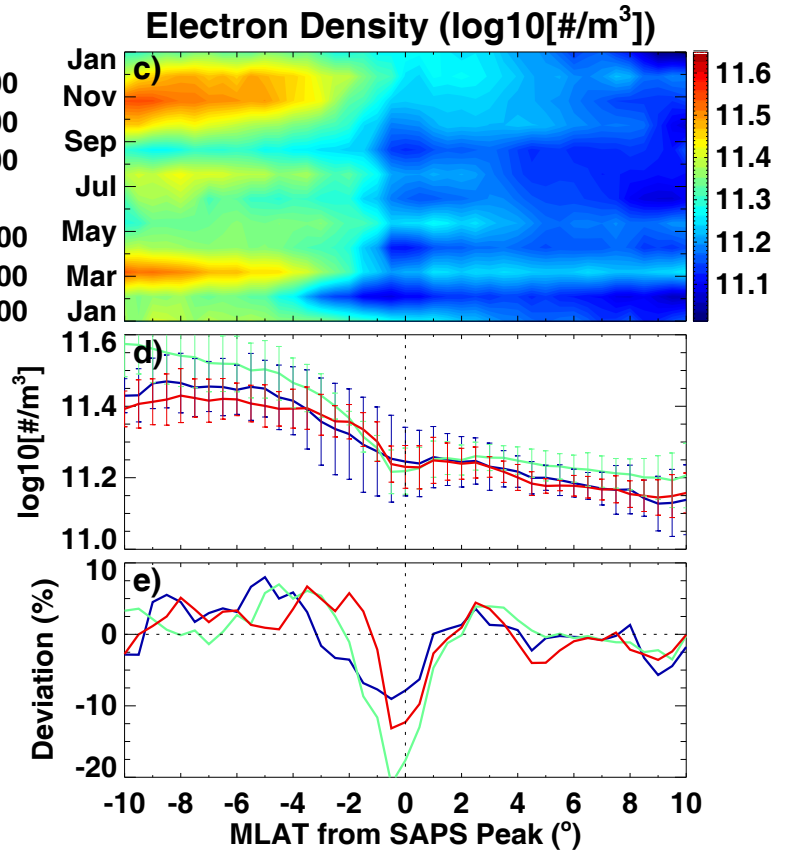
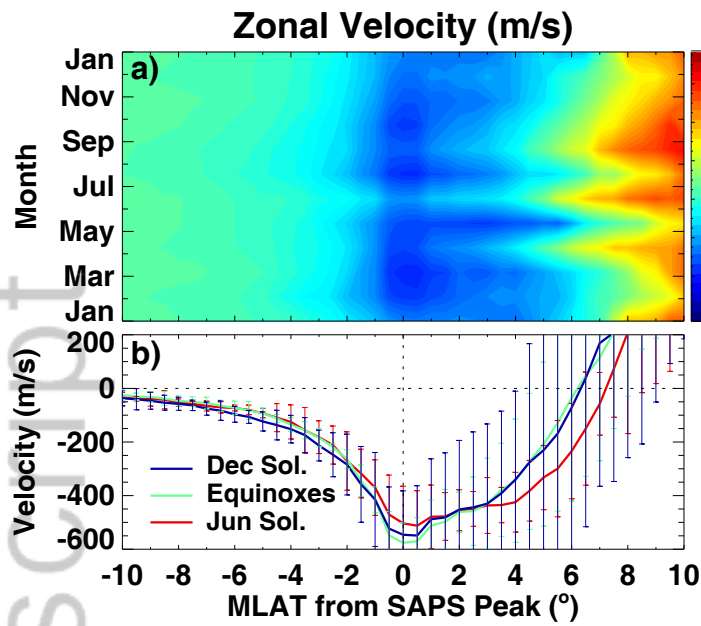
e) $kp \leq 3$



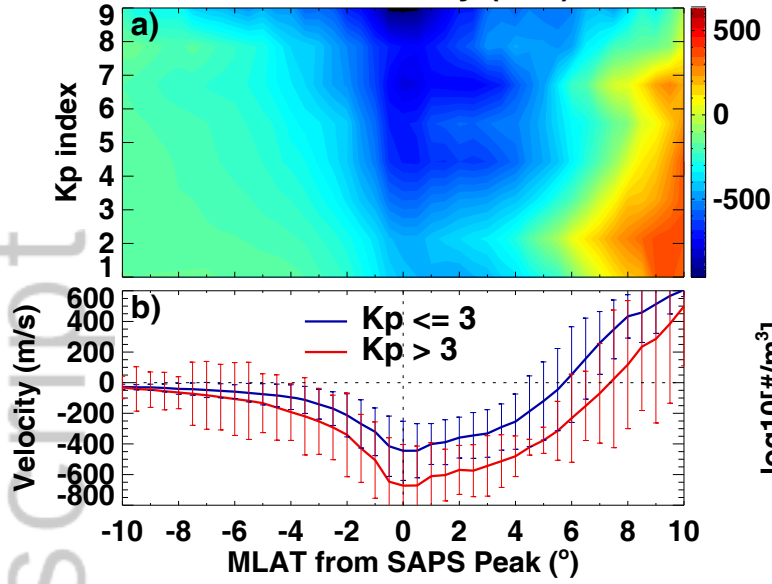
f) $kp > 3$



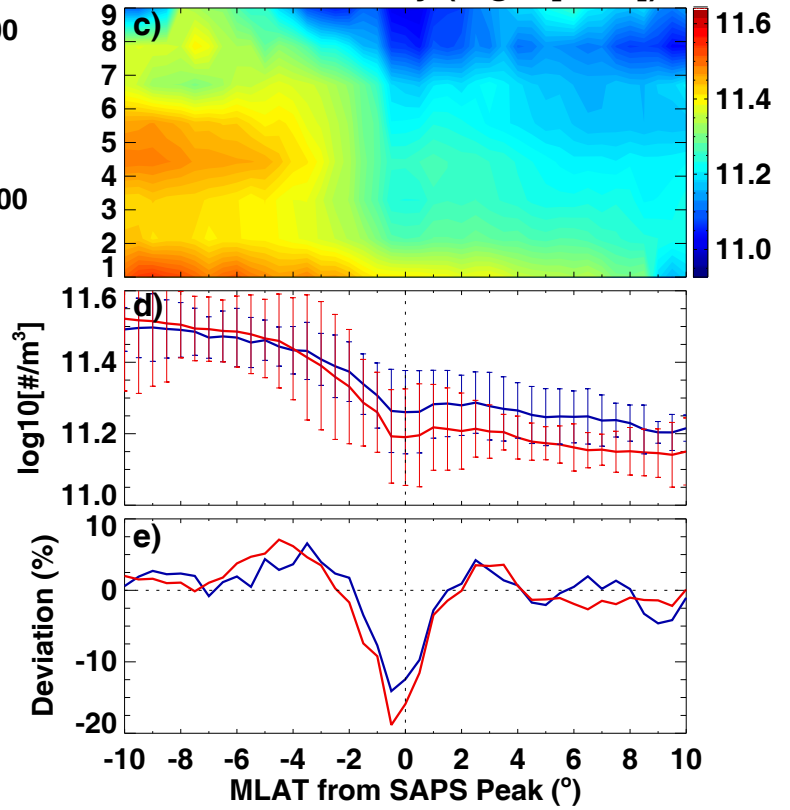




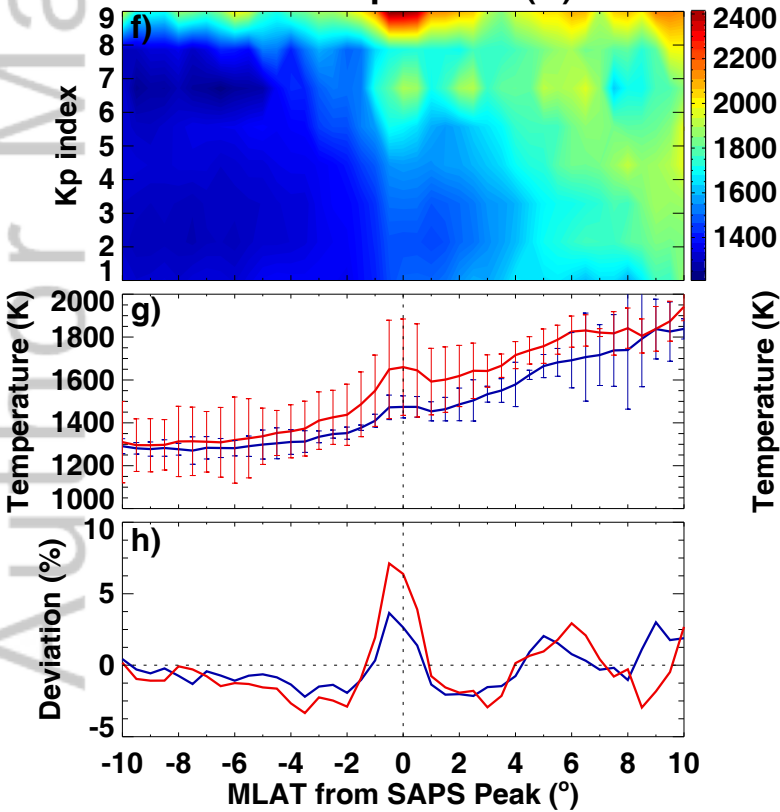
Zonal Velocity (m/s)



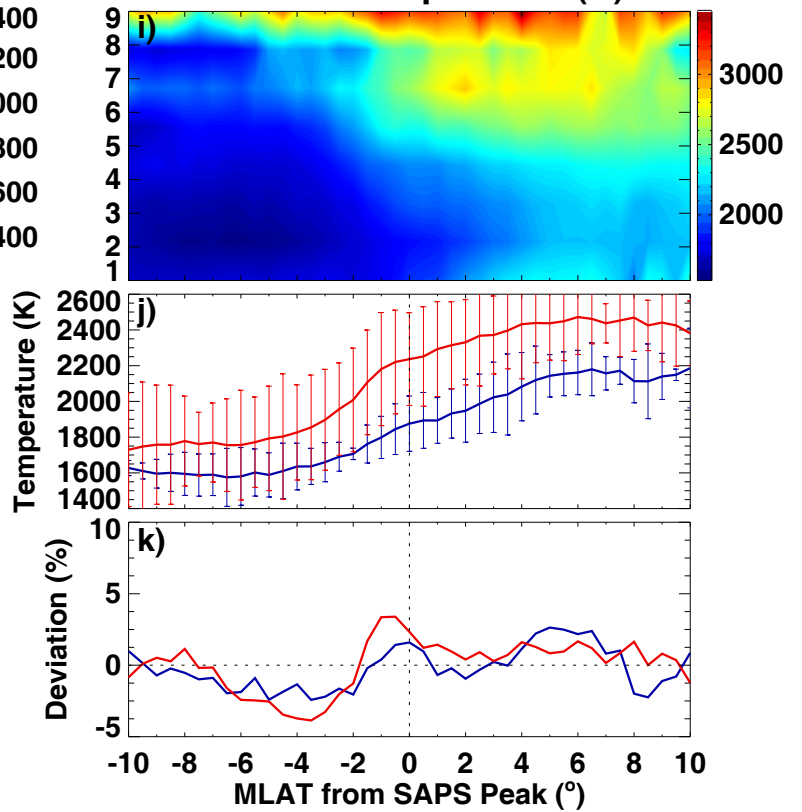
Electron Density (log10[#/m³])



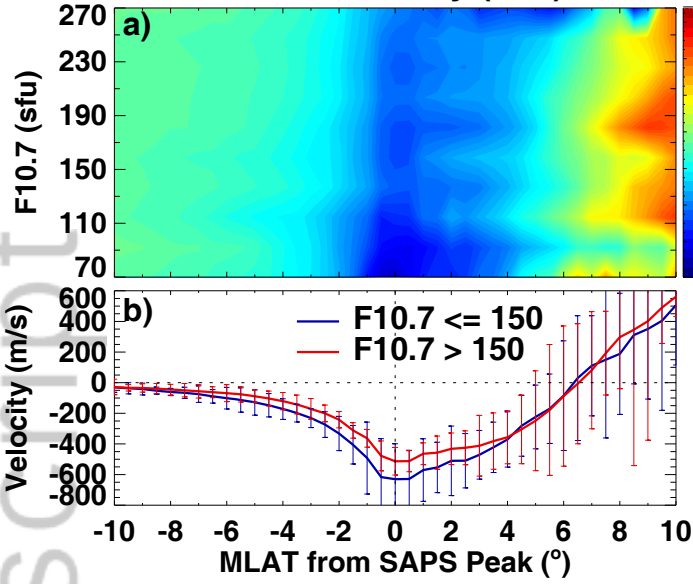
Ion Temperature (K)



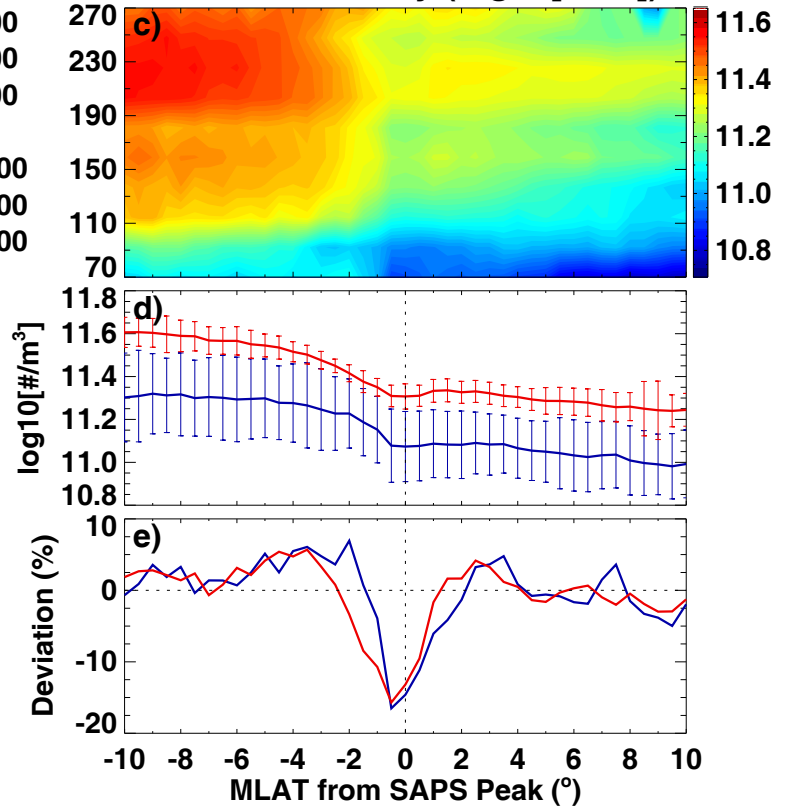
Electron Temperature (K)



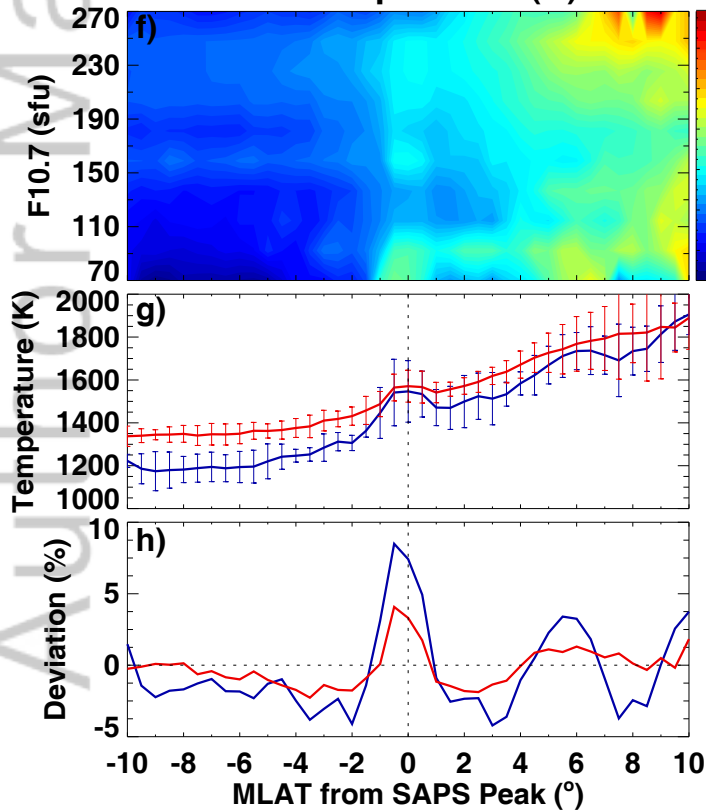
Zonal Velocity (m/s)



Electron Density (log10[#/m³])



Ion Temperature (K)



Electron Temperature (K)

